The role of galaxy mergers in the evolution of massive galaxies in the local Universe

Alfredo Carpineti
Astrophysics Group

Department of Physics
Imperial College London

—

Thesis submitted for the Degree of Doctor of Philosophy to
Imperial College London

· 2014 ·

Abstract

This Thesis presents a study of the nature of the different stages of galaxy mergers that lead to the formation of massive galaxies. In particular we look into the properties of infrared bright mergers, spheroidal post-mergers and star-forming early-types and how their properties compare and contrast with the properties of regular late and early-type galaxies. The aim of this thesis is to expand our knowledge of the merging process and to find a justification for the variability of the more active early-type galaxies. These studies were performed by extracting all the possible information from different surveys. For the optical analysis we used the Sloan Digital Sky Survey (SDSS), while we used surveys conducted by IRAS and GALEX for infrared and ultraviolet data respectively.

To better understand the mergers/massive galaxies connection we performed the first detailed analysis of spheroidal post-mergers, as well as the first infrared-blind study of the properties of merging galaxies and produced a multi-wavelength catalogue of local star-forming early-type galaxies. We also looked at the more general galaxy population by constructing the largest morphological survey of far-infrared selected objects, which provided us with the first estimate of how different morphologies (but mergers in particular) contribute to the local SF budget. The results show the pivotal role played by mergers in the formation of stars and evolution of galaxies in the local Universe.

Per Mamma e Papà,
per il loro amore, la loro pazienza e il loro supporto...

... e per Tata.

All you really need to know for the moment is that the Universe is a lot more complicated than you might think, even if you start from a position of thinking it's pretty damn complicated in the first place.

Douglas Adams

Contents

Abstract **1**

List of Tables **9**

List of Figures **12**

Declaration and Copyright **13**

Acknowledgments **14**

Publications **17**

Foreword **18**

1 Formation and evolution of galaxies in the Universe **19**

1.1 The standard Universe 20

1.1.1 From the Big Bang to proto-galaxies 20

1.1.2 Galaxy formation 20

1.2 Morphologies in flux: the role of mergers in galaxy evolution 27

1.3 Models and simulations: breakthroughs and limitations of computational astronomy 28

1.3.1 N-body simulations 29

1.3.2 Semi-analytic models (SAMs) 30

1.4 The role of observations 32

2 The tools for observing galaxy evolution **33**

2.1 The Sloan Digital Sky Survey 33

2.2 GALEX and IRAS 35

2.3 The different ways to estimate the Star-Formation rate of a galaxy . . 37

2.4 Emission line diagnostics 39

2.5 Environment estimation: Number density versus Mass 42

2.6 Direct observation of mergers in the optical . . . 43
2.6.1 Construction of Galaxy Zoo merger catalogue . . . 44
2.6.2 The merger fraction f_m: quantifying Galaxy Zoo mergers . . . 45
2.6.3 Properties of the mergers in the GZ catalogue . . . 48
2.7 Finding plausible evolutionary steps for the formation of massive galaxies . . . 53

3 The far infrared properties of galaxy mergers 55
3.1 The merger sample and basic properties . . . 56
3.2 Dependence of SFR on environment, system mass and mass ratio . . . 62
3.3 Cool ULIRGs as products of sub-L* mergers? . . . 65
3.4 Emission line activity . . . 67
3.5 Timescale of ULIRG formation along the merger sequence . . . 68
3.6 Discussion . . . 72

4 Spheroidal Post-Mergers 74
4.1 Introduction . . . 74
4.2 The Sample . . . 77
4.3 Local environments . . . 77
4.4 Colours and emission line activity . . . 80
4.5 Reconstructing the progenitors . . . 82
4.6 Discussion . . . 86

5 Star-forming Early-type galaxies 88
5.1 Introduction . . . 88
5.2 A sample of FIR-detected early-type galaxies . . . 90
5.2.1 Control samples . . . 92
5.3 Environment . . . 94
5.4 Colours, star formation and properties of the inter-stellar medium . . . 94
5.5 Emission line analysis . . . 100
5.6 Discussion . . . 100

6 The contribution of galaxy mergers to the star-formation rate in the local Universe 103
6.1 Introduction . . . 103
6.2 The morphological classification . . . 104
6.3 The colour magnitude distribution and nuclear emission line activity of IIFSCz galaxies . . . 104

6.4 The star-formation main sequence for different morphologies 108
6.5 The morphological contribution to the total star-formation budget of the Universe 110
6.6 Discussion 114

7 Conclusions **118**
7.1 Introduction 118
7.2 Merging galaxies as seen in the infrared 119
7.3 Post-merger galaxies with spheroidal morphologies 119
7.4 Star-forming early-type galaxies 120
7.5 The morphological classification of the IIFSCz 121
7.6 Overall conclusions 122

Bibliography **123**

List of Tables

2.1 Percentages of ionisation-types for volume-limited Galaxy Zoo merger and control galaxies 51

4.1 SDSS ID, RA, DEC, r-band *fracdev*, environment parameter ρ, spectroscopic redshift and stellar mass for our sample of postmergers . . . 78

List of Figures

1.1 A schematic representation of the discrepancy between theory and observation of the luminosity function 22
1.2 The Hubble classification scheme for galaxies 25
1.3 The Antennae Galaxies 26
1.4 A schematic version of the merger tree concept. 29

2.1 Comparison between the different ways to estimate the Star-Formation rate of a galaxy 38
2.2 Examples of BPT diagnostic diagrams 41
2.3 The Colour Magnitude diagrams of the Galaxy Zoo merger sample . . 49
2.4 Spectral type-colour-mass relations 50
2.5 The environment distribution for control population and Galaxy Zoo mergers 52
2.6 A schematic merger timeline 54

3.1 An SDSS ugriz composite image of an IRAS-detected merger in our sample. 57
3.2 The SFR calculated from the IRAS FIR luminosity plotted against the SFR calculated the Hα 57
3.3 Predicted FIR flux for mergers that were IRAS-*undetected* 58
3.4 Masses and SDSS spectroscopic redshifts for the IRAS-detected and IRAS-undetected mergers. 59
3.5 Infrared Luminosity and SFR of the IRAS-detected mergers 61
3.6 The distribution of the star-formation rates for the IRAS mergers and for a control sample of relaxed galaxies 62
3.7 The merger star formation rate plotted against the merger mass ratio. 63
3.8 The total stellar mass is plotted against the star-formation rate and against the specific star formation rate 64
3.9 The star formation rate of the IRAS-detected mergers and the LTG control sample plotted against the dark matter halo mass. 65
3.10 The luminosity distribution of a group of cool ULIRGs 66

3.11 The emission line activity of the IRAS-detected mergers 67
3.12 The SDSS images of the ULIRGs 70
3.13 Measured separations of the LIRGs in the sample and the timescale for their coalescence 71

4.1 SDSS images of our sample of spheroidal postmergers. 75
4.2 The *fracdev* parameter in the optical r band for our visually selected sample of spheroidal post-mergers. 76
4.3 The values of the environment parameter (ρ) for the sample 79
4.4 The $(u-r)$ colour-mass relation of the spheroidal postmergers compared to a control sample of early-type galaxies from the SDSS 79
4.5 Histogram of $(u-r)$ colour of the SPMs, ongoing mergers from the catalogue of Darg et al. and a control sample of early-type galaxies from the SDSS 80
4.6 Emission-line analysis of the SPMs compared to the ongoing mergers from Darg et al. 81
4.7 Comparison of the colours of the spheroidal postmergers to a simple model, designed to approximate the stellar content in these galaxies . 83

5.1 The sensitivity of UV to small mass fractions of a young stellar population 89
5.2 Examples of the 5 morphological star-forming ETG sub-classes 91
5.3 Comparison of the environments of our SF ETGs with an elliptical control sample 93
5.4 UV-optical colours of the FIR-detected ETGs, the early-type control sample and the late-type control sample 93
5.5 An example of the output SED produced by `MAGPHYS`. 95
5.6 TOP: `MAGPHYS`-derived star formation rates (SFRs) of the FIR-detected ETGs and LTG control sample. BOTTOM: Specific SFRs of FIR-detected ETG split by morphological sub-categories. 96
5.7 Stacked probability distributions of the dust mass from `MAGPHYS` for all FIR-detected ETGs & Dust-to-stellar mass ratio vs SSFR of the FIR-detected ETGs. 98
5.8 Estimated molecular gas mass of the FIR-detected ETGs. 101
5.9 Summary of ionisation mechanisms in our FIR-detected ETGs from our BPT analysis 101

6.1 SDSS images of the 3 morphological classes. In order we have a spheroidal, a late-type galaxy and a merger. 105
6.2 The u-r versus the absolute magnitude in the r band for the IIFSCz . 106
6.3 TOP: We plot the CMD for the spheroidals and LTGs in the catalogue. BOTTOM: We plot the CMD for different emission line classes. 107
6.4 SFR as a function of galactic stellar mass for our galaxy sample . . . 109
6.5 The plot shows the group mass as an environment density indicator for the different morphologies in the IIFSCz. 110
6.6 The linear fits for SF main sequence are plotted in this figure. 111
6.7 This pie chart shows the percentage of the star formation budget apportioned in terms of morphological class 112
6.8 These pie charts show the percentage of the star formation budget apportioned in terms of morphological class and environment 113
6.9 These pie charts show the percentage of the star formation budget apportioned in terms of morphological class and stellar mass 113
6.10 This pie chart shows the percentage of the star formation budget apportioned in terms of morphological class plus an estimation of the contribution to the SF budget by the undetected galaxies 115

Declaration and Copyright

This thesis is my own work, except where explicitly indicated in the text.
The copyright of this thesis rests with the author and is made available under a Creative Commons Attribution Non-Commercial No Derivatives licence. Researchers are free to copy, distribute or transmit the thesis on the condition that they attribute it, that they do not use it for commercial purposes and that they do not alter, transform or build upon it. For any reuse or redistribution, researchers must make clear to others the licence terms of this work

Alfredo Carpineti
March 2014

Acknowledgments

While a PhD is ultimately a solo endeavour, it is not possible to achieve it without the help, contribution and support of others. My first thank you goes to my biological family Mum and Dad, my wonderful sister, my grandparents, Richi e Vale, Zio Alberto, Zia Antonella e Zia Raffi, Mauro and all the aunties and uncles and cousins.

The second thank you goes to my logical family, the people that in the course of my life has come on board and help me become in the man I am today.

Xenia, there's no way I can ever thank you enough for your impact in my life. I love all your flaws and count myself lucky for all your qualities. Sei la mia roccia e il mio faro.

Davide, you're the brother I found in the world. You're my oldest friend, the one that always make me laugh no matter what, the one I can count on sharing a wall with every christmas mass.

Henry, our paths are diverging soon but it doesn't matter because we're not going anyway. You're one of the most important people in my life and there's not enough time-space to tear us apart.

Felix, words fail me when I try to express how important you are to me. The truth is that you make me a better man, and I can't be more thankful of knowing you.

Richard, you are my Imperial constant. In the last five years I've seen you more than any other person in the list. Life would be much different if I didn't have someone to discuss the trivial and the cosmic with every single morning.

Stuart, how do I even begin to explain Stuart Haylock's impact in my life? Well,

you know the rest and I'm very grateful for it.

Amooo, amooooooo, amooooooooo!! Grazie di tutto amo.

Chris, you were the first person I told I got the Ph.D., we have known each other for five years and I still can't believe how lucky you are to have me in your life. You're welcome.

Matt, you put up with so much of my craziness and you're always a laugh. Thanks for being such a good friend.

Daniele, I'm finishing my Ph.D. while you're starting yours. Thank you for your support and I hope I can give back what you gave me even though you're merely studying bio-physics.

Socha, I don't tell you enough how utterly incredible you are. After all you are an engineer and you still managed to make my acknowledgements shortlist... you must be doing something right.

Francesco, sono 8 anni che studio astrofisica e scommetto che se te lo chiedono tu continui a rispondere che faccio l'astrologo. Non ti sorprendere che continuo a retrocederti. Grazie di tutto.

Cyprian, I can't fathom the fact that some time soon I won't be able to pop by your office for a chat whenever I want. Thank you man, you're the best.

Nathalie, you are the Bonnie to my Clyde, the Thelma to my Louise. I'm really grateful for all the amazing time I spent with you and the girls.

Ashley, whenever I need some English help, or infrared advice or a video of a cat riding a roomba you were there for me. Thank you hun, you're the best.

Michael, thank you for the constant distractions of gigs, shows and general amazingness

Caroline, how can I not thank my wife? You have abandoned me several times but whenever I needed you were there either giving me advice or telling me off for

being stubborn. Something only a wife would do.

Daniel, you had a huge impact on me and you inspire me to go back to London. Thank you for being in my life.

Harsit, you have been patient and the google/wikipedia of the astro postgrads. Thank you very much for all your help.

Ryan, thank you for all the talks, all the concerts, all the time and all the wine.

And last but not least, to Chris who got here at the right time to see me finish the thesis and I am glad I got to share this with him
Thanks also to all the other friends I met along the way, especially Ivano, Daniele, Pietro, Matteo, Sara, Valeria, Keith, Iona, Alex, Rob, Tom, Russell, Seb, Nick, Tim, Josh, Darren, Aaron, Camilla, Dave, Craig, Phil.

Last but absolutely not least are the people that actually help me in my academic career. Sugata has been a terrific supervisor, guiding me through the whole charade and making me cultivate my independence. I'm grateful to Steve for giving me a second chance, and to Yvonne and Dave for all the advice and the time they both have dedicated to me. I'm also thankful to Dan, Chris and Kevin for their contributions, inputs and help in my publications and I'm very grateful to the astro group for the last four years especially Will, Daniel, Mitesh, Laura, Charlotte, Cat, Tot, Murray, Simon, Dan, Marissa, Andrew and Shyam.

Publications

- "Spheroidal post-mergers in the local Universe"
  Carpineti A., Kaviraj, S.; Darg, D.; Lintott, C.; Schawinski, K.; Shabala, S., 2012, MNRAS, 420, 2139

Foreword

This thesis is based on work carried out at Imperial College London between November 2009 and April 2013.

Chapter 1

Formation and evolution of galaxies in the Universe

Galaxies are massive, gravitationally bound systems that consist of stars, planets, gas, dust, and dark matter. They are fundamental components of the Universe, linking the very big and very far to the local and relatively small. Studying galaxies is essential to obtain a rounded cosmological picture. For this reason, galaxy formation and evolution is one of the most active fields of theoretical and observational astronomy. Its findings influence every other astronomical topic as galaxies connect the holistic view of cosmology to the exhaustive analysis of stellar physics. The detailed process of how galaxies form is still a major open question. In the '60s and '70s there were two schools of thought: top-down formation and bottom-up formation. In top-down theories (such as the Eggen-Lynden-Bell-Sandage model[1] or the Zeldovic pancake[2]), protogalaxies form in a large-scale simultaneous collapse lasting about one hundred million years. Subsequently, these huge structures break down in smaller clumps which collapse to form the objects we see today (Eggen, Lynden-Bell & Sandage, 1962; Zel'dovich, 1970). In bottom-up theories small structures form first, and then a number of such bodies accrete to form a larger galaxy. This model was first proposed by Leonard Searle and Robert Zinn (Searle & Zinn, 1978). Modern theories are bottom-up theories modified to take into account the

[1] In the Eggen-Lynden-Bell-Sandage model (Eggen, Lynden-Bell & Sandage, 1962), disk galaxies form through a monolithic collapse of a large gas cloud. As the cloud collapses the gas settles into a rapidly rotating disk becoming what we see nowadays

[2] An approximation can be used to describe an ellipsoid of gas at supergalactic scale, that will model the collapse as occurring most rapidly along the shortest axis, resulting in a pancake form. This approximation assumes that the ellipsoid of gas is sufficiently large that the effect of pressure is negligible and only gravitational attraction needs to be considered. That is, the gas will collapse without being significantly perturbed by outward pressure.

dark components of the Unverse, namely dark matter and dark energy[3].

1.1 The standard Universe

The way structures form, how they change in time and how they influence each other is imprinted upon the structure of the Universe from the very beginning. To understand how galaxies have evolved over cosmic time, the current cosmological model has to be briefly discussed.

1.1.1 From the Big Bang to proto-galaxies

The commonly accepted cosmological model of the Universe is based on the Big Bang. It proposes that the Universe started as a singularity which went through a phase of rapid exponential expansion (known as inflation) over 13 billion years ago. After cosmic inflation ended, the Universe continued its expansion and started breaking into its fundamental components in various processes which are poorly-understood. The latest theory (i.e. The ΛCDM model[4] (Sahni, 2004)) describes the Universe as composed of normal matter, dark matter and dark energy .

Most of this early epoch sees a complete dominance of photons over the rest of the Universe. As the radiation dominated Universe expands, its temperature drops to the point where the post-inflationatory quark-gluon plasma can condense into protons and neutrons. Then, nuclear fusion forms the nuclei of light elements. This period is known as nucleosynthesis.

1.1.2 Galaxy formation

While appearing smooth on large scales, we know that the Universe is inhomogenous on small scales. These inhomogeneities were already present at a redshift of $z \sim 1000$ as shown by detailed analysis of the Cosmic Microwave Background (Komatsu et al., 2009; Dunkley et al., 2009). Around this time, the energy density of these atomic

[3]Dark energy is a hypothetical form of energy which accelerates the expansion of the Universe.

[4]Λ stands for the cosmological constant which is currently associated with a vacuum energy or dark energy inherent in empty space. Λ explains the current accelerating expansion of the cosmos. Current estimates put dark energy to be about ∼ 69% of the energy density of the present universe. CDM, cold dark matter, is a form of matter necessary to account for gravitational effects observed in very large scale structures that cannot be accounted for by the quantity of observed matter. Dark matter is described as being cold, non-baryonic, dissipationless and collisionless. This component is currently estimated to constitute about 26% of the density of the universe. The remaining 5% of the universe, according to this model, comprises all matter and energy observed as baryons and electromagnetic radiation.

nuclei was equal to the energy density of the photons; this signs the beginning of the matter dominated Universe.

At this stage, according to the ΛCDM paradigm, the density fluctuations start growing due to their self-gravity. They will mostly affect dark matter, as CDM dominates over the baryons by a large factor. The cold dark matter starts to gravitationally collapse in the overdense regions increasing their density, while the under dense regions decrease their density contrast. (Steinmetz & Navarro, 2002). The overdense regions will evolve into the dark matter halos which host galaxies.

After recombination baryons start falling into the large dark matter halos (Blumenthal et al., 1984; White & Rees, 1978; Peebles, 1982). As these halos gain mass, dark matter stays mostly on the outskirts of these proto-galaxies. It cannot dissipate as it can only interact gravitationally, and it cannot form clumps, due to its small cross-section (Bertone, Hooper & Silk, 2005). The baryons, on the other hand, can condense in gas clouds which form the seeds of galaxies (Fall & Efstathiou, 1980; Dalcanton, Spergel & Summers, 1997; Mo, Mao & White, 1998; Hatton et al., 2003). An important piece of evidence for the early appearance of galaxies was found in 2006, when the galaxy IOK-1 with an unusually high redshift of 6.96 was discovered. This corresponds to just 750 million years after the Big Bang (Iye et al., 2006). Several other very high redshift galaxies have since been found, the latest by Riechers et al. (2013).

These primordial high density clouds begin to contract, and the first stars appear within them (Komiya et al., 2009). These objects, called Population III stars, are composed almost entirely of hydrogen and helium and are very massive (between 10-100 $M_{\odot}$), implying an extremely short lifetime (Heger & Woosley, 2002). These stars rapidly burn their hydrogen and explode as supernovae, releasing heavy elements into the interstellar medium. There are hypotheses (Madau & Rees, 2001; Schneider et al., 2002) that the resulting black holes can merge to form super massive black holes (SMBHs) and quasars, but scientists are yet to find conclusive evidence of this scenario (or Population III stars themselves).

1.1.2.1 Luminosity function expectations, active galactic nuclei and supernovae

The galaxy formation conundrum is a complex one: its aim is to mathematically explain how the variety of structures in the Universe formed from a random Gaussian distribution of density fluctuations. To do so, we need to characterise the galaxies according to measurable parameters and provide estimates for their distribution in both time and space. The Schechter luminosity function (Schechter, 1976) supplies

us with these exact tools.

$$\phi(L) = \frac{\phi_\star}{L_\star}\left(\frac{L}{L_\star}\right)^{\alpha} \exp\left(\frac{L}{L_\star}\right) \tag{1.1}$$

where ϕ represents the number of galaxies per luminosity bin per megaparsec cubed, $\phi_\star$ is a normalisation factor based on the abundance of bright galaxies, and $L_\star$ is the characteristic luminosity. The value of $L_\star$ is established empirically. The characteristic luminosity is the luminosity at the point where the function goes from the exponential profile to the power law. Essentially, this function represents a parametric description of the space density of galaxies based on the luminosity yielded by observations. Unfortunately the shape of ϕ does not match the theoretical expectation from the mass function of dark matter halos as we can see in Figure 1.1.

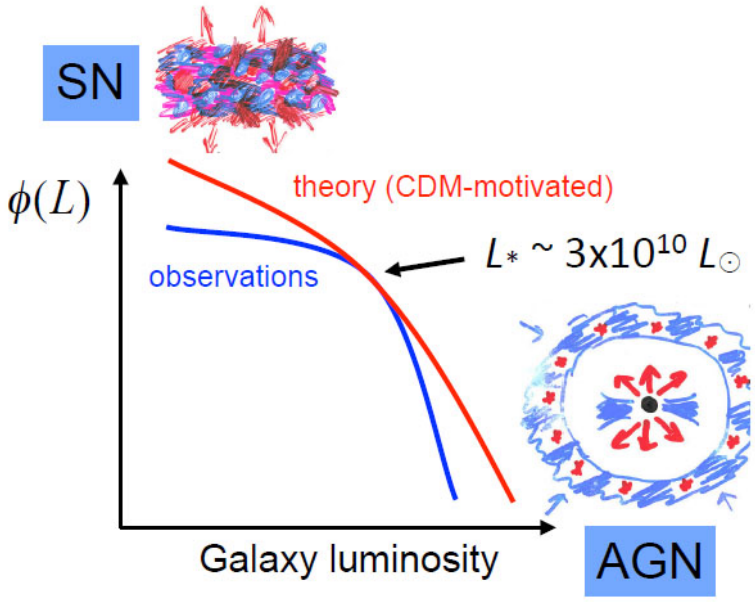


Figure 1.1: A schematic representation of the discrepancy between theory and observation of the luminosity function from Silk & Mamon (2012). The plot shows the impact of feedback on the size and number of galaxies in the Universe. There are fewer low luminosity galaxies than expected because Supernovae feedback will irreversibly disrupt the star-formation cycle for the smallest objects. At the high end luminosity, AGN feedback has the biggest impact: strong galactic winds will disperse and heat up the gas curbing the highest luminosity these objects can reach.

Feedback mechanisms may allow us to reconcile theory and observations. At the low-luminosity end, supernova explosions and the resulting winds are the main mechanism to disrupt and disperse the gas reservoir of galaxies. But when it comes

to massive galaxies, SNe cannot stop the cold stream of gas from the intergalactic medium, and we require powerful AGN feedback from a supermassive black hole. SMBHs appear to play a key role in actively regulating the growth of galaxies by limiting the total amount of matter added (Di Matteo, Springel & Hernquist, 2005). When the SMBH is accreting a large quantity of in falling material it can have a very high Eddington luminosity; this will push the residual infalling gas in kiloparsec wide winds. These winds heat the interstellar medium quenching the star-formation in the galaxy.

1.1.2.2 Early epoch, downsizing and low-mass galaxies

Within a billion years of a galaxy's formation, key structures like globular clusters, the central super-massive black hole (SMBH), and Population II stars begin to appear (Machacek, Bryan & Abel, 2001). Population II stars are relatively metal-poor objects which lead to the formation of a SN enriched interstellar medium (Venkatesan, Nath & Shull, 2006; Schaerer, 2003; Renzini, 1977). The early Universe is very turbulent, as dark matter halos interact and combine, and the gravitational pull counteracts feedback mechanisms. Conventional galaxies are born in this complex environment which has many characteristic that are yet to be fully understood.

We know that the bottom-up hierarchical formation paradigm is not linear, in the sense that the stellar population in massive galaxies can (and did) form before smaller galaxies. This phenomenon, called *downsizing*, might appear like the opposite of bottom-up, but results naturally from the hierarchical clustering process of dark-matter halos. Downsizing implies that the most massive galaxies in the Universe have formed on much shorter time scales. The less massive and younger galaxies are affected by non-trivial baryonic processes. They are also influenced by the early galaxies' effect on the intergalactic medium, which is the gas reservoir for the younger galaxies. Downsizing is not at all in contrast with the bottom-up hierarchical model. Downsizing refers principally to the formation of stellar population in galaxies and this does not necessarily coincide with the mass assembly of dark matter halos. In other words massive galaxies assemble from smaller galaxies at earlier epochs after which their star formation ceases (e.g. via feedback). So, on average their stellar populations appear older than that of smaller galaxies which continue to form stars.

The phenomenon of downsizing seems to hold across a wide range of masses. The only difference is that for low-mass galaxies the star formation was probably suppressed more quickly as previously mentioned. This is very important, because low-mass galaxies, also known as dwarf galaxies, outweigh their larger counterparts

in the Universe and are a cardinal feature of galaxy formation. Dwarf galaxies cover a large array of morphological types, star-formation rates, metallicities, and gas content. Due to the proclivity of our instruments and surveys to the Malmquist bias[5], they are still very mysterious.

1.1.2.3 Galactic structure formation: disks and spheroids

There is no one galaxy identical to another, but over the last century people have tried to categorise them with respect to their general properties. Historically galaxies have been classified according to their apparent shape which is commonly known as the Hubble sequence (Hubble, 1926; Sandage, Sandage & Kristian, 1975). This morphological classification scheme divides the galaxies into four classes based on their appearance: spirals (late-type), lenticulars, ellipticals (early-type) and irregular (Figure 1.2). Even though it is very useful, the Hubble scheme is far from perfect. The distinction between two close Hubble types is often completely arbitrary: physical structures are often at odds with each other (a small bulge does not necessarily mean a wider spiral) and the Hubble sequence breaks down at high redshifts, where most of the rapidly evolving faint blue galaxies are "morphologically peculiar" (Bunker et al., 2000; Papovich et al., 2005; Kriek et al., 2009). Still, even though it is only indirectly related to measurable physical quantities, it is the most commonly used, and its classes are important because morphological differences are related to different evolutionary paths. Spiral galaxies are disk-shaped conglomerates with dusty, curving arms containing stars, gas and dust, and a central concentration of stars known as the bulge. Young, hot blue stars are common in these galaxies as they are considered gas rich. Spirals form from the original protogalaxies.

A collapsing system of dark matter and gas has a certain amount of angular momentum due to tidal torques from inhomogeneities in the primordial matter distribution (Hoyle, 1949; Barnes & Efstathiou, 1987; Padmanabhan, 1993). To form a galaxy the gas needs to cool down. It does that by radiating energy and collapsing in the potential well. Angular momentum cannot be radiated away and is conserved. According to the galaxy formation paradigm, the angular momentum of a protogalaxy is the factor that regulates its growth. When it reaches a certain size, the angular momentum will be sufficient to balance the pull of the gravitational potential and it will stop contracting. This picture is fairly in agreement with the galaxies we actually observe (Fall & Efstathiou, 1980; Mo, Mao & White, 1998).

[5]The Malmquist Bias is the selection bias of observational astronomy. Luminous objects are over-represented in magnitude-limited surveys.

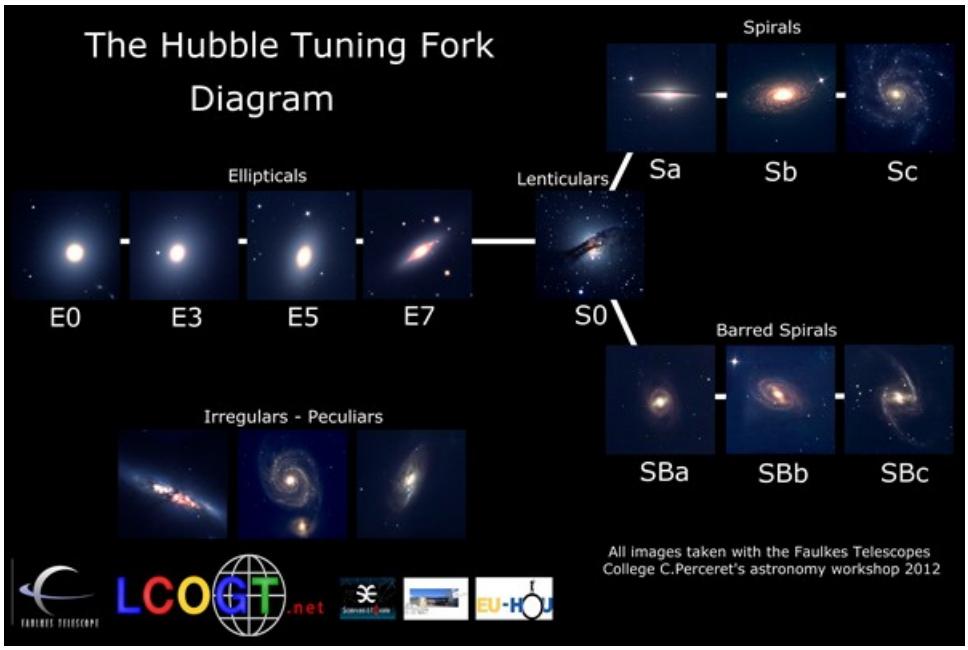


Figure 1.2: The Hubble classification scheme or Hubble tuning fork (from the College Christiane Perceret's astronomy workshop 2012). Galaxies are divided into irregulars, lenticulars, spirals, and ellipticals. Spirals are then divided into two main subclasses by the presence of a central bar. Both barred and regular spirals have an ulterior division depending on the tightness of their spiral arms. Elliptical galaxies are, instead, assigned a number depending on their ellipticity (i.e. an E0 is very circular, an E1 is less so, etc).

When the angular momentum and the accretion are balanced, the gas and dust start accumulating around the central bulge, settling in what will become the galactic disk (Noguchi, 1999) and undergoing a major burst of star formation (Verma et al., 2007).

Galaxies will continue to absorb in-falling material from high velocity passing by clouds and dwarf galaxies in the neighbourhood. Acquiring more and more gas (mostly hydrogen and helium) results in the re-ignition of the life/death cycle and the production of heavier elements through supernovae explosions (Foster & Boss, 1996; Larson, 2003). Eventually the star formation rate slows down to a small fraction of the total stellar mass of the galaxy, leaving the galaxy to age, and become progressively redder. There are two main reasons for this: the first reason is that the gas supply is decreasing as the Universe ages. The second is that feedback processes are continually ejecting gas out of the system. Over time both these reasons cause the gas supply to decrease.



Figure 1.3:]
The Antennae Galaxies (NGC 4038 and 4039) photographed by Hubble Space Telescope (16 October 2006)

Ellipticals, as the name suggest, have an approximately ellipsoidal shape and a smooth, nearly featureless brightness profile. Elliptical galaxies are believed to form after strong interactions (sometimes several) between galaxies (Mihos & Hernquist,

1996a; Bender, 1996), which is a highly gas and time consuming event. For this reason, they are generally gas poor, and they have an old, red stellar population.

1.2 Morphologies in flux: the role of mergers in galaxy evolution

Galaxy mergers are violent interactions between galaxies. They occur when two (or more) galaxies collide. This interaction can radically alter the overall structure of the progenitors due to the tidal forces between the galaxies and the friction between the gas and dust moved around in the process. It is important to note that the way the two cores spiral into the common centre of mass also has effects on the final configuration of the system. Because of the vast distances between stars and the long timescale of mergers, they do not involve direct star or star cluster collisions. The exact effects of such mergers depend on a wide variety of parameters such as collision angles, speeds, and relative size/composition.

If two galaxies of approximately the same size collide at suitably wide angles and relatively low speeds it is called *major merging* and the progenitors' morphologies are irreversibly altered. In the resulting galaxy most of the dust and gas will disperse through a variety of feedback mechanisms (often including active galactic nuclei). Galaxies approaching at high speed will only perturb each other, creating irregular objects known as *fly-by*.

If one of the galaxies is significantly larger than the other, the larger will often 'eat' the smaller, absorbing most of its gas and stars, while the larger one remains mostly undisturbed. This is often referred to as 'galactic cannibalism' or *minor merging*, where the mass ratio between the two galaxies is less than 1:3. The Milky Way is currently absorbing smaller galaxies such as the Canis Major Dwarf Galaxy, and possibly the Magellanic Clouds. The Virgo Stellar Stream (VSS) is thought to be the remains of a dwarf galaxy that has been mostly merged with our home Galaxy. The gas and dust stolen by the larger galaxy from the smaller one during a minor merger are believed to induce star formation (Kaviraj et al., 2009).

We mentioned how ellipticals evolve from spirals during mergers. It is important to note that galaxy mergers were a very common phenomenon in the early Universe, and the majority of galaxies were peculiar in their morphology (Bunker et al., 2000; Papovich et al., 2005; Kriek et al., 2009). The tidal forces between two galaxies will induce gravitational stripping of interstellar gas and dust that makes up spiral arms, producing a long train of stars known as a tidal tail (Khochfar & Silk, 2009).

A beautiful example of this formation can be seen in the Antennae Galaxies (Figure 1.3).

Galaxy merging is thought to be an important driver of the evolution of the visible Universe (e.g. Steinmetz & Navarro, 2002). Mergers are believed to drive strong star formation episodes (Mihos & Hernquist, 1996b), they may contribute to the growth of supermassive black holes (Cox et al., 2006a) and they are expected to produce morphological transformations (Toomre, 1977). Major mergers between equal mass progenitors are thought to lead to the formation of early-type galaxies, largely independent of the original morphologies of the progenitors (e.g. White & Frenk, 1991; Barnes, 1992; Cole et al., 2000). Repeated minor mergers appear to be able to produce the same effect (e.g. Bournaud, Jog & Combes, 2007; Naab, Johansson & Ostriker, 2009). Observational evidence for the role of mergers in creating early-type galaxies is suggested by the presence, in many ellipticals, of morphological disturbances such as shells, ripples and tidal tails (e.g. van Dokkum, 2005; Ferreras et al., 2009; Kaviraj, 2010) and recent merger-driven star formation (Kaviraj et al., 2008, 2009, 2011). A better understanding of mergers will give us better insight into the evolutionary histories of elliptical galaxies.

We have seen that a key feature of the ΛCDM cosmogony is a hierarchical bottom-up formation paradigm, with smaller bodies accreting to form progressively larger ones (White & Rees, 1978; Searle & Zinn, 1978). More evidence that galaxy evolution is really bottom-up comes from the connection between merger events and star-formation histories. As time passes, mergers of two systems of equal size become less common due to the shape of the cosmic web. By z=0 density peaks in the Universe (which are essentially where the massive galaxies lie) are quite far apart, and consequentially, the collision cross section is small. Large-scale interactions have become rarer, therefore most bright galaxies have remained fundamentally unchanged for the last few billion years. The net rate of star formation peaked approximately ten billion years ago (Heavens et al., 2004; Panter et al., 2007).

1.3 Models and simulations: breakthroughs and limitations of computational astronomy

Mergers can easily explain the hierarchical build-up of galaxies, but some properties of both early-type and late-type galaxies (percentage of dust, star formation, general structure, nuclear activity) need a more detailed theoretical description if we want to use the theory to make predictions in our observations. The theoretical work is

based on the concept of merging trees, a schematic illustration of the merger history and growth of the dark matter halo of an object (see Figure 1.4). The mathematical

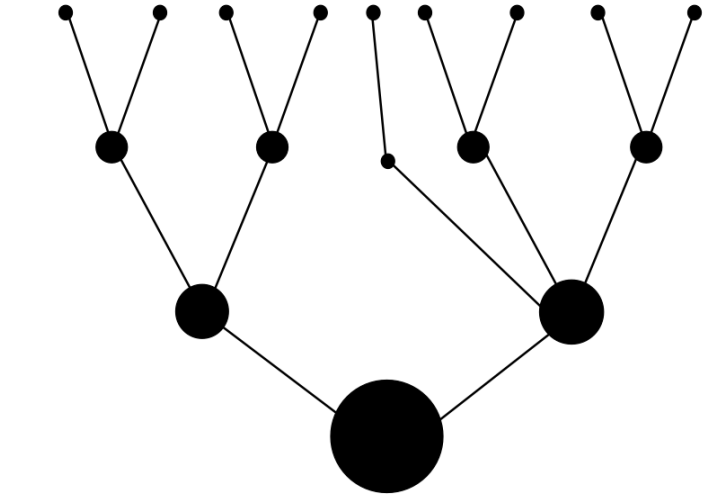


Figure 1.4: The growth of the dark matter halo can be traced by using merger trees. In this figure the bottom node represent the halo at redshift zero, while the seven top nodes are primordial halos. The time line goes from top to bottom.

interpretation of merger trees is given by the extended Press-Schechter formalism (Press & Schechter, 1974), which is a formal estimation of the number of object more massive than some specific mass M within a given volume of the Universe. Thanks to this formula it has been possible to lay the basis for strict model construction.

1.3.1 N-body simulations

The first approach to construct a simulated Universe was made in the 1960s with the development of N-body simulations (von Hoerner, 1963). Computer programs were constructed for the purpose of simulating star-clusters and galaxies (and eventually galaxy clusters). They started with the basic but difficult task of predicting the dynamical evolution of a system of N gravitationally interacting objects. This is known as the N-body problem. The dynamical evolution is extracted by numerically solving the 6N differential equations that define the motion for each member of the system (Hernquist, 1988; Carlberg, 1988; Bertschinger, 1998; Springel et al., 2005; Tweed et al., 2009).

These simulations are very powerful in giving an accurate description of a system with a relatively small number of objects, but when it comes to galactic or cosmological simulation we start to encounter problems. To simulate a galaxy correctly, it is necessary to take into account every star, gas cloud, the supermassive

black hole, etc. which leads to a dynamical system of billions of objects. This implies that there are N^2 particle interactions that need to be computed. Directly solving the equations of such a system is too computationally expensive to be pursued.

Simplifications were implemented to refine and ease the workload of these simulations. There are two main methods and they both discretise the space of the simulation. In the *tree method* (Barnes & Hut, 1986) space is divide in cubes with individual interactions only happening between adjacent cubes and a generic total interaction from particles away from our selected cube. The *Particle-Particle Particle-Mesh method*, discretise the space as a grid (mesh) of density values in addition to the straight particle-particle sum between nearby particles (Bouchet & Kandrup, 1985). For a gravitational potential, this is solved using a Fourier transform of the gravitational Poisson equation

The main advantage of an N-body simulation is that the results are robust, accurate and completely general. The drawbacks, even taking into account ways to reduce computational time, are lack of finer details, oversimplification of systems and rigidity in your simulation. Another drawback of pure N-body models is that they do not include hydrodynamics. The user cannot tweak the equations to make the simulation more lifelike (Barnes & Hut, 1989; Goodman, Heggie & Hut, 1993). These disadvantages become very important when we start dealing with the intricacy of a galaxy merger. It is clear that a direct N-body simulation of the merger trees is an evidently limited construction of a very complex problem, so scientists have been trying to work with a more flexible approach: the semi-analytical models (Kauffmann, White & Guiderdoni, 1993; Cole et al., 2000; Somerville, Primack & Faber, 2001) .

1.3.2 Semi-analytic models (SAMs)

Semi-analytic modeling is a modular technique to improve our knowledge of galaxy formation. By approaching the problem with the most detailed approximation of galaxy physics, these models can predict a wide array of properties. Starting from the descriptions of key physical ingredients, it is possible to extract information for the galaxy population at any redshift. The modularity facilitates the expansion and the exploration of alternative hypotheses, and allows to refine the simulations when new physics or better theoretical explanations come out. Semi-analytic models can be used to push the resolution of standard simulations forward.

These models have the WMAP cosmology as the initial condition (Spergel et al., 2007; Dunkley et al., 2009) and the distribution and morphology of low redshift

galaxies as the final condition. The constraints are given by the cosmological parameters $H_0, \Omega_0, \Omega_\Lambda, \Omega_m, \Omega_B$, the shape and the normalisation of the power spectrum of primordial linear fluctuations. SAMs also necessitate the introduction of free parameters to take into account issue that can only be solved in a phenomenological way. Among these issues we find shock heating and radiative cooling (Kereš et al., 2009), photoionization suppression (Efstathiou, 1992; Shapiro, Giroux & Babul, 1994; Somerville, 2002), star formation episodes (Hopkins, Quataert & Murray, 2012), supernovae heating and SN-driven winds (Hopkins, Quataert & Murray, 2012), AGN accretion and feedback (Bower et al., 2006), chemical evolution, stellar populations, and dust. All these physical processes are described by *ad hoc* analytic formulae which are then implemented in the model.

1.3.2.1 Limitations of SAMs

Taking into account the physical processes to be solved analytically, we end up with models involving a large number of obvious free parameters in addition to theoretical assumptions which have been buried in their implementation. SAMs are very successful in reproducing the general characteristic of the evolving galaxy population. The unavoidable complexity of their structure implies an extensive degree of uncertainty as to the uniqueness of any particular implementation. Even accepting that a perfect agreement with observations is a scientific impossibility, we find the outputs of SAMs cannot be used to produce realistic synthetic galaxies. Testing the observations with the simulated data is of paramount importance to asses the validity and the extent of our theoretical models. Most simulations lack a deep analysis of baryons and radiation, and it is necessary for a simulated model to be able to characterise the internal processes and not merely predict the right results for the parameters being simulated.

A solution to some of these issues has been brought forward by Hatton et al. (2003), where a hybrid N-body/SAM approach was designed and tested against observations. The new models are in good agreement with the observations of a variety of properties from morphology to luminosity correlations, disk sizes and fundamental planes.

The direction in which these studies lead points to confident predictions for a full set of observational data. While the exponential growth of computational power has aided our aim of detailed simulations of galaxy mergers, we are still far away from an exhaustive forecast of a galaxy's past.

1.4 The role of observations

Although simulations are not perfect their contribution to modern astronomy is undeniable. Since White (1978) and Aarseth & Fall (1980), simulating galaxy mergers have become a necessity: mergers happen on such long timescales that only by being able to see a fast forward version can we understand and predict the various phenomena that shape a galaxy. Simulations have tried to cover all the possible bases necessary to have a coherent model theory of galaxy evolution, from specific parameter like merger rates (Lacey & Cole, 1994) to the testing of the full hierarchical paradigm (Cole et al., 2000), from the impact of major merging (Mihos & Hernquist, 1994b; Springel & Hernquist, 2005; Mihos & Hernquist, 1996b) to the consequences of minor mergers (Mihos & Hernquist, 1994a; Naab, Johansson & Ostriker, 2009).

But what is the role of observations in the world of computational astronomy? Even if the time of an overflow of new discoveries is behind us, but observation cannot be relegated to the mere fact-checking of modelling results. Looking into the cosmos is a fundamental component of astronomy and its impact is further reaching than testing model A versus model B. Simulations are limited by the power of our machines and by the intrinsic fallacies of our theories. Only by a insightful characterisation of galaxy properties across time and space will we be able to have a complete understanding of galaxy evolution. This characterisation can only come from a large and open study of galaxy properties across a wide range of wavelengths so that models can take into account all the peculiarities of the ever-changing galaxies.

Chapter 2

The tools for observing galaxy evolution

To obtain clear observational evidence on various processes and stages of galaxy evolution, we need to employ large imaging surveys and use the most appropriate techniques to extract relevant parameters. Throughout this chapter, we will examine the surveys, telescopes and techniques used in this project. In Section 2.1 we explore the Sloan Digital Sky Survey. In Section 2.2 we discuss the GALEX and IRAS surveys. We discuss emission line diagnostics in Section 2.3, and in Section 2.4, we look at environment estimation. In Section 2.5, we discuss Galaxy Zoo and the Galaxy Zoo merger catalogue. Finally, the goal of this project is articulated in Section 2.6.

2.1 The Sloan Digital Sky Survey

Galaxy merging is an incredibly slow process on human timescales, so the best observational approach is to collect a large array of observed mergers, compose an extensive picture of the process, and use commonalities to build up a detailed timeline. The main requirement for this kind of analysis is a vast data set. The most comprehensive catalogue of this type is the *Sloan Digital Sky Survey* (SDSS), comprising more than one million galaxies in its spectroscopic sample (York et al., 2000). The SDSS is a major imaging and spectroscopic redshift survey. SDSS uses a dedicated 2.5 metre f/5 modified Ritchey-Chrétien wide-field altitude-azimuth telescope in New Mexico. The telescope achieves a wide (3°) distortion free field by using a large secondary mirror and two corrector lenses. It is equipped with two special-purpose instruments. The first is an optical camera that can image 1.5 square degrees of sky at a time; it has mapped, since the year 2000, over 35% of the

sky. The telescope's camera is made up of thirty CCD chips each with an individual image field size of 2048x2048 pixels, arranged in five rows of six chips. The telescope scans the sky in great circles at the sidereal rate. The full camera has approximately 120 Megapixels. The pixel size is of 24μm, or 0.396" on the sky.

The second instrument is a pair of optical fibre spectrographs that measures the spectra of (and distances to) more than 600 galaxies and quasars in a single observation. To be certain that the fibres do not flex during exposure, they are permanently attached to the image rotator. Data from the imaging survey are explored to consistently pick a representative sample of every class of objects. Once an object is selected for spectroscopy, a hole of its position (with respect to a field) is drilled in an aluminium plate. Every field in which spectra are to be acquired requires a unique plate. A single fibre is then positioned in the hole and fed to the spectrograph. The photometry and the spectroscopy produce about 200 GB of data nightly; to deal with this enormous information flow, a custom-designed set of software pipelines is employed. SDSS has consistent astrometry over a wide field, with no tracking error issues, as the telescope was purposely built to use the drift technique. This keeps the telescope fixed and makes use of the Earth's rotation to record small strips of the sky, as the image in the focal plane drifts along the CCD chip. The spectroscopic limit for the survey is $m_{AB} = 17.6$.

SDSS takes images using a photometric system of five filters (u, g, r, i and z), with effective wavelengths of 355.1, 468.6, 616.5, 748.1 and 893.1 nm respectively. The filters are arranged on the five rows of the camera chips (placed in the order r, i, u, z, g) with a 5σ detection limit for point sources in 1" seeing at 22.3, 23.3, 23.1, 22.3, 20.8 respectively. The camera is kept at a temperature of 190 K using liquid nitrogen. The time for passage over the entire photometric array is of 5.7 minutes, with an integration time per filter of 54.1 seconds. Calibration is carried out using the United States Naval Observatory 1 metre telescope and their network of established standard stars. The survey collects photometric observations of around 500 million objects and spectra for more than 1 million objects. Both photometric and spectroscopic observation can be used to extract various parameters of astronomical importance, as we will see in the following sections. We will be using data from the first eight years of operations (SDSS-I, 2000-2005; SDSS-II, 2005-2008). In this timeframe, SDSS obtained deep images of more than a quarter of the sky in five optical bandpasses, and created 3-dimensional maps containing more than 930,000 galaxies and 120,000 quasars.

To obtain unabridged knowledge of these objects, we need to look beyond optical wavelengths; only by composing an exhaustive compendium of their properties, can

we understand the full impact of galaxy evolution.

2.2 GALEX and IRAS

Optical light is only a fraction of the emission we can collect from astrophysical objects, and integrating optical and non-optical quantities is increasingly important for constraining the true properties of galaxies. The importance of expanding our wavelength range cannot be overstated, and to complement the data from SDSS, we employ the data available from the space telescopes GALEX and IRAS.

The Galaxy Evolution Explorer (GALEX) is an orbiting space telescope which observes the Universe in ultraviolet light. GALEX employs a 50 centimetre modified Ritchey-Chrétien f/6 telescope with four specific channels: far-UV (FUV) and near-UV (NUV) imaging, and FUV and NUV spectroscopy (Martin et al., 2005). The primary mirror is coated in Aluminium-Magnesium Fluoride and has a 3 metre focal length, with a field of view of 1.2°. An optics wheel is used to set an opaque position, a Calcium Fluoride imaging window or a Calcium Fluoride grating prism (grism) in the beam. The spectroscopic observation of the instrument is secured by using the multiple dispersion angles provided by the grism. This technique can be employed to remove overlap effects in the spectrum. Employing a dichroic beam splitter allows simultaneous broad-band UV photometry in two passbands: NUV $(1750 - 2750)$ Å and FUV $(1350 - 1750)$ Å, with effective wavelengths of 2267 Å and 1516 Å respectively. Thanks to its aspherical surfaces, the beam splitter also acts as an aberration corrector. The NUV detector has a red blocking fold mirror responsible for a sharp long wavelength cutoff. This filter reduces contamination from the optical and zodiacal light backgrounds. A blue edge filter, to block the airglow of the Lyα, OI[1304 Å] and OI[1356 Å] lines, is placed on the FUV detector. GALEX was launched in 2003 for a 29 month mission, which was subsequently extended.

GALEX's scientific goal is to expand our understanding of galaxy evolution. By using UV light, one can delve into how galaxies, the basic structures of our universe, evolve and change across 10 billion years of cosmic history. Additionally, GALEX observations are burrowing into causes of star formation during the cosmic dawn, when most of the stars and elements we see today originated. GALEX's goal has been achieved by completing five surveys. The main one is the All-Sky survey, run to a sensitivity of $m_{AB} \simeq 20.5$, taking ten 100 second exposures of 1° fields. There can be up to 1000 objects in a 1° field. The medium imaging survey covers 1000 square degrees and has an extensive overlap with SDSS. With a magnitude

limit of $m_{AB} \simeq 23$ and very accurately matched SDSS photometry, this survey is fundamental in studying the star-formation histories of galaxies. There are three other notable surveys produced by GALEX, a deep and ultra-deep imaging survey ($m_{AB} \simeq 26$) in specific low extinction, low zodiacal and diffuse galactic background regions; a nearby galaxy survey aiming to studying the UV properties of some of the closest 200 galaxies to the Milky Way; and finally, an array of spectroscopic surveys: a wide-field which covers the full deep-imaging surgery; a medium-deep survey that follows up on the central 8 square degrees; and a deep spectroscopy survey that extensively covers the central 2 square degrees. UV observations are useful because the UV is dominated by the hot, young and massive main sequence stars. The UV is therefore a good tracer of recent and ongoing star formation. It is almost an order of magnitude more sensitive to recent star formation than the traditional optical filters that are available from SDSS.

The Infrared Astronomical Satellite (IRAS) observed the Sky from the other end of the optical spectrum. Launched in 1983, IRAS was the first observatory to perform an all-sky survey at 12, 25, 60, and 100 micron wavelengths (Neugebauer et al., 1984a). It had a Ritchey-Chrétien f/9.6 telescope with a focal length of 5.5 metres and an aperture of 0.57 metres. The mirrors were made of beryllium and cooled to approximately 4 K. The focal plane accommodated the survey detectors, visible star sensors for position reconstruction, a low resolution spectrometer and a chopped photometric channel. The focal plane assembly was located at the Cassegrain focus of the telescope and was cooled to about 3 K using superfluid helium. The survey array was composed of 62 rectangular infrared detectors, organised in such a way that any real point source would be seen by at least two detectors in each wavelength band. The Low Resolution Spectrometer was a slitless spectrometer sensitive from 7.5 to 23 μm with a resolving power of about 20. Due to lower-than expected temperature in the focal plane, the chopped photometric channel's data is very difficult to use.

IRAS was in a sun-synchronous near-polar (99 degree) orbit, which precessed by about a degree each day. The full Sky was divided into 12 *lunes* bounded by ecliptic meridians 30 degrees apart. The satellite scanned each lune in overlapping strips, with the end result of having 96% of the sky covered by at least two hours-confirming scans and 66% was covered by an extra observation which was performed following a different methodology. For the same source, every hour-confirming scan was taken several months apart, and may be affected by foreground variation and different detector response.

IRAS discovered about 350,000 sources; not all of them have been identified. Its

resolution ranged from 30 arcseconds at wavelength 12 micrometers to 2 arcminutes at wavelength 100 micrometers. IRAS detected a wide variety of sources, such as dust rings around stars, asteroids, comets, the infrared cirrus (cloud-like filaments of warm dust) as well as a significant number of extragalactic objects. For example, about 20% of the sources detected are starburst galaxies in the middle of an intense episode of star-formation. IRAS was designed to catalogue fixed sources, so it scanned the same region of sky several times in its ten months of activity. Its life was constrained by the limited amount of coolant that could be included in the satellite.

Similarly to UV observations, using IR data greatly improves our analysis. UV and optical light is often reprocessed into IR by obscuring gas and dust; hence having access to the IR enables you to balance the energy budget of the objects one is studying. This is necessary when trying to extract a complete picture of galaxy formation

2.3 The different ways to estimate the Star-Formation rate of a galaxy

It might be useful to visualise how the different star-formation rate estimators (from Kennicutt (1998)) relate to each other. To do so we compose a sub-sample of the Imperial Infrared Faint Source Catalogue (Wang & Rowan-Robinson, 2009) made of objects with an optical spectrum and GALEX detection. The value we get from the luminosity in the far infrared is compared with the other tracers, namely $H\alpha$ and UV monochromatic luminosity. The far infrared luminosity, the $H\alpha$ line and the monochromatic UV should all be good tracers of star-formations because they, directly or indirectly, are hugely enhanced by the presence of a very young stellar population as mentioned in the previous section. We use equations

$$SFR_{FIR}(\mathrm{M_\odot yr^{-1}}) = 4.5 \times 10^{-44} \mathrm{L}_{FIR}(\mathrm{ergs\ s^{-1}}), \tag{2.1}$$

and

$$SFR_{H\alpha}(\mathrm{M_\odot yr^{-1}}) = 7.9 \times 10^{-42} \mathrm{L}_{H\alpha}(\mathrm{ergs\ s^{-1}}), \tag{2.2}$$

from Kennicutt (1998) to calculate the star-formation rate from FIR and $H\alpha$, respectively. We also use the following equation still from Kennicutt (1998) to calculate

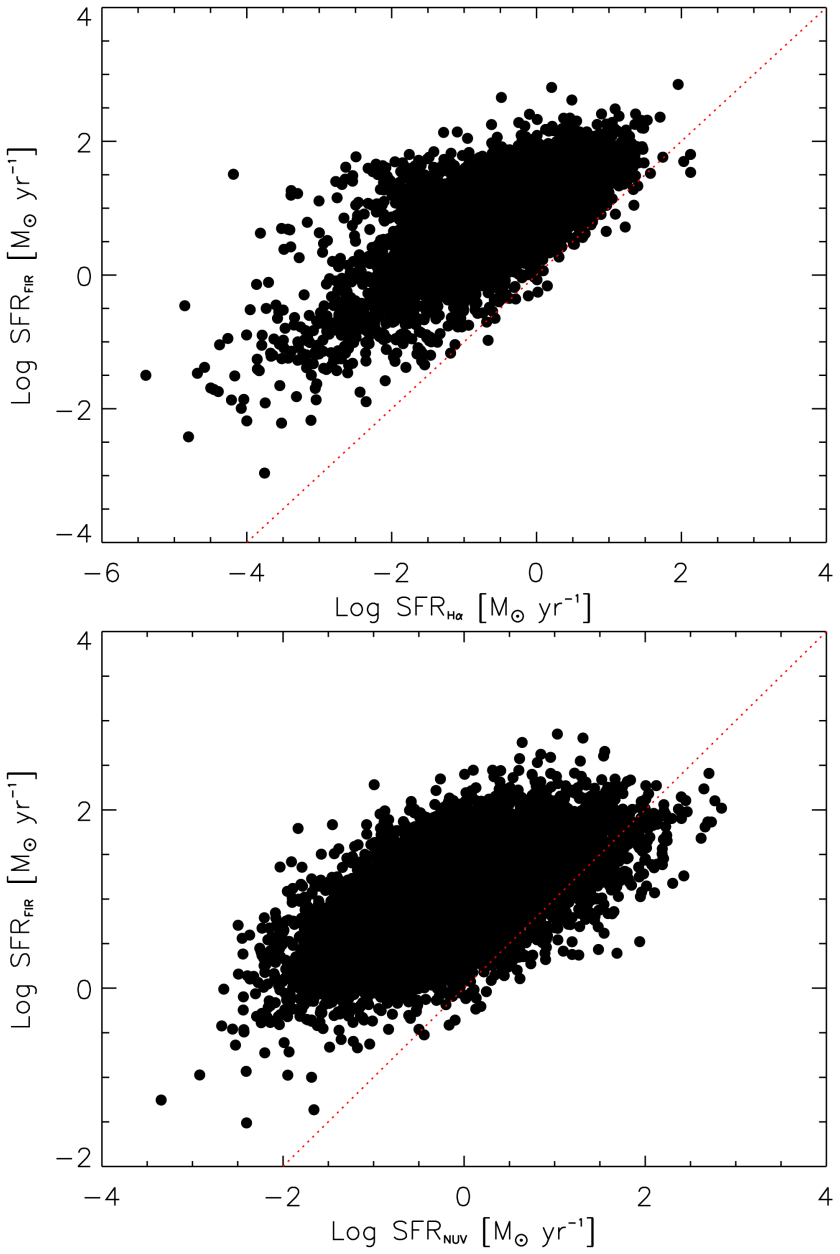


Figure 2.1: TOP: SFR_{FIR} vs $SFR_{H\alpha}$. We see that $H\alpha$ follows the right trend but underestimates the SFR (in some cases by several orders of magnitude). The most likely cause for this is the dependence of the parameter on extinction. BOTTOM: SFR_{FIR} vs SFR_{UV}. We see the limitation of the UV as a tracer for IR-bright galaxies.

the SFR from the ultraviolet:

$$SFR_{UV}(\mathrm{M_\odot yr^{-1}}) = 1.4 \times 10^{-28} \mathrm{L}_\nu(\mathrm{ergs\ s^{-1}\ Hz^{-1}}), \tag{2.3}$$

In Figure 2.1, we plot the $SFR_{H\alpha}$ and the SFR_{UV} versus the SFR_{FIR}. In the top plot we see that, while the $H\alpha$ follows the general trend of the distribution, it underestimates the SFR of our galaxies. This could be due to an array of reasons going from uncertainties in the galactic extinction to the initial mass function, to the assumption that all massive star formation is traced by ionising gas. In the bottom panel we see that UV is an even worse tracer when it comes to star-formation in infrared bright galaxies; this is expected. The UV tracer is much more affected by extinction than Hα; it could also depend on the IMF shape, since it mostly traces the young massive star population ($\geq 5M_\odot$). It is important to note that equation 2.3 needs a nearly-flat spectrum as a working assumption which might not necessarily be the case for our galaxies. Both the extinction and the deviation from a flat UV spectrum contribute in making UV light unreliable in tracing SFR for our objects. The galaxies plotted in Figure 2.1 are a representative sample of the galaxies we are going to encounter in this thesis, and contains both relaxed galaxies and a significant number of peculiar and interactive galaxies. As we are planning to study quickly changing dynamic objects that can have a considerable amount of dust, we will consider the far-infrared the correct estimator although this is just an approximation as not every galaxy that we will encounter will be dust rich.

2.4 Emission line diagnostics

The vast majority of galaxies we might study have narrow emission lines (narrow compared to the Hydrogen Lines) from ionisation of the interstellar medium (ISM). These narrow lines are from so called forbidden transitions. Permitted lines are those which occur very rapidly (e.g. the lifetime of Balmer Lines is $\sim 10^{-8}s$), while forbidden lines are long-lived or metastable states, with lifetimes of $\sim 10^4 s$. The somewhat misleading name refers to the fact that their emissions happen only in very low densities (impossible to recreate in a laboratory) in order for the electrons to survive in higher orbits without collisions for enough time to emit these rare wavelengths. These lines are commonly found in astrophysical plasma and the most common ones belong to nitrogen ([N II] at 654.8 and 658.4 nm), sulphur ([S II] at 671.6 and 673.1 nm), and oxygen ([O II] at 372.7 nm, and [O III] at 495.9 and 500.7 nm).

Specific emission line ratios can be used as powerful probes of the condition of the ISM; emission line ratios sample different regimes of temperature, density, and energy and this enables us to investigate the processes that are responsible for the ionisation (e.g the central AGN or star formation) and their relative proportions. Photons emitted by AGN are more energetic than those emitted by young massive stars in the HII regions. This implies that the collisionally excited lines will be brighter than the recombination lines one would find if ionisation was caused by stars alone. Using spectroscopy it is possible to highlight this effect. The technique to use the forbidden lines to learn more about galaxies was developed by Baldwin, Phillips & Terlevich (1981) (hence the name BPT) and subsequently refined by others (Veilleux & Osterbrock (1987); Kauffmann et al. (2003); Kewley et al. (2006) to mention a few). But while this diagnostic is powerful, it has its limits: no detailed description of the central engine or the star-formation rate can be taken from it.

Throughout this thesis the emission line ratios are computed using the public GANDALF code (Sarzi et al., 2006). GANDALF is a simultaneous emission and absorption lines fitting algorithm, designed to separate the relative contribution of the stellar continuum and nebular emission in the spectra of nearby galaxies, while measuring the gas emission and kinematics. This method has been used to derive ionised-gas maps and kinematics of the SAURON sample (Sarzi et al., 2006).

We use four optical emission line ratios [OIII]/Hβ, [NII]/Hα, [SII]/Hα, and [OI]/Hα to separate star-forming regions, Seyfert nuclei and Low-Ionisation Nuclear Emitting regions (LINERs). We assign these classes to all galaxies with $S/N > 3$ in all the Hα, Hβ, [OIII], [SII], [OI] and [NII] lines. Those galaxies which do not fall under this category ($S/N < 3$) are classified as quiescent. Every sample we classify is thus divided into:

- (0) Quiescent
- (1) Star-forming (SF)
- (2) Mixed SF/AGN
- (3) AGN (Seyfert/LINER)

Examples of BPT diagrams can be seen in Figure 2.2. We see that, depending on the strength and the type of the lines, the position of an object on the plot will change. This permits us to divide the parameter space into areas where the different types of galaxies reside, and are easily identified. The different areas are defined by particular equations. The Kauffmann et al. (2003) prescription is the divider between the SF

objects and the AGN-dominated galaxies. It takes the form of:

$$\log\left(\frac{[OIII]}{H\beta}\right) = \frac{0.6}{\log\left(\frac{[NII]}{H\alpha}\right) - 0.05} + 1.3 \tag{2.4}$$

This line is the dashed blue line in the left plot in Figure 2.2. It identifies the upper limit for emission line measurement for pure SF galaxies. The red line, on the other hand, is the upper limit for the most intense starburst and is defined as:

$$\log\left(\frac{[OIII]}{H\beta}\right) = \frac{0.61}{\log\left(\frac{[NII]}{H\alpha}\right) - 0.47} + 1.19 \tag{2.5}$$

Everything to the right and above this line is identified as a pure AGN hosting galaxy (Kewley et al., 2006). The above equation and the analogue ones for the [SII] and [OI] plots, along with divisions for the Seyferts, LINERs, and Composite HII-AGN types (solid blue lines), were developed by Kewley et al. (2006). The [NII] plot is, when possible, the preferable one to construct. The heating of an AGN significantly increases the [NII] line creating a clear demarkation between the AGN dominated galaxies and the star-forming ones, as it can be seen in Figure 2.2.

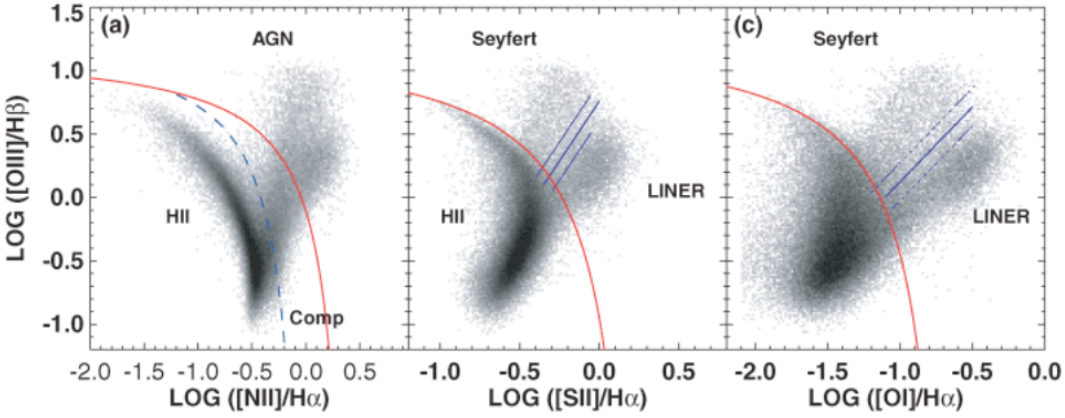


Figure 2.2: An example of 3 different BPT diagrams from the Kewley et al. (2006) paper. The red solid line represents the extreme starburst classification (following equation 2.5 for the left plot), the Kauffmann et al. (2003) pure star-formation line (blue dashed, following equation 2.6 for the [NII] plot), and Seyfert-LINER line (blue solid) are used to separate galaxies into HII region-like, Seyferts, LINERs, and Composite HII-AGN types.

2.5 Environment estimation: Number density versus Mass

An important parameter that drives the evolution of galaxies is their local environment. In this work we will look at two environment estimators. The first estimator looks for the number density of neighbours around our target galaxy. This is quantified by $\rho_g(ra, dec, z, \sigma)$ (Schawinski et al., 2007a), which is defined as a weighted sum of all the neighbours (from the SDSS DR6) within the ellipse

$$\left(\frac{r_a}{3\sigma}\right)^2 + \left(\frac{r_z}{3c_z\sigma}\right)^2 \leq 1 \tag{2.6}$$

where r_a is the distance on the sky in Mpc to each surrounding galaxy, r_z is the distance along the line-of-sight in Mpc to each surrounding galaxy, and σ is an arbitrary radius (we will use $\sigma = 2$ Mpc across the thesis). The environment parameter is defined as:

$$\rho_g = \frac{f(mass)}{\sqrt{2\pi}\sigma} \exp\left[-\frac{1}{2}\left(\frac{r_a^2}{\sigma^2} + \frac{r_z^2}{c_z^2\sigma^2}\right)\right] \tag{2.7}$$

where $f(mass)$ is a linear function of the absolute r band so that brighter galaxies count more and the parameter c_z scales the value of σ along the line of sight to compensate for the finger of god effect (see Schawinski et al. (2007a) for more details)[1], such that ρ_g increases the closer a neighbour is to the selected galaxy. The two merging galaxies are considered a single system, otherwise the calculations will be incorrect (as ρ_g is sensitive to nearby objects).

The range of ρ_g can be divided to get an intuitive idea of what it would correspond to. Obviously, a galaxy with the lowest value $\rho_g = 0$ has no neighbours in a σ radius. Values $0<\rho_g<0.1$ are consistent with a field environment. Galaxies with a $0.1<\rho_g<1$, are in intermediate environments, while anything larger is a cluster (Schawinski et al., 2007a). To get an empirical idea we should point out that if we pick a galaxy with $\rho_g = 1$ we would have approximately ten other randomly distributed L* galaxies in a sphere of radius $\sigma = 3$ Mpc.

The second estimator is the Yang et al. (2007) group mass catalogue. In this case, the environment parameter is the (dark matter) halo mass of the galaxy. This is estimated from the characteristic luminosity of the components. This analysis

[1]The finger of god is an effect in observational cosmology that causes clusters of galaxies to be elongated in redshift space, with an axis of elongation pointed towards the observer. It is caused by a Doppler shift associated with the peculiar velocities of galaxies in a cluster.

begins with estimation of the luminosity of the group:

$$L_{group} = \sum_i \frac{L_i}{f_c(L_i)} \tag{2.8}$$

where L_i is the luminosity of each galaxy in the group and f_c is the luminosity-dependent incompleteness of the survey. This can be expanded to include the total luminosity of the group using:

$$L_{total} = L_{group} \frac{\int_0^\infty L\phi(L)dL}{\int_{L_{lim}}^\infty L\phi(L)dL} \tag{2.9}$$

where $\phi(L)$ is the luminosity function as defined in Equation 1.1 and L_{lim} is the minimum luminosity we are able to observe at the redshift of the group. This set of equations is called the *Conditional Luminosity Function* formalism, and was developed in Yang et al. (2005); in the same paper it was shown that the mass of a dark matter halo M_h associated with a group is tightly correlated with the total luminosity of all member galaxies down to some luminosity. Using the semi-analytic models of Kang et al. (2005) they were able to estimate the halo mass for many objects in the SDSS DR4 catalogue.

2.6 Direct observation of mergers in the optical

Simulations in recent years give a detailed explanation of the merging process (Robertson et al., 2006; Cox et al., 2006a,b; Ruszkowski & Springel, 2009), but more work is required: to cover the theory behind galaxy mergers, we will need to solve several problems (SMBH accretion, feedback, and the final parsec problem[2] (Milosavljević & Merritt, 2003) among others). All simulations to date, even with good results, have the same flaw: the only comparison between the model and the observation is performed at the end. Obviously, they began their analysis from a sensible starting point, but all characteristics of the mergers are assumed a priori. There is no step-by-step control mechanism. Simulated merger processes are not compared with real ones. To implement this system one would need a vast knowledge of visually inspected merger events.

Automated techniques can extract mergers from survey images, all of which

[2]The final parsec problem is concerned with the merging of supermassive black holes. When the separation between two SMBH is less than a few tens of parsecs, the pair form a gravitationally bound system which cannot merge. Various solutions have been proposed, but we are yet to find conclusive proof.

have made significant contributions to the merger literature; however, these have limitations. For example, merger studies are often based on samples of *close pairs*[3] but involve an inherent (albeit well-motivated) assumption that the close-pair system will eventually merge (e.g. Patton et al., 2000). Close-pair techniques can also be biased against minor mergers, since the smaller merger progenitor is often fainter than the spectroscopic limit of the survey in question. Similarly, mergers and merger remnants can be identified via structural parameters, such as concentration and asymmetry (e.g. Conselice, Blackburne & Papovich, 2005). While this technique has achieved significant success in probing the merger population in modern surveys (e.g. Conselice, Rajgor & Myers, 2008), it is difficult to define a parameter space uniquely occupied by mergers, and typically, the results must be calibrated against results of visual inspection (Jogee et al., 2008). Although automated strategies have improved in recent years, these remain less robust than direct visual inspection. To visually classify such a high number of galaxies, a comparable number of eyes are needed.

2.6.1 Construction of Galaxy Zoo merger catalogue

Galaxy Zoo (GZ) is an internet-based user interface to catalogue galaxy images from the SDSS, according to morphology. A complete description of the project can be found in the paper by Lintott et al. (2008), which demonstrates how public users in large numbers (over 500,000 volunteers participating in GZ) are as good as experts in identifying morphologies. The advantages of using volunteers are twofold. Computer programs have limited success when it comes to classifying galaxies, and are not able to discover unusual objects or structures. GZ volunteers are quickly trained with a short tutorial about general classes of galaxies, and are tested before they are signed up to the program. No previous knowledge of astronomy is required to become a volunteer.

The website itself is simply structured. Its interactive page displays a JPEG image of an area of sky, centred on a randomly chosen galaxy from the sample. The image is a colour composite of the three middle filters (g,r,i). Its scale is of $0.024R_p$ arc-seconds per pixel, where R_p is the Petrosian radius for the galaxy. Using the *SDSS data release 6* (York et al., 2000; Adelman-McCarthy et al., 2006) volunteers are instructed to classify galaxies into the following categories:

[3]Close pairs are normally defined using a projected distance of 30 kpc and a line of sight velocity differential ($\Delta z \leq 500$ km s^{-1}) (Patton et al., 2000)

- Ellipticals (e)
- Spirals (s)
- Star/Bad image (b)
- Merger(m)

Every user is weighted based on the number of classifications and every classification is weighted by the user's weights and the general agreement. A more detailed classification has been completed, thanks to the second iteration, Galaxy Zoo 2, but it was not used in this work.

2.6.2 The merger fraction f_m: quantifying Galaxy Zoo mergers

This preliminary classification was used by Darg et al. (2010b) to build a merger catalogue of over three thousand objects. The raw parameter f_m, called the weighted-merger-vote fraction, is used to select the correct galaxies from the whole sample. f_m simply quantifies the probability that a certain image was in fact the image of a merger.

$$f_m = \frac{W n_m}{n_{e,s,b,m}} \tag{2.10}$$

The parameter f_m ranges from 0 to 1 so that an object with $f_m = 0$ should look nothing like a merger and $f_m = 1$ should look unmistakeably so. The f_m values are calculated by taking the number of merger classifications (n_m) for a given Galaxy Zoo object and dividing it by the total number of classifications ($n_{e,s,b,m}$) for that object multiplied by a weighting factor W that measures the quality of the particular users that have assessed the object. The quality of an individual user is determined by measuring to what extent that person agrees with the majority opinion for all objects the individual has viewed (Lintott et al., 2008). The merger catalogue consists only of objects whose spectroscopic redshift lies in the range $0.005<z<0.1$. The magnitude limit of SDSS spectroscopy is $r<17.77$, which corresponds to an absolute magnitude M_r of < -20.55 at $z = 0.1$. So the minimum stellar mass they consider at $z = 0.1$ is $10^{10} M_\odot$. The quality of the SDSS images beyond a redshift of 0.1 rapidly diminishes, leading to unreliable visual classifications of galaxy morphology. The lower limit is set at $z = 0.005$: the reason for this is to remove Galactic stars. The number of SDSS objects peaks near $z = 0.08$ and only a few percent have $z<$ 0.02.

The number of SDSS objects that survive the spectroscopic redshift cut is

304,182 from 790,220. To find mergers within this set, an additional cut of $0.4<f_m<1.0$ was applied, leaving 4198 GZ objects with spectra. The reason behind the cut on the weighted-merger-vote fraction was the high occurrence of false positives (which are virtually non-existent in the interval $f_m>0.6$). A second layer of visual inspection was used to:

- remove any non-merging systems
- visually select an appropriate SDSS object to represent the merging partner
- assign morphologies to the galaxies in each merging system

These are discussed below.

Removal of non-merging systems The three principal causes for misclassification for $f_m<0.6$ are:

- projection of galaxies along the line of sight
- projection of nearby stars onto distant galaxies
- cases which are borderline mergers

Galactic projections occur when two galaxies have similar celestial coordinates but are separated by a significant radial distance. This case is easy to spot and to deal with when both galaxies have spectral redshifts. However, most of the GZ candidate systems had only one redshift. Spotting a projection in such cases can only be performed through visual examination of the image for signs of interaction. The choice to use only systems with $f_m > 0.4$ meant, however, that the need for such elaborate decisions is rare.

Stellar projections are the most common problem, but they are easily dealt within the SDSS catalogue itself. Stellar objects are determined with an accuracy greater than 98% by looking whether they have a point like or extended emission. 'Border-line' cases involve galaxies that are morphologically disturbed but do not necessarily merit the term 'merger'. Most galaxies are merging with something, from simple secular accretion ('merging' with gas and molecules from the intergalactic medium) to cannibalising a small galaxy (minor merger), to collision with a galaxy roughly its own size (major merger); so only cases where there was a clear and strong morphological disturbance were included in the catalogue.

Visual selection of a partner To create a catalogue of merging pairs, it may be necessary to manually select an appropriate SDSS object as a partner for each object supplied by GZ with f_m>0.4. To do so, an IDL routine is used that allows for the rapid examination of the image and photometry of all objects within 30" of the GZ object given by the Neighbours table in the SDSS database. Finally, the partner object is selected by 'visual-plausibility', since it is still the most reliable method. Most merging systems are binary mergers, and have a simple, straightforward classification, since in the GZ merger catalogue they can either have

- (a) spectra centred on both galaxies or
- (b) a spectral object centred on one galaxy and only photometry on the other.

However, not all strongly-perturbed systems appear in a simple binary mergers state. There are cases where

- (c) galaxies are in the final stages of a merger and its progenitors are no longer distinguished by the SDSS pipeline (*postmergers*),
- (d) a galaxy has been perturbed by a close encounter with a neighbour no longer in view (*fly-by*) and, occasionally,
- (e) a merging system involves three or more galaxies.

This range of possibilities makes merger taxonomy a more complex task. The construction of the merging-pairs catalogue is unique for these cases: For case (a) they straightforwardly pick two spectral objects to represent our merging pair. If the merger companion does not have a spectrum, then the best photometric object available is visually selected to represent the merging partner (case b). For cases (c) and (d), a merging partner is not selected at all, because they usually occur when only one galaxy core is apparent with the peripheries undergoing extensive tidal disruption, meaning that there is no photometric object to represent the perturbing body. These are included in the merging catalogue but not in the merging pair catalogue. The same goes for case (e), where they have a multiple galaxies merger. After these distinctions, the catalogue contains 3003 pairs of galaxy mergers.

Assigning merging morphologies Four classifications are used to assign morphologies to each SDSS object in the merging-pairs catalogue: E, S, EU, SU. The E and S classifications label those galaxies which have sure morphology, respectively ellipticals and spirals, and in which no appeal to colour was necessary. The EU

and SU are for those galaxies which, even after visual inspection, cannot be classified with absolute certainty as ellipticals or spirals. The 'unsure' morphologies are usually more distant objects, with image resolution too poor to clearly distinguish features such as spiral arms. Choosing between EU and SU can be very difficult and is based mostly on apparent surface brightness profile and, in very difficult cases, on colour.

A simple way to select morphology in SDSS is via the SDSS *fracdev* parameter measured in the optical bands (usually the r band is used) that ranges from 0 to 1. This is a measure of the goodness-of-fit of a de Vaucouleurs profile to a galaxy's surface-brightness, or in other words, how well the surface brightness of a galaxy as a function of the apparent distance is described by the de Vaucouleurs' law (de Vaucouleurs, 1948). Ellipticals tend to have a fracdev ~ 1, indicating a good fit to a de Vaucouleurs profile, whereas spirals have a wide distribution. The morphological categories S, SU, EU and E of the merging-pairs catalogue have mean fracdev values of 0.48, 0.85, 0.93 and 0.94 respectively, fitting qualitatively with our expectations. The high value of 0.85 for the SU category suggests some contamination by bulge dominated discs or ellipticals. This is expected, since distant, poorly-resolved spirals can look like ellipticals (Bamford et al., 2009).

2.6.3 Properties of the mergers in the GZ catalogue

The GZ merger catalogue (Darg et al., 2010a) has been used to study the basic properties of merging systems in the local universe. Here, we summarise some properties of the SDSS merger population:

Colour-Magnitude relation Examining luminosity and colour of the GZ merger sample is important, as it provides information on their internal properties. It is also valuable to have a better understanding of the qualitative effect that including the 'unsure' categories has on the whole sample. In Figure 2.3 we can see the volume-limited samples, for two sets: the upper set where the colour distributions are plotted for just the sure morphologies and then the lower set where all merger morphologies are plotted. Comparing the colours of the control morphologies to the merger morphologies, it is interesting to see that the overall means for $u - r$ are similar between the control and merger samples. The merger-spirals (S+SU) are bluer by $\Delta < u - r > \sim 0.05$ magnitudes than their control counterpart. However, the merger ellipticals (E+EU) have a slightly redder mean compared to the control ellipticals with $\Delta < u - r > \sim 0.15$ magnitudes. The overall merger distributions have a more prominent red tail (due to the long time scale of merging events)

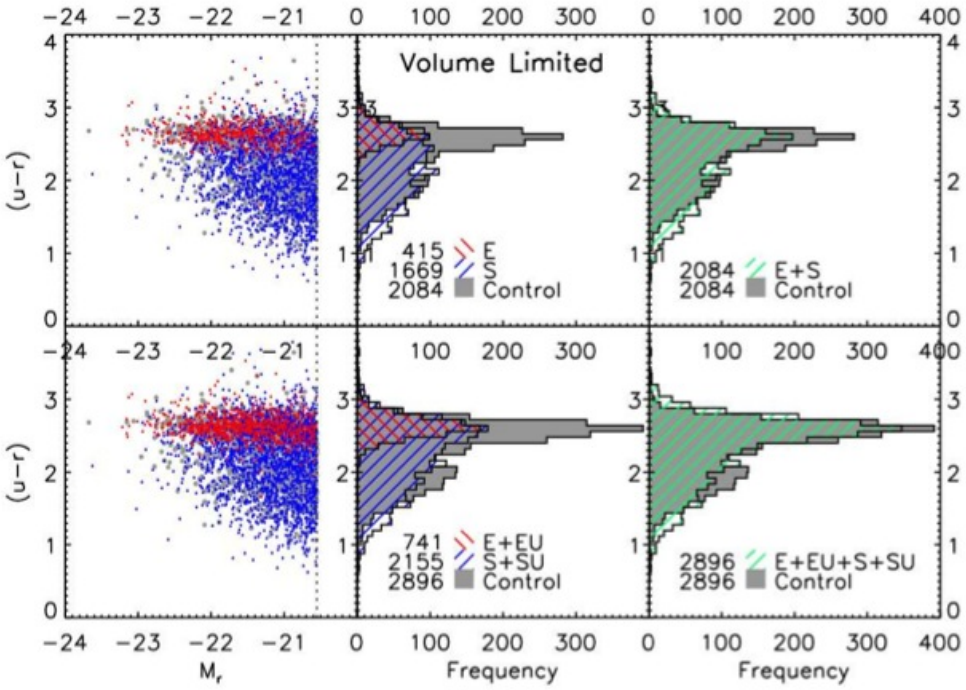


Figure 2.3: Optical colour-magnitude diagrams of the individual galaxies involved from the merger sample (coloured) and from the control sample (grey). The k-corrected rest-frame magnitude limit is M_r<20.55 (dotted vertical line). In the top panels, we see the distributions for only 'sure' morphologies, while in the bottom panels we see them for any morphology (Darg et al., 2010a).

compared to the control distributions, and so the previous result should not be a surprise, since this might be due to a selection effect: spiral mergers are easier to spot and have a longer interaction timescale; Darg et al. (2010a).

AGNs, Star-Forming or Quiescent signatures in galaxy mergers. Darg et al. (2010a) has determined the major source of ionisation in the control sample and in the merging catalogue, using emission-line diagnostics as we discussed earlier in this chapter. In Figure 2.4, we see colour-mass relations for different spectral types of mergers. We see that star-forming mergers occupy smaller-mass regions dominated by spirals, while quiescent types occupy higher-mass regions dominated by ellipticals. The AGN categories seem to occupy intermediate-mass regions. The

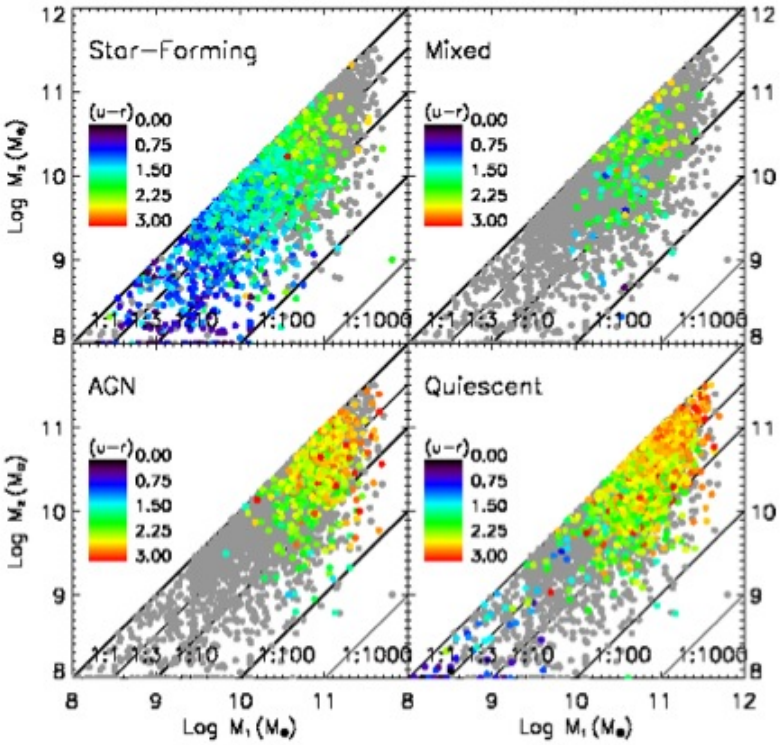


Figure 2.4: Spectral type-colour-cass relations. Mass and colour are plotted for all 3003 systems. The log of the Mass for the two mergers are plotted against each other, and the $u-r$ colours are given through a colour gradient. Masses are calculated following Bell et al. (2003). The diagonal lines represent mass ratios between the progenitors. The panels show the population split into its various spectral types: Quiescent, Star-Forming or AGN. No magnitude limitation is imposed for an enhanced view of mass build-up in relation to these properties (Darg et al., 2010a).

lack of star formation and AGN activity in high-mass galaxies suggests that their

fuel supply has been exhausted, whereas the lack of AGN activity in low-mass gas-rich galaxies suggests that either AGN do not form there (perhaps because they have insufficiently massive black holes at their centres to generate substantial ionisation) or that their AGN signatures are obscured by the high gas content and star-formation rates (SFRs).

When we examine Table 2.1, we see that the fraction of AGN in mergers appears no different from the control sample; ($\sim 23 \pm 1\%$ compared to $\sim 24 \pm 1\%$). The situation is different when samples is split according to morphology: the fraction of AGN in merging spirals is slightly less than in their control counterparts ($\sim 23 \pm 1\%$ compared to $\sim 29 \pm 2\%$), but the AGN signatures might be obscured by high star-formation rates (common for spirals) and disrupted gas content in merging galaxies. These star-formation rates are seen to be higher for merging spirals ($59 \pm 2\%$) compared to control spirals ($31 \pm 2\%$). The sample of ellipticals in mergers, by contrast, resembles that of the control ellipticals when split into ionisation types, except that none are star-forming types. Both merging and control ellipticals are dominated by quiescent types ($81 \pm 7\%$ and $73 \pm 3\%$) and have the same fraction of AGN ($18 \pm 3\%$ and $20 \pm 2\%$). In short, the internal ionisation properties of ellipticals appear basically unaffected by the merging process.

Type	S-Merger	E-Merger	S-Control	E-Control
Star-Forming	51 ± 2	0 ± 1	25 ± 2	6 ± 1
Mixed	8 ± 1	0 ± 1	6 ± 1	2 ± 1
AGN	15 ± 1	18 ± 3	23 ± 2	20 ± 2
Quiescent	26 ± 1	81 ± 7	46 ± 3	73 ± 3
All Star-Forming	59 ± 2	0 ± 1	31 ± 2	8 ± 1
All AGN	23 ± 2	18 ± 3	29 ± 2	22 ± 2

Table 2.1: Percentages of ionisation-types for volume-limited merger and control galaxies. The 'All AGN' and the 'All Star-Forming' lines are the sum of the AGN and mixed and the Star-Forming and mixed, respectively. The errors are Poisson-Counting errors rounded up to the nearest integer (Darg et al., 2010a).

The environment parameter in the GZ merger catalogue The environment parameter used by Darg et al. in the GZ merger catalogue is the ρ_g (see eq 2.7). Figure 2.5 shows a plot of the ρ_g distribution from the GZ merger catalogue and the GZ local galaxy population (to act as a control sample) with background shading representing our different environments. The sample as explained in the previous paragraph was volumed-limited, and to have a more exact result, 'unsure' morphologies were left out. Both merger and control samples peak in intermediate

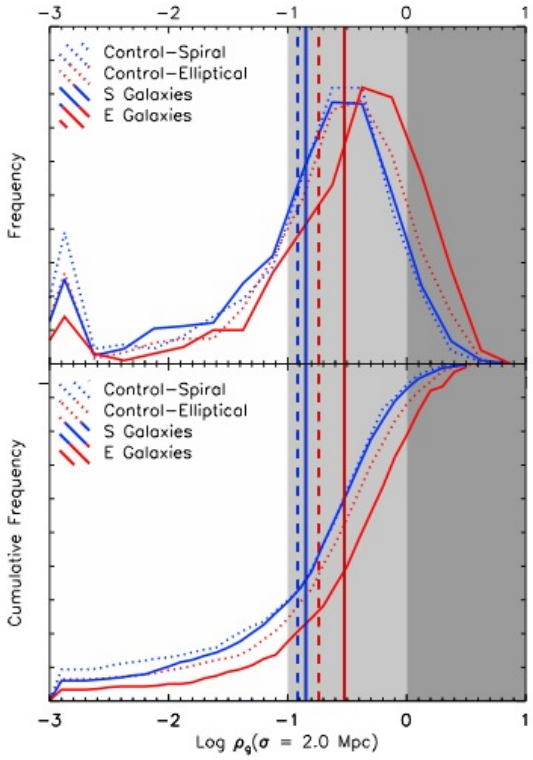


Figure 2.5: Distribution of ρ_g for control population and mergers. The distributions in the upper panel are scaled to have unitary area. $\rho_g = 0$ was set to $\rho_g = 10^{-3}$ to avoid Log(0) errors (hence the spike near -3). Vertical lines mark the mean value of ρ_g for the samples. The shading in the background is an indicator of environment type. The unshaded-white area corresponds to the *field environment*. The middle shade corresponds to *intermediate environments*. The darkest shade corresponds to the *cluster environment*. (Darg et al., 2010a)

environments, with elliptical mergers occupying a slightly denser environment than their control counterparts. The spiral mergers, on the other hand, do not show any major differences compared to their control sample, but perhaps favour a slightly less dense neighbourhood. When combining morphologies, the mergers are, overall, in virtually identical environments as the control sample; this is expected as the control sample is consistent with the probable merger parents population (Darg et al., 2010a).

2.7 Finding plausible evolutionary steps for the formation of massive galaxies

The main idea behind this project is to probe galaxy evolution along the merger sequence and study the properties of the early-type galaxies that are thought to lie at the end of that sequence. In Figure 2.6, we see a schematic representation of a general merger event. If we accept the merger scenario as the most likely mechanism to form early type galaxies (ETGs), we need to find evidence of the existence of all missing links between merging galaxies and ETGs: working backwards from a gas-poor elliptical galaxy, we need to find star-forming ETGs (to explain the blue colours), spheroidal post-mergers (to explain tidal features, dust and disturbances) and bright infrared mergers (to explain the lack of gas). Luckily, not only is there a significant number of these objects in the sky, but these peculiar classes and their properties can help us constrain conditions required to form early-type galaxies at low redshift.

In the following chapters we provide observational analysis and results on different stages of the merger process. In Chapter 3 we focus on highly star-forming mergers by looking at their properties in the infrared. Chapter 4 is dedicated to the analysis of spheroidal post-mergers, a *missing-link class* between mergers and early-type galaxies. A further analysis in the area of active and unrelaxed early-types is conducted in Chapter 5. Chapter 6 is concerned with the morphological classification of local infrared-bright galaxies and a general investigation of their properties. Finally, conclusions are provided in Chapter 7.

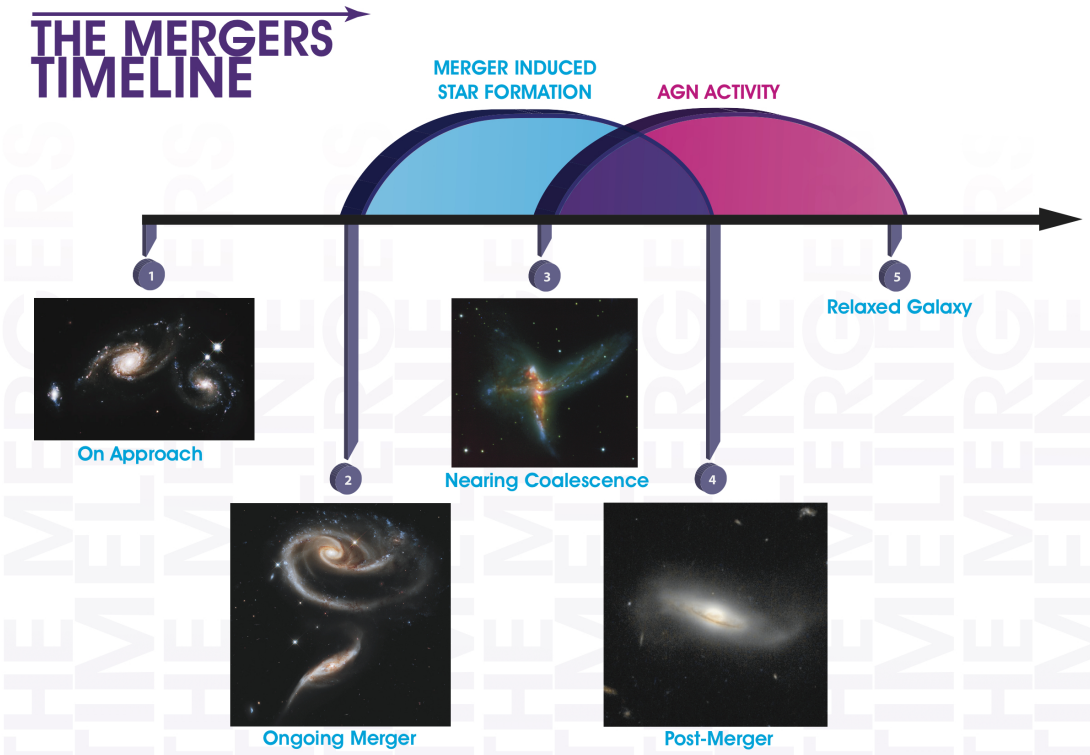


Figure 2.6: This is our own schematic representation of a general merger timeline. We divided the merging process into five phases: Galaxies on approach, Merging, Coalescing, Post-merging and relaxed. The peaks of star-formation activity and AGN activity are shown to be flat and extensive. This graphic choice symbolises the lack of detailed evidence on the exact moment and relative intensities of the peak of these two processes.

Chapter 3

The far infrared properties of galaxy mergers

In the previous chapter, we mentioned several studies (e.g. Kleinmann & Keel (1987); Sanders et al. (1987); Hutchings & Neff (1987); Vader & Simon (1987); Sanders et al. (1988a,b); Sanders & Mirabel (1996); Clements et al. (1996); Hopkins et al. (2006); Younger et al. (2009)), which looked at the properties of infrared-detected galaxy samples and then, via visual inspection, found direct or indirect evidence of merging. Given the important role played by mergers in the infrared (IR) universe, a *blind* infrared survey of mergers is a desirable enterprise. In other words, it is useful to start with a complete sample of mergers and then study their infrared properties (an opposite approach to what has typically been employed in the past). In this chapter, we pursue such a study by combining a large, *visually-selected* sample of mergers in the local universe ($z < 0.1$) from Galaxy Zoo with their far-infrared properties derived using data from IRAS.

The choice of a low-resolution instrument like IRAS might seem somewhat peculiar in the current age of relatively high spatial-resolution IR astronomy e.g. using instruments like Herschel. However, IRAS surveys provide all-sky coverage which makes it possible to gather statistically significant samples after cross-matching with a large optical surveys like the SDSS. More importantly, the coarseness of the IRAS beam (1.5'×4.7') is an advantage in complex, *spatially-extended* systems like galaxy mergers, especially in the local Universe. For the mergers studied here, the IRAS beam always encompasses *both* progenitors, allowing us to study the mergers as a *single* object and avoid deblending of the constituent regions of the merging system.

While much of our understanding of galaxy evolution has traditionally come from UV-optical astronomy, modern efforts have increasingly leveraged instruments in the infrared (Neugebauer et al., 1984a; Pilbratt et al., 2010). A substantial

fraction of the luminosity of a galaxy in the UV-optical wavelengths is absorbed by interstellar dust and re-emitted in the infrared (Spitzer, 1978). Indeed, around 50% of all the energy produced by star formation (and AGN) over cosmic time has been absorbed by molecular clouds and re-emitted in the far-infrared (FIR) waveband ($3.5 - 1000\mu$m), forming the Cosmic Infrared Background (e.g. Puget et al., 1996; Fixsen et al., 1998; Pei, Fall & Hauser, 1999; Hauser & Dwek, 2001; Dole et al., 2006).

In star-forming systems like mergers, obscuration is likely to be a particularly important issue, since the star formation in the dusty cores of these systems may be obscured, making it challenging to measure the total star formation activity accurately via the UV or optical wavelengths (Spitzer, 1978; Kennicutt, 1998; Pei, Fall & Hauser, 1999). However, while the UV-optical signatures are likely to be affected, the star formation can be better studied using the FIR wavelengths, as the peak of emission from cold dust in the star forming regions lies in the FIR (e.g. Shu, Adams & Lizano, 1987; Pei, Fall & Hauser, 1999; Chary & Elbaz, 2001). Thus, the FIR luminosity is a sensitive tracer of the young stellar populations (Lonsdale Persson & Helou, 1987; Kennicutt, 1998; Lehnert & Heckman, 1996; Meurer et al., 1997; Kewley et al., 2002; Law, Gordon & Misselt, 2011) and has been shown to correlate well with the star formation rate (Kennicutt, 1998).

The structure of this chapter is as follows. In Section 3.1 we describe the sample of Galaxy Zoo mergers that underpins our study and describe its basic properties. In Section 3.2 we explore how the IR luminosity and the associated star-formation rate is related to the properties of the mergers (e.g. total system mass, mass ratio, local environment etc.). In Section 3.3 we test if ultra-luminous infrared galaxies are the product of sub-L_* progenitors. In Section 3.4 we study the optical emission-line activity in our sample and, in Section 3.5, we explore the timescales over which LIRGs turn into ULIRGs along the merger sequence. We summarise our findings in Section 3.6.

3.1 The merger sample and basic properties

Our sample of visually-classified mergers was produced via the Galaxy Zoo (GZ) project (Lintott et al., 2008). GZ is uniquely powerful in detecting rare classes of objects like mergers, which can only reliably be selected via direct visual inspection of galaxy images. At the time this study was performed GZ had enlisted over 500,000 volunteers from the general public to morphologically classify, through visual inspection, the entire SDSS DR6 spectroscopic sample (York et al., 2000;

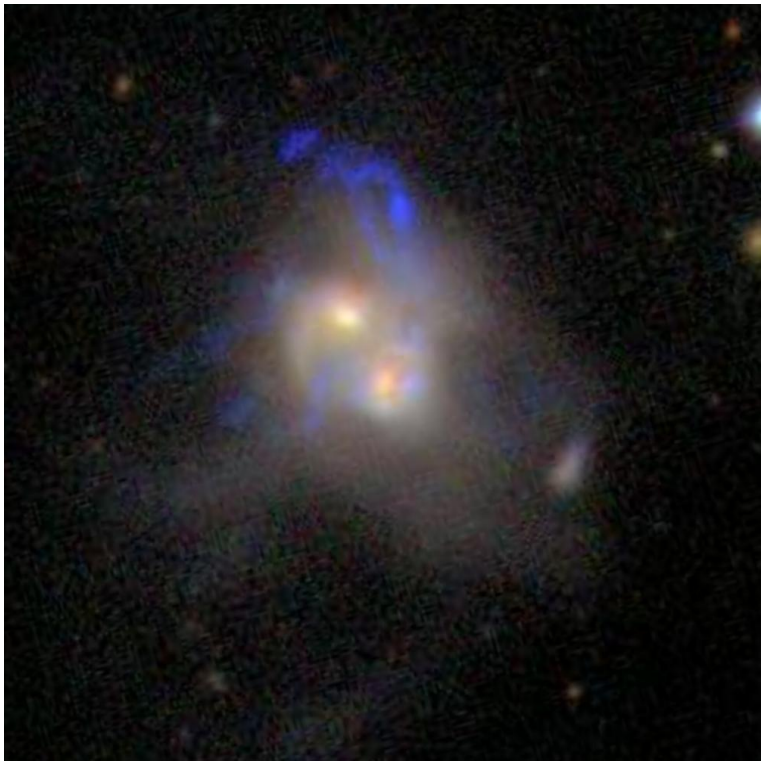


Figure 3.1: An SDSS ugriz composite image of an IRAS-detected merger in our sample.

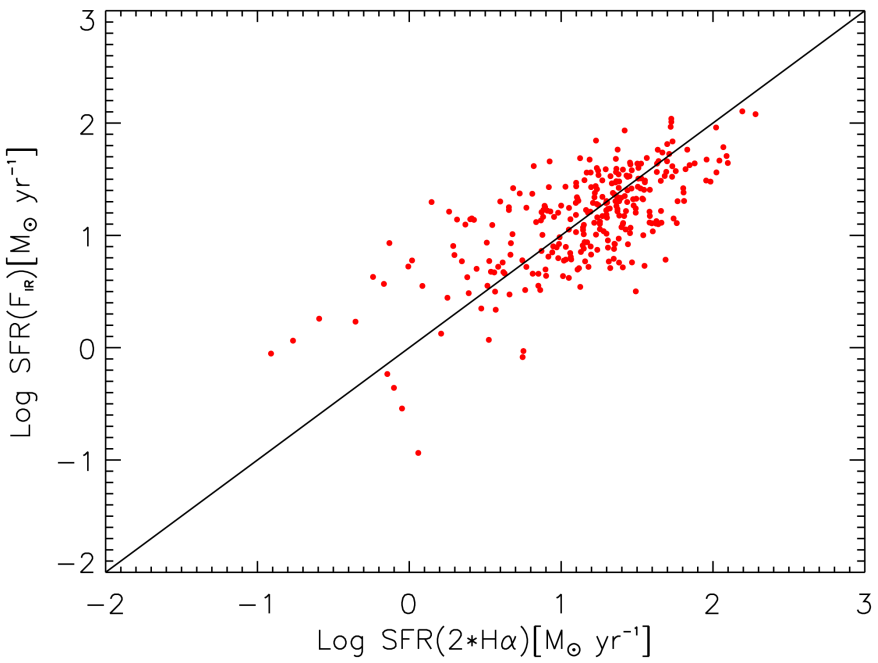


Figure 3.2: The SFR calculated from the IRAS FIR luminosity plotted against the SFR calculated from twice the Hα luminosity of the merger progenitor that has an SDSS spectrum. We find a reasonable correlation between these two quantities.

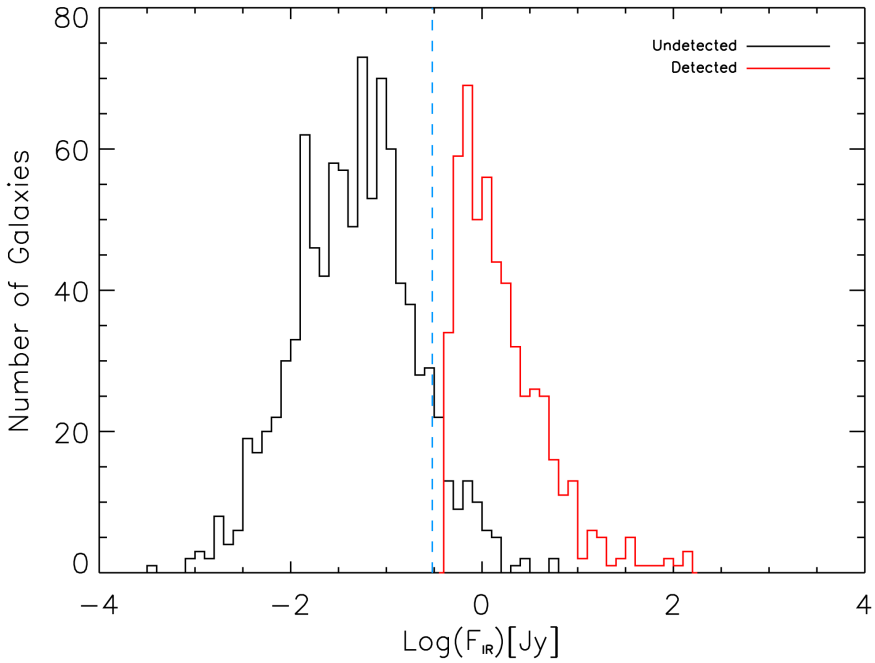


Figure 3.3: Predicted FIR flux for mergers that were IRAS-*undetected*, calculated using twice the Hα luminosity of the merger progenitor that has an SDSS spectrum (the IRAS-detected mergers are shown in red). The nominal IRAS detection limit is shown as the vertical dashed line.

Adelman-McCarthy et al., 2008). This included the compilation of the largest, most homogeneous sample of merging systems in the local Universe to date, as described in Chapter 2 (Darg et al., 2010a,b). The final sample of Galaxy Zoo mergers which was used for this study contains 3373 objects, unbiased in morphology and local environment and with mass ratios typically between 1:1 and 1:10.

The Galaxy Zoo merger sample was cross-matched with the Imperial IRAS-FSC Redshift Catalogue (IIFSCz; Wang & Rowan-Robinson, 2009), a sample of ∼60,000 galaxies selected at 60 μm from the IRAS Faint Source Catalogue (FSC; Moshir, Kopman & Conrow, 1992). The IIFSCz catalogue provides far-infrared (FIR) fluxes based on the best-fitting infrared templates of Rowan-Robinson et al. (2008). For the flux limit at 60μm ($f(60) > 0.36$ Jy) 90 per cent of the sources have spectroscopic redshifts from the SDSS. Recall that an IRAS-based analysis is useful here, because the large IRAS beam size of 1.5'×4.7' (at 60μm, Neugebauer et al., 1984a,b) allows us to study the entire merging system as a single source. The SDSS mergers are isolated systems, so contamination by nearby sources within the IRAS beam is negligible. An example SDSS image of an infrared-detected merger is shown in Figure 3.1.

Cross-matching the Darg et al. GZ merger sample with the IIFSCz yields

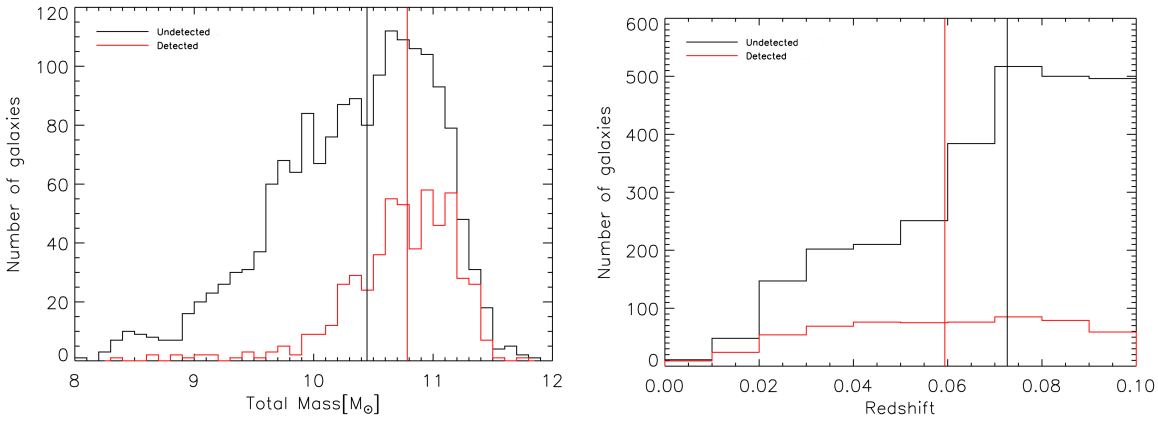


Figure 3.4: Masses (left) and SDSS spectroscopic redshifts (right) for the IRAS-detected (red) and IRAS-undetected (black) mergers. Median values are indicated using the vertical lines.

606 mergers (18% of the Darg et al. merger sample). 594 mergers are spiral-spiral merging pairs and only 12 have an elliptical progenitor. There are 274 LIRGs (40%) and 10 ULIRGs (2%) in our sample, with the ULIRGs typically being nearly-coalesced, i.e. in the very final stages of the merger. Note that the Darg et al. merger catalogue is slightly biased *against* ULIRGs, since they typically do not show two merging nuclei with tidal bridges between them, which are the main criteria for a galaxy pair to be defined as a merger in GZ.

It could be argued that a similar analysis could have been performed using, for example, Hα measurements from the SDSS itself. Hα is a line in the Balmer series which occurs when a hydrogen electron falls from its third to second lowest energy level. It is a spectral line with a wavelength of 656.28 nm, and it is found in emission in AGNs, HII regions and planetary nebulae. The crucial limitations of extracting the SFR from Hα are its sensitivity to uncertainties in dust extinction and the initial mass function, and the assumption that all of the massive star formation is traced by the ionised gas (Kennicutt, 1998). A way to solve some of these issues is to have detailed Hα maps of the galaxies, and then apply corrections to establish the amount of dust extinction. The most common estimators are the Balmer decrement and the Case B recombination rate. The Balmer decrement is the ratio between Balmer lines. Under laboratory conditions:

$$\frac{H\alpha}{H\beta} = 2.86$$

but if there is dust between the emitter and the observer, this ratio will become greater than 2.86 as micron-sized dust particles selectively dim shorter-wavelengths

(Baker & Menzel, 1938). The Case B recombination similarly employs emission lines, since it is a way of measuring the total recombination rate using only recombinations to excited states. This technique is preferentially applied to optically thick regions. Under equilibrium conditions, there is a balance between photoionization and recombination rates, which allows us to measure the UV ionizing luminosity of an astronomical object from the intensity of line radiation emitted by the surrounding ionized gas alone. In the ionization-bounded case the entire ionizing flux is absorbed within the nebula and it is re-emitted as an Hα photon under certain conditions. Understanding this rate helps us to understand what kind of stars and what kind of nebulae there are in these regions (Osterbrock & Ferland, 2006).

The other problems that plague Hα are related to the quantity and the age of stars. More gas is ionised by young massive stars so to evaluate the goodness of the assumption the caveat is to know how exactly the gas is being ionised. Gas can be ionised by AGNs, shocks (both from supernovae and AGNs), and stars. To characterise their contributions we need to understand exactly how they impact interstellar gas and birth clouds. This is not at all trivial; traditionally the AGN and shocks contribution are simply subtracted from the total Hα luminosity based on the average luminosity of local objects (e.g. Shioya et al. (2008)). This could lead to an incorrect estimate for the stellar component of the $\mathrm{SFR}_{H\alpha}$. The older stellar population contribution is estimated directly from the IMF. This means that if the estimate of the shape of the mass distribution of stars is wrong, we might be severely misestimating the SFR from Hα.

In addition to these general limitations, in our specific case using Hα is problematic largely due to the how SDSS collects spectroscopic information. Firstly, the SDSS fibre only detects Hα flux from the core regions of galaxies. Secondly, SDSS suffers from 'fibre collisions' i.e. it cannot take simultaneous spectra of two objects within 55" of each other (which is always the case for merging systems) in a single visit. This leaves us typically with Hα information on only one of the merger progenitors.

Before we begin our analysis we briefly compare the IRAS-detected mergers to their undetected counterparts. Only one of the merger progenitors typically has an SDSS spectrum and therefore a measured $H\alpha$ luminosity. Nevertheless, for the *IRAS-detected* mergers, we notice that a reasonable correlation exists between the FIR (i.e. 8-1000 μm) star formation rate, calculated using equations 2.1 and *twice* the SFR derived from 2.2 (as calculated following Kennicutt, 1998) of the merger progenitor that has an SDSS spectrum(see Figure 3.2). Mergers have a higher fraction of young stars compared to relaxed galaxies, for this reason we believe the

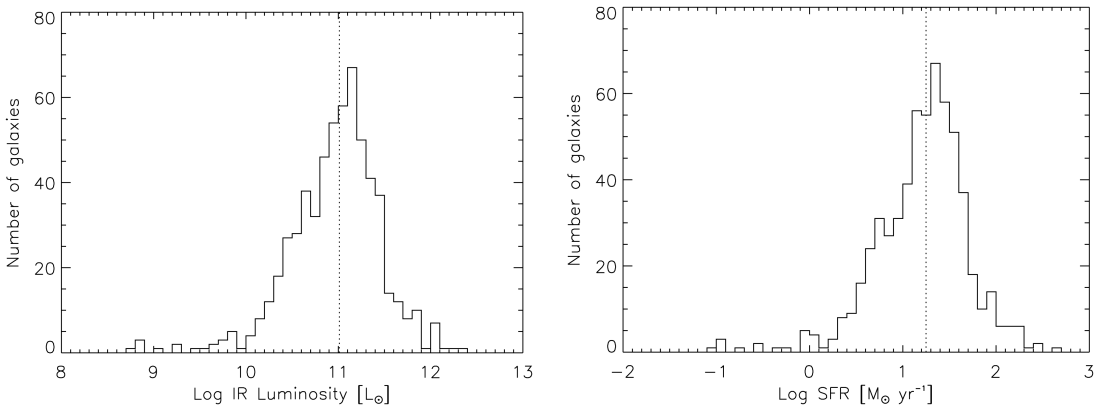


Figure 3.5: The distribution of FIR(i.e. 8-1000 μm) luminosity of the IRAS-detected sample of galaxy mergers (left) and the corresponding star-formation rate (right), following Eqn 4 in Kennicutt. The dashed lines are median values. (1998).

correlation in Figure 3.2 is tighter than what we found in the previous chapter.

The extinction-corrected $H\alpha$ luminosity used here is computed using the GANDALF code (Sarzi et al., 2006), described in Chapter 2. Exploiting this correlation, we can estimate (albeit crudely) the FIR flux distribution of the undetected galaxies by using twice the $H\alpha$ luminosity of the progenitor that has an SDSS spectrum. In Figure 3.3 we show the predicted FIR fluxes for the undetected systems (black) and the FIR fluxes of their detected counterparts (red). The nominal IRAS detection limit is shown using the blue dashed line. As might be expected from the IRAS-undetected mergers their predicted FIR fluxes (in a simplistic way from the $H\alpha$ luminosity of the one progenitor that has an SDSS spectrum) overwhelmingly lie below the detection limit. Indeed the detected and undetected merger populations separate relatively cleanly on either side of the detection limit.

In Figure 3.4 we compare the masses and redshifts for the detected and undetected mergers. The stellar masses have been estimated using SDSS optical photometry, via the calibrations of Bell et al. (2003). The mass distributions are similar, with medians separated by $\sim$0.3dex (which is roughly the uncertainty in the stellar mass estimates). The redshifts are also similar with median values for the detected and undetected of 0.06 and 0.072 respectively. The similarity in the masses and redshifts of the detected and non-detected samples suggests that the non-detection in IRAS of is more due to intrinsic differences in the mergers themselves rather than the undetected systems being smaller or further away.

In our sample of IRAS-detected mergers, the FIR luminosity (L_{FIR}) ranges from around $10^9 L_\odot$ to over $10^{12.3} L_\odot$, with a median $\sim 10^{11} L_\odot$, which corresponds

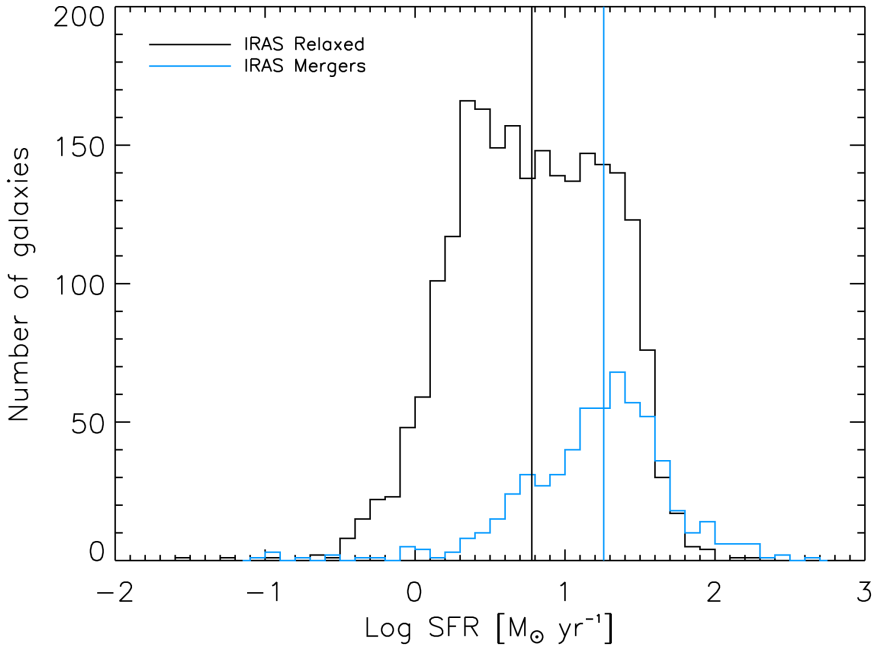


Figure 3.6: The distribution of the star-formation rates for the IRAS mergers and for a control sample of relaxed galaxies (either early-type or late-type galaxies, but no irregulars) detected by IRAS.

to a median star-formation rate of $15 M_{\odot}$ yr^{-1} (see Figure 3.5). In Figure 3.6 we compare the SFRs of the IRAS-detected mergers to that of a control sample of 2285 IRAS-detected galaxies in the same redshift and r-band magnitude ranges that are not in mergers. The IRAS-detected mergers show significantly elevated SFRs, with a median SFR enhancement of over 0.5 dex.

3.2 Dependence of SFR on environment, system mass and mass ratio

In this section we study how the SFR of mergers are influenced by their local environment and by their internal properties (total stellar mass and mass ratio).

In Figure 3.7 we study the dependence of the SFR on the (stellar) mass ratio. We find no apparent dependence between the mass ratio of the merger and the SFR in the merging galaxies. Indeed 'minor' mergers (those with mass ratios less than 1:3) also seem capable of producing IR-bright galaxies, including LIRGs and systems that are close to the ULIRG luminosity. Our empirical analysis thus suggests that major mergers are not the only process that can trigger strongly star-forming systems, somewhat in contradiction with the wider literature (Di Matteo, Springel & Hernquist, 2005; Cox et al., 2006a,b). Minor mergers can play an equally influential

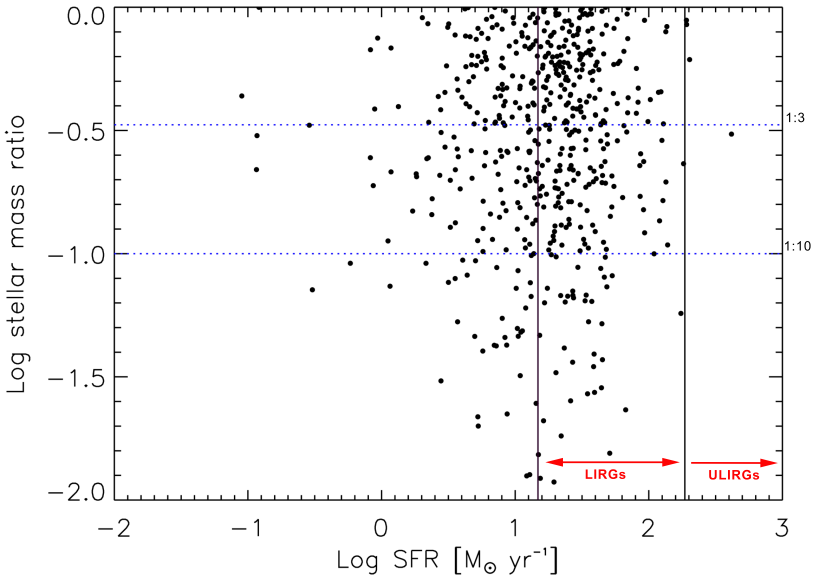


Figure 3.7: The merger star formation rate plotted against the merger mass ratio. The dashed horizontal lines represent the 1:3 and 1:10 ratio lines. From left to right the solid vertical lines represent the LIRGs locus and the ULIRGs locus. There is no significant trend between SFR and mass ratio. It is also important to note that minor mergers play a significant role in the formation of LIRGs.

role in triggering such strong star formation episodes.

In Figure 3.8, we study the star-formation and specific star-formation rate against the total stellar mass of the system. The top plot of this figure indicates that the SFR is positively correlated with the mass of the system, with LIRGs and ULIRGs residing mostly at the higher end of the mass spectrum. This is true for the mergers and the control sample. The difference between the two is a definite enhancement of SFR. This enhancement is mass independent as we can see in the bottom plot. There we see how the specific star formation rate (SSFR) correlates the total stellar mass of the system. The SSFR is the SFR per unit mass and in the plot, we can see, it has a similar trend to the SFR versus mass plot. Again we see a significant enhancement in the merger sample; the trends are plotted by using a one-sigma binned fit. A one-sigma binned fit is a simple way to graphically express the median trend of a distribution per error bin.

In Figure 3.9 we study the dependence of the merger SFR on local environment. We use the Yang et al. environment catalogue (Yang et al., 2007) to estimate the environment of our galaxies and compare them to a control sample of late-type galaxies (LTGs). Yang et al. estimate the dark matter halo mass of individual SDSS galaxies, that can be used as a proxy for the local environment of the galaxy. Across the range of environments sampled by our mergers, we do not find a strong

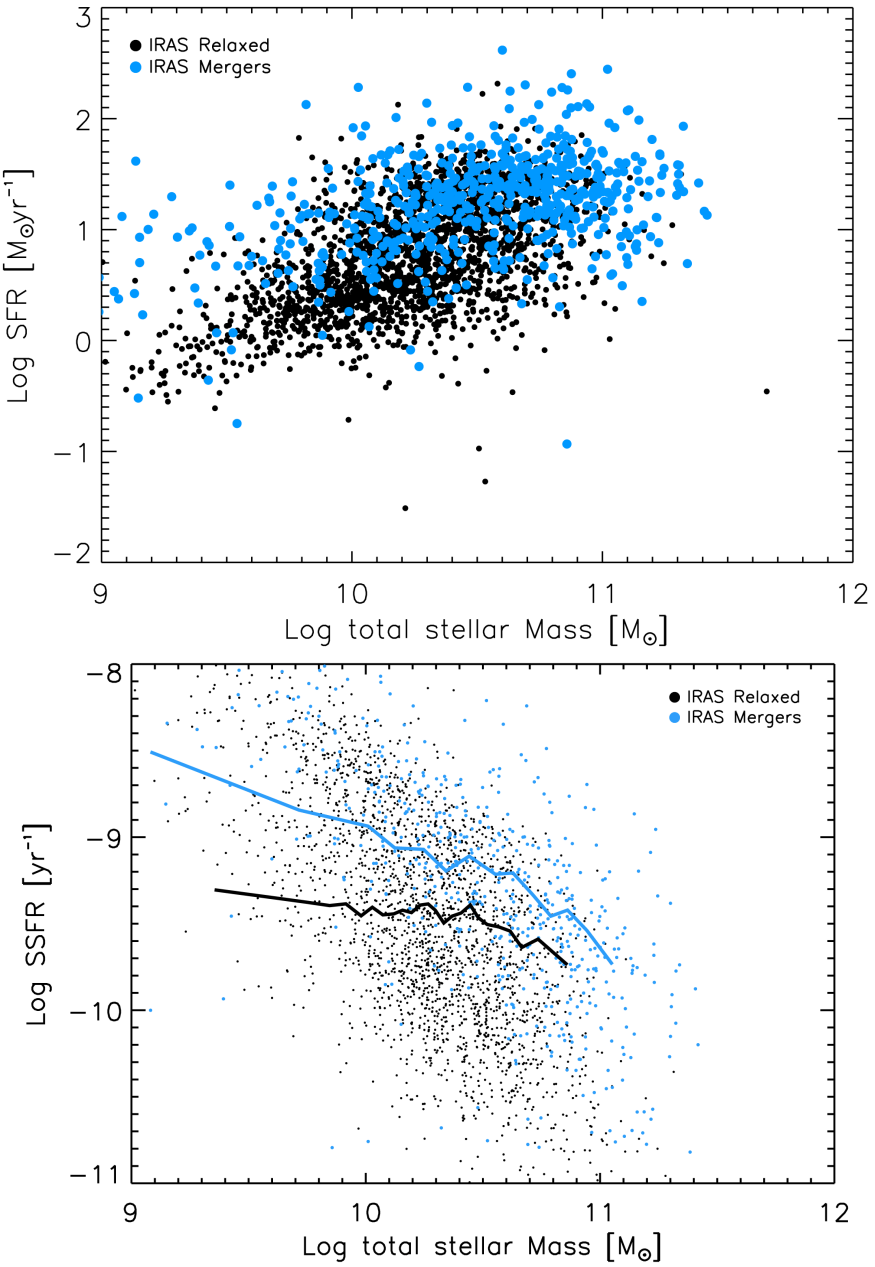


Figure 3.8: TOP: The star formation rate and the total stellar mass for the merger system and the control sample, with the mergers in blue and the relaxed control in black. From this plot and Figure 3.7 we see that the star formation rate correlates with the total stellar mass of the system but shows no correlation with the mass ratio. BOTTOM: The total stellar mass is plotted against the specific star formation rate. The solid lines are the one-sigma binned fit for the two distributions. It is clear from this plot that there is a significant enhancement of the SFR in mergers.

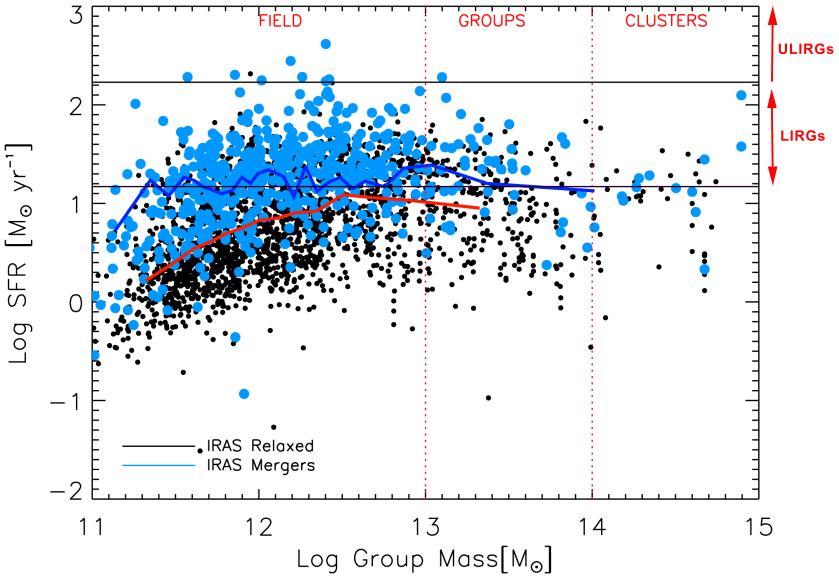


Figure 3.9: The star formation rate of the IRAS-detected mergers (blue) and the LTG control sample (black) plotted against the dark matter halo mass, which is used as a proxy for environment. Typically halos with masses less than 10^{13} $M_{\odot}$ are considered to be the 'field'. Halos with masses between 10^{13} $M_{\odot}$ and 10^{14} $M_{\odot}$ are considered to be 'group'-like environments, while haloes with masses greater than 10^{14} $M_{\odot}$ host clusters (Kaviraj et al., 2009). The plot also shows the one-sigma binned fit of the mergers (dark blue) and control sample (red).

correlation between the SFR in merging galaxies and the local environment. The relationship between SFR and environment in the mergers is similar to that in the control sample, except that the mergers show an enhancement in SFR of around a factor of 2.5, largely irrespective of environment. In agreement with previous studies (Hwang et al., 2010; Darg et al., 2010b; Carpineti et al., 2012), we find that, like the general merger population, the IRAS-detected mergers tend to favour lower-density environments. Most of the IRAS-detected mergers are found in groups and the field (95% of the sample favours such low-density environments), with ULIRGs exclusively inhabiting the field.

Our results thus suggest that the star formation activity in mergers is correlated more strongly to the total stellar mass of the system, with the system mass ratio and local environment being of secondary importance.

3.3 Cool ULIRGs as products of sub-L* mergers?

In the paper by Colina et al. (2001) it has been claimed that cool ULIRGs (ULIRGs with a $f25/f60 < 0.2$) are supposed to be mergers of sub-$L*$ galaxies. The char-

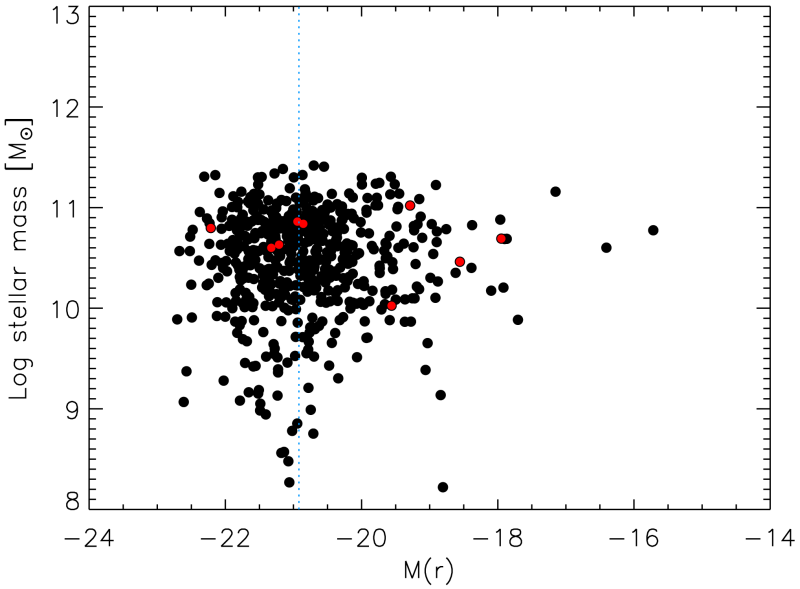


Figure 3.10: We calculated the luminosity of a group of cool ULIRGs (ULIRGs with a $f25/f60 < 0.2$) in red. The dashed line corresponds to the M_r for an $L*$ galaxy, which is -20.92 for $h = 0.75$. We find that only 2 of our 9 ULIRGs have a luminosity less than $0.5L*$, while another 2 are definitely super-$L*$ ($1.32L*$ and $2.43L*$). The median luminosity for for the 9 ULIRGs is $0.96L*$ ($M_r \sim -20.88$). The black dots are the other objects in the sample. The values are for the brightest object in the system.

acteristic luminosity was discussed in section 1.1.2.1. Sub-$L*$ galaxies are objects which have a M_r less than -20.92 for $h = 0.75$. The objects in their sample were single objects, so their result is not based on direct observation of ULIRG progenitors. Having a sample of merger ULIRGs, which is also infrared blind, give us a unique chance to test their findings. In our sample 9 out of 10 ULIRGs are cool (the other one has $f25/f60 = 0.22$ and $M_r = -21.09$), so we are in a good position to test their findings. From the Schechter function (Schechter, 1976) we extract the absolute magnitude in the r-band for an $L*$ galaxy: $M_r = -20.3 + 5 \log h$, where h is the Hubble parameter. If we assume that coalesced ULIRGs were formed by equal luminosity galaxies, then we find that only 3 of our 9 cool ULIRGs have a luminosity less than $0.5L*$, while another is definitely super-$L*$ ($2.43L*$). The median luminosity for the 9 ULIRGs is $0.96L*$ ($M_r \sim -20.88$). These results are shown in Figure 3.10.

Looking at the luminosity of our ULIRGs we find that they are mostly $L*$ galaxies, with few exceptions both in the sub-$L*$ and super-$L*$ categories. This is not what was found in the literature (Colina et al., 2001), where cool ULIRGs are claimed to be formed mostly by sub-$L*$ galaxies. This result complements well the result in the previous paragraph: dimmer galaxies can through merging, produce an

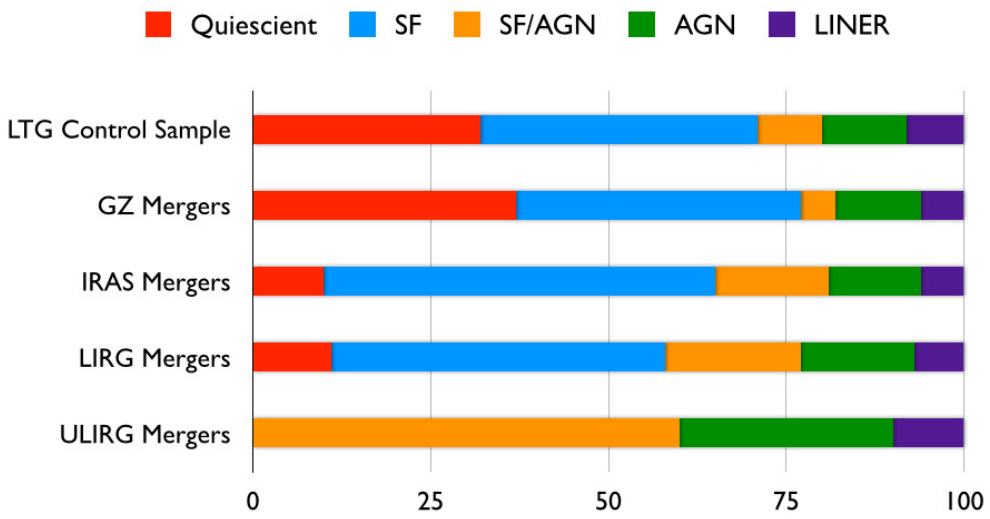


Figure 3.11: We have used the BPT technique to learn more about the emission line activity of our sample of galaxies. We divided the sample into 3 categories (Full, LIRG and ULIRG) and compare it with the original galaxy merger sample and the control-sample. We can see a clear increase of the AGN fraction with increasing IR luminosity (and hence SF), which could play quite an important role in the transition from LIRGs to ULIRGs

incredibly bright and highly star-forming object but they cannot be arbitrarily dim.

3.4 Emission line activity

We use optical emission-line ratios (see Baldwin, Phillips & Terlevich (1981); Veilleux & Osterbrock (1987); Kauffmann et al. (2003); Kewley et al. (2006)) to study the ionisation mechanisms in the IRAS-detected mergers and probe the connection between AGN activity and IR luminosity. We use two standard optical emission line ratios ([OIII]/Hβ and [NII]/Hα), to separate galaxies that are 'star-forming', 'Seyferts', 'LINERs', or 'composite' (i.e. contain both star formation and AGN), using a signal-to-noise (S/N) threshold of 3. Galaxies which do not have S/N $>$ 3 in all four lines are classified as 'quiescent'. The ratios are computed by using the public GANDALF code, which is described in Chapter 2.

In Figure 3.11 we split the IRAS-detected mergers into these emission-line categories and study how they change with IR luminosity. We also perform an equivalent analysis for the parent Galaxy Zoo merger sample and our control sample of late-type galaxies. The majority (71%) of the IRAS-detected mergers are classified as star-forming and a significant minority (35%) host an AGN. Mergers that are LIRGs exhibit a slightly higher incidence of AGN with respect to the general

infrared-detected merger population and the control sample. However, in mergers that are ULIRGs, the ionisation is dominated by the AGN (Figure 3.11). Seven out of the eight ULIRGs in our merger sample have a Seyfert-type AGN, while the other is classified as a LINER. This result is consistent with the recent literature which suggests that AGN become active in the *later* stages of a merger (Schawinski et al., 2007a; Darg et al., 2010a; Wild, Heckman & Charlot, 2010; Carpineti et al., 2012) and also with the findings of past studies (Sanders & Mirabel, 1996; Clements et al., 1996; Risaliti et al., 2000; Hopkins et al., 2006; Chakrabarti et al., 2007; Younger et al., 2009; Treister et al., 2009, 2010; Iwasawa et al., 2011) which suggest that AGN play an important role in the formation and evolution of ULIRGs - at least 50% (and up to 75%) of the ULIRGs explored in past studies show an AGN signature.

3.5 Timescale of ULIRG formation along the merger sequence

Although our sample of ULIRGs is small (recall from the discussion in Section 1 that the GZ merger catalogue is likely biased against ULIRGs, because it was not designed for systems that are 'postmergers'), we find a clear morphological segregation between LIRGs and ULIRGs in our sample. In Figure 3.12 we present the SDSS images for all the ULIRGs in our sample. Half the ULIRGs are apparently in an advanced merging state (the projected distance between their cores is less than 4 kpc in all cases), while the other half have already coalesced (i.e. it is not possible to resolve two cores in the SDSS images). In comparison, 98% of LIRGs have a core separation greater than 4 kpc (as shown in the top plot in Figure 3.13). Assuming that an evolutionary transition occurs from LIRG to ULIRG as star-formation increases along the merger sequence (Sanders & Mirabel, 1996; Clements et al., 1996; Dasyra et al., 2006), it is instructive to explore how quickly the LIRG-to-ULIRG transition takes place along the merger sequence. An estimate – albeit crude – can be derived for this 'coalescence timescale' using the typical separations of the LIRGs in our merger sample and the velocity dispersion of the groups that they inhabit (which is a measure of the typical relative velocities of objects in a group).

Recall that there may be a selection bias in the merger sample against ULIRGs. This is because the visual selection of mergers in GZ favours systems that have two separate cores rather than those that are in a post-starburst configuration with a single core. We therefore briefly check whether the ULIRGs in the merger sample

are representative of ULIRGs in general by extracting all 121 ULIRGs in the IIFSCz at $z < 0.1$ and inspecting their SDSS images. We find that in this general ULIRG sample, more than 90% of the systems are ones in which the cores have already coalesced while the outskirts remain disturbed, very similar to the ULIRGs in the merger sample. The *postmerger* nature of ULIRGs in the Darg et al. sample thus appears to be a typical characteristic of these systems, as has been shown in the past literature (Sanders & Mirabel, 1996; Clements et al., 1996; Dasyra et al., 2006).

In the bottom plot of Figure 3.13, we estimate a timescale for LIRGs to transform into ULIRGs along the merger sequence. To find the distance between objects we use the projected separation using the angular separation on the sky, since the line-of sight separation cannot be computed. To estimate a coalescence timescale we also require an estimate for the relative velocities of the individual galaxies. While we do not have the information to measure either the relative transverse or line-of-sight velocities (except in the 32 systems where we can measure the relative line-of-sight velocities), we use the velocity dispersion of the groups hosting these systems as an estimate for the relative velocities of the two progenitors. Note that the actual relative velocity of each LIRG in question may indeed be different to the group velocity dispersion. However, given the data available, a more accurate estimate of the relative velocity in our individual LIRGs is not possible. Following Yang et al. (2007), we estimate a group velocity dispersion for our merging LIRGs using:

$$\sigma = 397\mathrm{kms}^{-1}\left(\frac{M_h}{10^{14}h^{-1}M_\odot}\right)^{0.3217} \tag{3.1}$$

where M_h is the dark matter halo mass (measured in $M_\odot$) from the Yang et al. (2007) SDSS group catalogue. This relation was developed theoretically using simulations, and it is not based on an empirical relation from the data, hence the improbable number of significant figures in the formula.

Dividing the separations by the group velocity dispersions then yields a estimate for the coalescence timescale for the merging LIRGs (Figure 3.13). From the distribution of coalescence timescales we estimate that the timescale for the LIRG to ULIRG transformation in our sample is 145 $\pm$120 Myr. Our empirically-determined value is in good agreement with N-body/SPH merger simulations, such as those performed by Torrey et al. (2012a,b) who find coalescence timescales of $\sim$ 200Myr. The low values of the timescales may indicate that *merging LIRGs turn into ULIRGs over reasonably short timescales comparable with the dynamical timescale.*

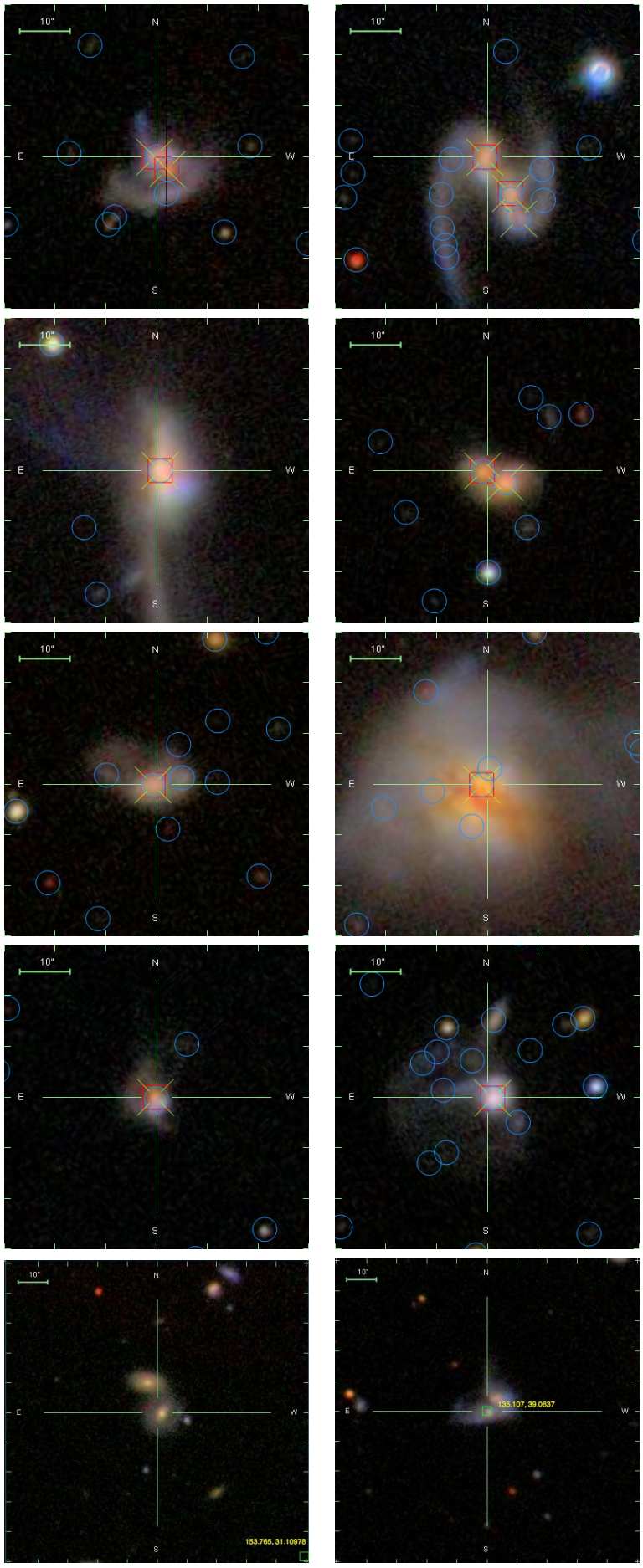


Figure 3.12: The SDSS images of the ULIRGs

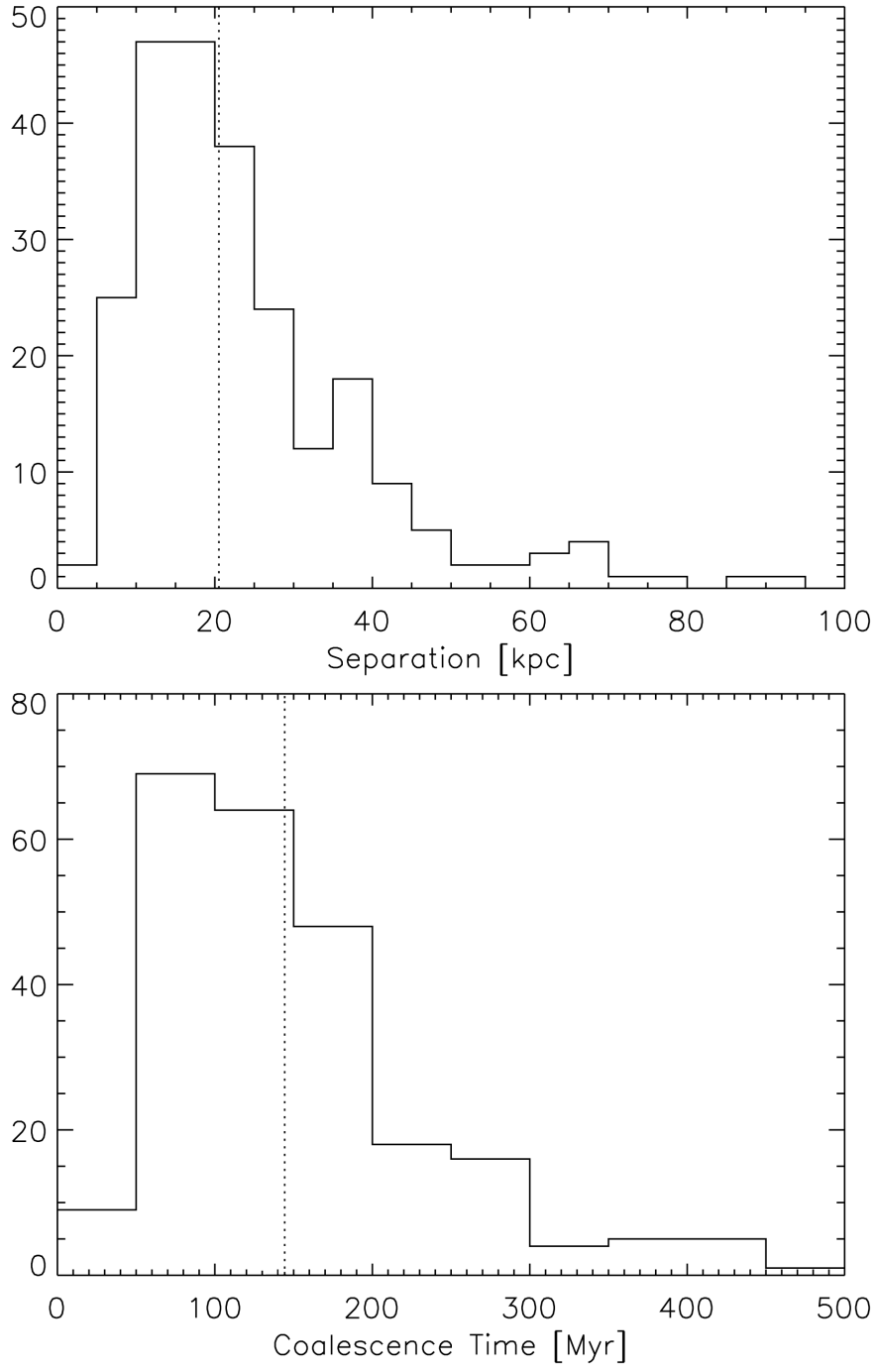


Figure 3.13: All the star-forming LIRGs in our sample have an average separation of 21 kpc. Assuming that these galaxies are the parent population of the ULIRGs, we find that the average time for a LIRG merger to coalesce is 145 $\pm 120 Myr$.

3.6 Discussion

In the last two decades it has become evident that the most infrared bright galaxies are undergoing some morphological transformation (Kleinmann & Keel, 1987; Sanders et al., 1987; Hutchings & Neff, 1987; Vader & Simon, 1987; Sanders et al., 1988a,b; Sanders & Mirabel, 1996; Clements et al., 1996; Hopkins et al., 2006; Younger et al., 2009; Hwang et al., 2010). Using the largest catalogue of visually-classified mergers we have looked at the connection between infrared brightness and morphology from the opposite angle: are interactions sufficient to generate an infrared luminous galaxy? Generally we have found that the answer is no. Only a small fraction of the Galaxy Zoo mergers are detected in the infrared by IRAS.

Understanding what separates infrared bright from infrared dim mergers is beyond the scope of this thesis and it would need a higher degree of sophistication (better constraint on infrared fluxes and positions, as well as better optical and spectroscopic data, etc) than is publicly available at the moment for these large surveys. The question is why some mergers have strong episodes of star formations and other do not. As we see in Figure 3.4 masses and redshifts may influence why a galaxy is undetected, but since infrared mergers are seen at every mass and at every redshift, the difference between detected and undetected galaxies has to be more subtle. We can hope that more sophisticated data in the next few years will lead to a more in-depth analysis of this sample with a better characterisation of the merger-infrared connection.

Our study reveals that mergers typically host higher levels of infrared flux (and therefore star-formation) when compared to a control sample of late type galaxies. Interestingly, we have not found a strong correlation between galaxy density and SFR in our mergers. An investigation of the variation of SFR with mass indicates that while SFR is intimately connected with the *total* stellar mass of the system, it shows very little dependence on the system mass ratio. We find that LIRGs (and possibly ULIRGs) can be formed without recourse to major mergers. A study of the nuclear emission-line activity shows that the fraction of systems with AGN generally increases with infrared brightness, with the nuclear emission in ULIRGs likely dominated by AGN activity.

Finally, we have explored the timescale for systems to transition from being LIRGs to ULIRGs along the merger sequence. Combining the typical separations of mergers that have LIRG luminosities and the velocity dispersion of the groups that they are likely to inhabit we have shown that the likely timescales for the LIRG to ULIRG transition is quite short, around a few hundred Myrs. Our analysis might be

unsophisticated but it is in agreement with expected results from the literature. I am confident that in the next few years more precise simulations (which can dispense of the over-simplifications associated with star-formation and AGN activities) will give a very strong constraint on the timescale and will clarify the remaining doubts on how the LIRG-to ULIRG evolution actually happens.

Chapter 4

Spheroidal Post-Mergers

4.1 Introduction

Studying how galaxies form and evolve is a fundamental step to better understanding our place in the Universe. The Universe is believed to follow a ΛCDM cosmology (e.g. Blumenthal et al., 1984; Freedman et al., 2001; Efstathiou et al., 2002; Pryke et al., 2002; Spergel et al., 2007). This model appears consistent with experimental measurements of the Cosmic Microwave Background (CMB) (e.g. Dunkley et al., 2009; Komatsu et al., 2009) and large scale clustering (e.g. Sánchez et al., 2009). A key feature of the ΛCDM cosmogony is a hierarchical bottom-up formation paradigm, with smaller bodies accreting to form progressively larger ones (White & Rees, 1978; Searle & Zinn, 1978). Small dark matter halos form first and subsequently merge to form bigger halos (e.g. Peebles, 1982; Blumenthal et al., 1984). Baryonic (gas) inflow into the gravitational potential wells created by these halos builds the stellar mass and central black holes in the first galaxies (e.g. Renzini, 1977; Fall & Efstathiou, 1980; Dalcanton, Spergel & Summers, 1997; Mo, Mao & White, 1998; Machacek, Bryan & Abel, 2001; Schaerer, 2003; Venkatesan, Nath & Shull, 2006). Observational and theoretical work has suggested that feedback from supernovae and Active Galactic Nuclei (AGN), powered by the central black holes, may regulate the star formation in galactic systems (e.g. Kauffmann et al., 2003; Di Matteo, Springel & Hernquist, 2005; Nesvadba et al., 2006; Schawinski et al., 2007b; Kaviraj et al., 2007b; Alatalo et al., 2011) (and perhaps also in systems in their immediate vicinity, see Shabala et al. (2012)) which plausibly produces the observed correlation between the mass of the central black hole and the stellar mass contained in spheroids at present day (e.g. Ferreras & Silk, 2000).

Mergers are known to play an important role in the formation of early-type galaxies (Mihos & Hernquist, 1996a; Bender, 1996, 1997), so an observational study

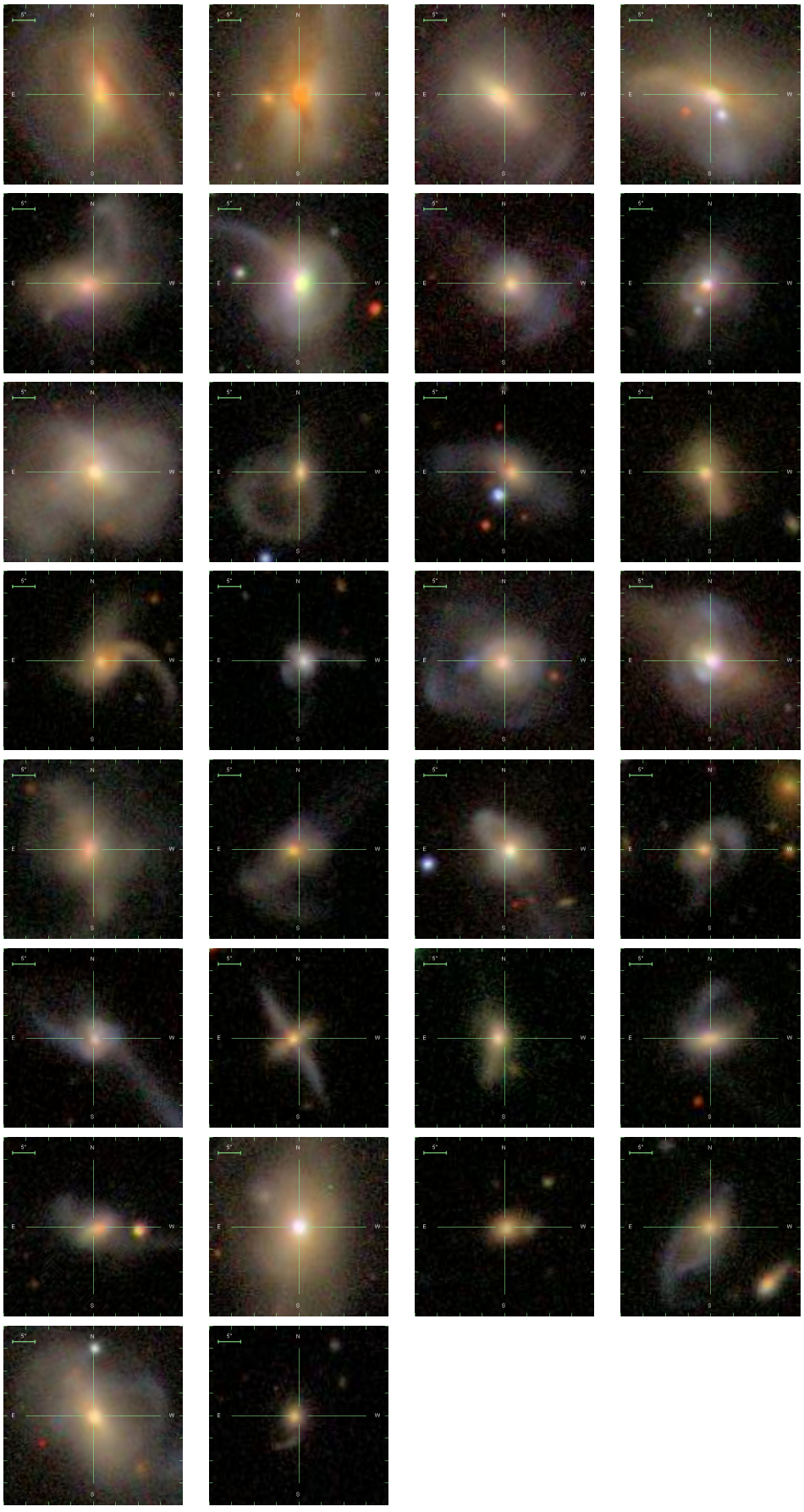


Figure 4.1: SDSS images of our sample of spheroidal postmergers.

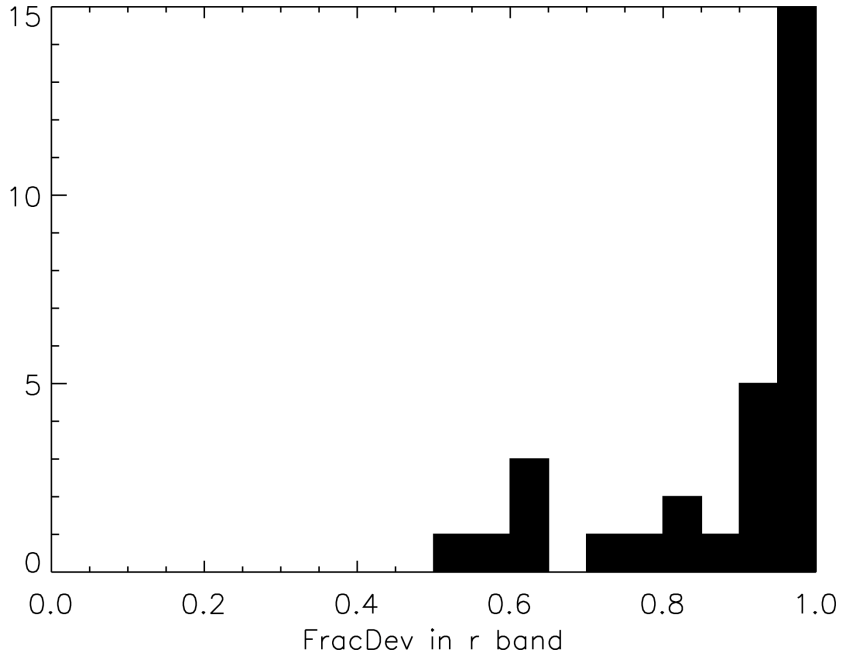


Figure 4.2: The *fracdev* parameter in the optical r band for our visually selected sample of spheroidal post-mergers. All galaxies have *fracdev* higher than 0.5 (most of them being higher than 0.8) consistent with them being bulge-dominated systems.

of merger remnants that are likely to evolve into early-type galaxies is desirable. A critical issue in studying post-mergers (and indeed mergers in general) is that perhaps the most reliable method for identifying mergers and merger remnants is by visual inspection of galaxy images.

As we discussed in Chapter 2, Darg et al. (2010b) has identified a population of 'post-mergers' in the preparation of the GZ merger catalogue. The class of galaxies consists in a system involving a single object which is morphologically disturbed (as a result of the recent merger) but in the final stages of relaxation. Now, if we aim to discover an intermediate stage in the formation of a massive elliptical galaxy we need to look for a subset of these objects in which the post-merger system has a dominant bulge, making them plausible progenitors of early-type galaxies.

In this chapter we will present an analysis of the spheroidal post-mergers (SPMs), and it is structured as follows. Section 4.2 is dedicated to the general properties of the sample. In Section 4.3 we study the local environments of our SPMs. In Section 4.4 we discuss their colours and emission line activity while in Section 4.5 we reconstruct the plausible progenitors of the SPMs. We discuss our results in Section 4.6.

4.2 The Sample

We construct a sample of *spheroidal* post-mergers (SPMs) from a parent sample of 370 post-mergers selected by Darg et al. As mentioned above, a postmerger is defined as a *single* object in which the morphological disturbances induced by the recent merger remain visible. In other words a postmerger represents the very final stages of the merger process (see Figure 2.6). We visually re-inspect this postmerger sample to select 30 objects which are clearly bulge-dominated (Figure 4.1). We note that non-bulge dominated post-mergers cannot be put in a single morphological category: they include disturbed or peculiar spirals, as well as many irregular objects.

As a sanity check of our visual classification, we use the SDSS parameter *fracdev* in the optical r band (see Table 4.1). *Fracdev* indicates the likelihood of the surface brightness profile to be modelled by a pure de Vaucouleurs profile (i.e. $fracdev \sim 1$ indicates a pure bulge, while $fracdev \sim 0$ represents a purely exponential or disk-like profile). Past work (e.g. Kaviraj et al., 2007a) has successfully used this parameter as a measure of morphology in large galaxy samples. In Figure 4.2 we plot the *fracdev* in the r band of our sample. All our SPMs have a *fracdev* greater than 0.5 (i.e. they are dominated by the 'bulge-like' profile), with most of them higher than 0.8, which is consistent with the results of our visual classification. Note that not all postmergers with high values of *fracdev* from the original sample of 370 were in fact bulge-dominated when inspected visually; a further example of the utility of employing visual inspection in conjunction with automatic techniques.

Following the estimated completeness of the Darg et al. merger sample, we expect the completeness of our SPM sample to be around 80%.

4.3 Local environments

We begin by exploring the local environments of our SPMs, using the environment parameter (ρ_g) defined by Schawinski et al. (2007a) and discussed in Chapter 2. Given the complex nature of post-mergers, we preferred this parameter to the Yang et al. because ρ is dynamically independent. The chaotic structure of our objects could bias the Yang et al. parameter to higher densities.

Knowing if the galaxy density plays a part in the evolution of galaxies is an important notion, so studying the environment should be a fundamental feature of any galaxy evolution study. The environment parameters for the sample are shown in Figure 4.3. We find that two galaxies in our SPM sample inhabit clusters ($\rho_g > 1$), while the rest are split between groups and the field. This result is expected since

SDSS ID	RA	DEC	FracDev in r	ρ	Redshift	Log(Mass)
587726102026453183	227.770	4.293	0.799	0.536	0.0420	11.552
587726102027239592	229.454	4.162	0.628	0.609	0.037	11.722
587731521205567501	132.978	40.835	1	1.08519	0.029	11.153
587731681194868806	139.212	45.700	0.948	0.084	0.026	11.073
587732484342415393	130.937	35.828	0.638	1.942	0.054	11.002
587733431923703839	253.789	26.664	0.940	1.017	0.035	11.163
587734948595236905	160.265	11.096	1	1.019	0.053	11.206
587735663161442343	153.992	39.243	1	0.547	0.0627	10.865
587735665845403787	221.437	51.580	0.894	0.0156	0.030	11.235
587735696984571992	201.726	56.889	1	0.207	0.090	11.172
587736585513795652	244.425	25.205	0.950	0.043	0.0311	10.294
587736586036969554	211.414	40.032	1	0.046	0.084	11.335
587738409785557168	143.447	10.811	0.711	0.00676	0.085	11.758
587738946141552732	169.385	37.963	0.943	0.098	0.096	10.799
587738947747053602	154.640	36.224	0.851	0.591	0.054	11.056
587739707951808602	227.963	23.151	1	0	0.052	11.171
587741533323526200	173.781	29.891	0.857	0.103	0.046	10.980
587741533859414124	171.142	30.095	1	0.148	0.055	10.722
587741600963690567	198.656	26.123	1	0.079	0.074	11.251
587741708326469917	128.289	15.398	1	0.219	0.076	10.802
587741709954121847	168.418	27.241	0.658	0.453	0.037	10.263
587742062680015040	176.183	23.162	1	0	0.048	10.621
587744874792222779	137.156	14.122	1	0.158	0.0882	11.080
588007005789683827	196.060	65.345	0.598	0.412	0.083	11.087
588013382183944595	119.951	27.838	0.536	0.0442	0.067	10.977
588015508746338312	31.566	-0.2914	1	0.529	0.0426	11.329
588017565490872652	187.554	11.770	0.922	1.459	0.089	11.012
588017705071214745	164.196	12.762	0.963	0.5035	0.092	11.421
588017978367934481	218.326	34.734	0.996	0.288	0.034	11.190
588017978895892603	193.458	39.738	1	0.259	0.092	10.814

Table 4.1: SDSS ID, RA, DEC, r-band *fracdev*, environment parameter ρ, spectroscopic redshift and stellar mass for our sample of postmergers. Stellar masses are estimated using the calibrations of Bell et al. (2003)

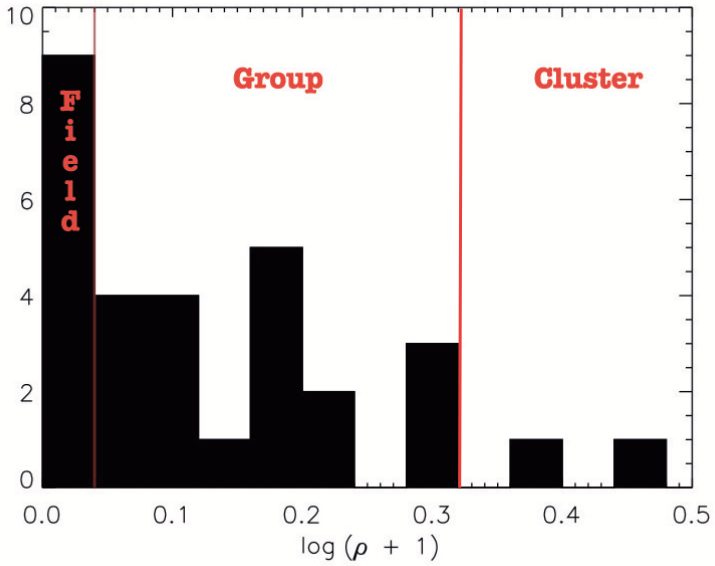


Figure 4.3: The values of the environment parameter (ρ) for the sample: two galaxies in our sample inhabit clusters ($log(\rho + 1) > 0.32$), with the rest split between groups ($0.04 < log(\rho + 1) < 0.32$; the 0.04 is due to the binning) and the field. See text for details.

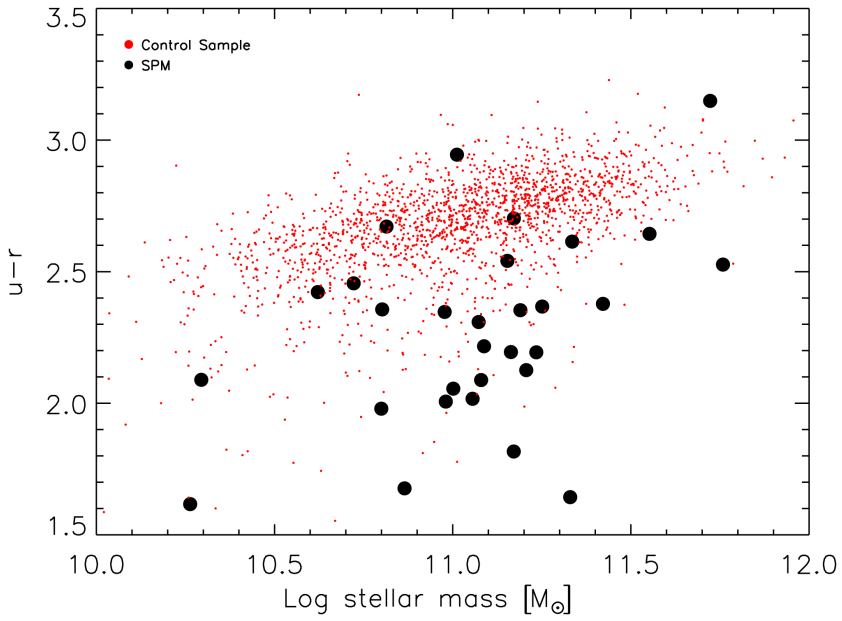


Figure 4.4: The $(u-r)$ colour-mass relation of the spheroidal postmergers (large black circles), compared to a control sample of early-type galaxies from the SDSS (red dots).

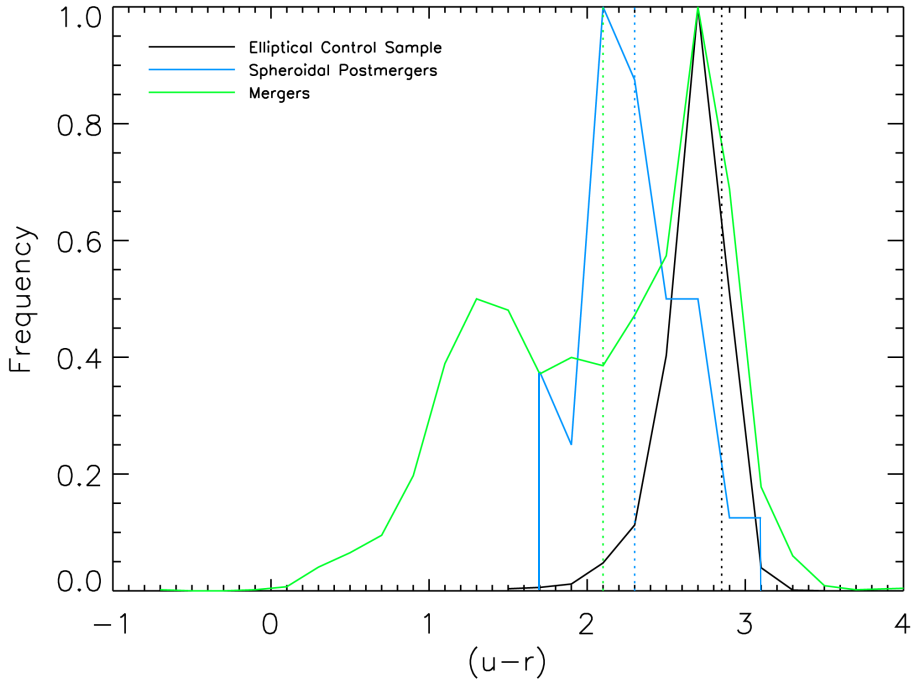


Figure 4.5: Histogram of $(u - r)$ colour of the SPMs, ongoing mergers from the catalogue of Darg et al. and a control sample of early-type galaxies from the SDSS. The dotted lines are the median values for the populations.

the high peculiar velocities of the galaxies in dense environments such as clusters make collisions unlikely. In very sparse environments, there are not enough galaxies around to produce many merger events, hence we find the post-merger population spread between intermediate and low-density environments.

4.4 Colours and emission line activity

We use the SDSS system to extract the *ugriz* colours for our SPMs. The colours are K-corrected according to the technique devised by Blanton & Roweis (2007) using the IDL routine `KCORRECT`(version 4.2). K-correction is used to obtain the precise flux measurement of a given astronomical object, independent of redshift, like it was in the rest frame.

In Figures 4.4 and 4.5 we compare the colours of the SPMs to both an early-type control sample and the *ongoing* mergers from Darg et al. The stellar masses used in Figure 4.4 are estimated using the mass-to-light ratio calibrations of Bell et al. (2003)

$$log_{10}(M/L) = a_\lambda + (b_\lambda \times color), \tag{4.1}$$

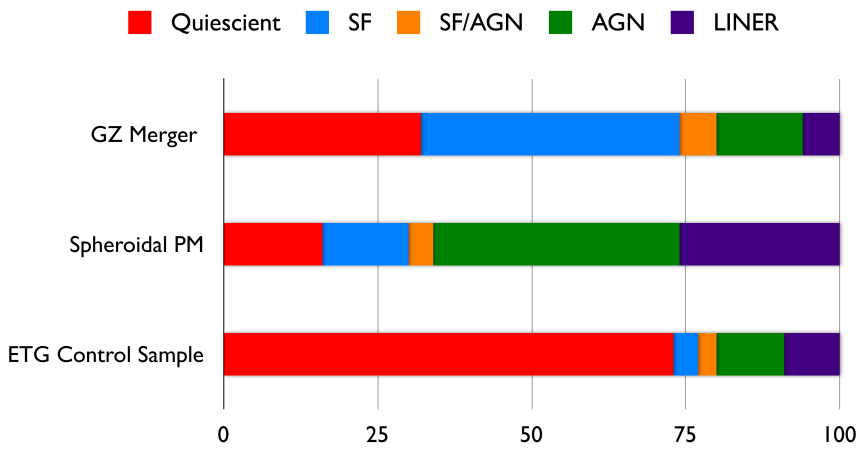


Figure 4.6: Emission-line analysis of the SPMs compared to the ongoing mergers from Darg et al., and a control sample of early-type galaxies from the SDSS. The dominant emission-line type in the ongoing mergers are star-forming galaxies, while the dominant type in the SPMs and early-type controls are AGN and quiescent galaxies respectively. The AGN phase appears to dominate the postmerger phase in the morphological sequence.

where M/L is in solar units, and a and b are coefficients depending on a specific colour (Bell et al., 2003). We then use the optical fluxes to calculate an optical Luminosity and finally compute the values for the stellar mass. According to Bell et al. (2003) the uncertainties on the mass are on the order of $\sim$ 0.1 dex in the optical. The early-type control sample is constructed using the GZ early-type galaxy catalogue restricted to the redshift and magnitude range of the Darg et al. mergers (see Darg et al., 2010b). Figure 4.4 shows that our objects occupy the same mass-space as the ETG population, although showing bluer colours. This is better shown in Figure 4.5 where we see that the vast majority (85%) of our SPM sample have bluer colours than the mean colours of the early-type control population. These blue populations are likely to contain both young stars formed in the recent merger as well as remnants of the blue stellar populations in the original progenitors. However, they are typically not bluer than the population of ongoing mergers from Darg et al. (2010), which suggests that the star-formation rate is subsiding in the post-merger phase. The presence of a significant fraction of SPM with colours consistent with early-types could be due either to a merger involving an ETG or to old SPMs.

There is still some debate on exactly when the star formation activity peaks during the merger process (Barton, Geller & Kenyon, 2000; Lambas et al., 2003; Nikolic, Cullen & Alexander, 2004; Di Matteo, Springel & Hernquist, 2005; Schawinski et al., 2009), our results suggest that it peaks prior to the final coalescence

of the merger progenitors, since the SPMs lie intermediate between the ongoing mergers and early-type control sample.

We use optical emission-line ratios (see e.g. Baldwin, Phillips & Terlevich, 1981) to explore the emission-line activity in the SPM sample and compare it to what is found in the control sample of early-type galaxies and the ongoing mergers from Darg et al. Emission lines are calculated using the public GANDALF code (Sarzi et al., 2006). The majority of the SPMs display Seyfert-like emission (42%) with the rest being either LINERs (26%), star-forming (16%), or quiescent (16%) objects (Figure 4.6). In comparison, the dominant emission-line type in the ongoing mergers is the star-forming population, while the dominant type in the control early-types are quiescent objects. Together with the higher fraction of LINERs in the SPMs (which are likely to be post-starburst galaxies, see e.g. Sturm et al. (2006); Sarzi et al. (2010)), and since it has not been possible to identify blue Compton-thick AGN in the local universe (Schawinski et al., 2009), our results suggest that these objects have gone through a gradual transition from being dominated by star formation in the merger phase to AGN activity in the post-merger phase, followed by quiescence when the objects have transitioned to being relaxed spheroids. While the small number of SPMs makes a robust conclusion difficult, our results suggest that, not only is there a delay between the onset of star formation and AGN activity, in agreement with several studies in the literature (Schawinski et al., 2007b; Wild, Heckman & Charlot, 2010; Darg et al., 2010a), *but that the peak of AGN activity may coincide with the post-merger phase of the merger process.* Note that, in this case, the delay between the onset of star formation and AGN activity could be expected to be around the coalescence timescale of the merger, which is around 0.5-1 Gyr for a major merger (Cox et al., 2006a; Lotz et al., 2008). This appears consistent with the time delays derived from spectral fitting in recent work (Schawinski et al., 2007b; Wild, Heckman & Charlot, 2010; Darg et al., 2010a).

4.5 Reconstructing the progenitors

In this section we explore the plausible progenitors of the SPM sample. Under the reasonable assumption that the sample of ongoing mergers in Darg et al. are the progenitors of the SPMs, we first search for merging systems which have a summed mass within 0.3 dex of the mass of the SPM in question. We use 0.3 dex as the tolerance because it is consistent with the typical mass error. We assume that major mergers of all morphological types (elliptical-elliptical, elliptical-spiral and spiral-spiral) produce spheroids (e.g. Khochfar & Silk, 2006) and that, from simple

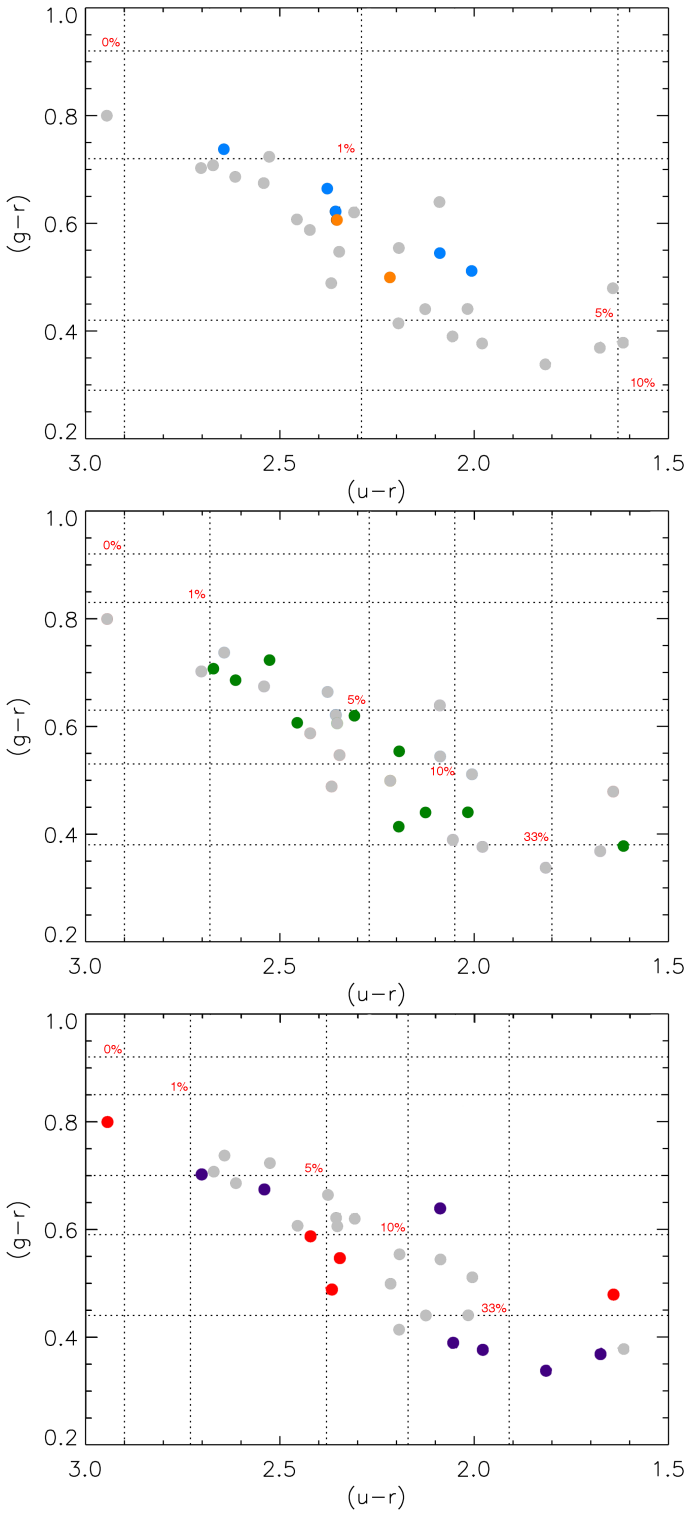


Figure 4.7: Comparison of the colours of the spheroidal postmergers to a simple model, designed to approximate the stellar content in these galaxies. TOP: The plot shows the model for a second burst at an age of 0.2 Gyr (grey dashed lines) and we compare it with the star-forming SPMs (blue star-forming, orange star-forming and AGN). MIDDLE: The second burst in this model is at 0.5 Gyr (grey dashed lines) and we overplot those SPMs that show AGN activity (green). BOTTOM: This model has a second burst at 0.6 Gyr of age (grey dashed lines) and it is used as a comparison for Quiescent (red) and LINER (purple) SPMs.

dynamical considerations, all minor mergers whose major partner is an elliptical will create a spheroid. Note that the merger catalogue of Darg et al. is not expected to be biased against minor mergers with mass ratios between 1:4 and 1:10. The median mass ratios for the SPMs, under these assumptions, are between 1:1.5 to 1:3, with a tail to lower values, suggesting that these systems are typically remnants of major mergers.

In most of our galaxies a significant minority of the stellar population is likely to have formed in the recent merger-driven burst of star formation; so another way to explore the morphologies of the progenitors is to estimate the amount of stars formed during the recent merger. To do so we make a simple comparison of the SPM colours to the expected colour of a passively evolving old population idealised early-type galaxy at the present day (e.g. Bower, Lucey & Ellis, 1992; Bender, 1997; Cox et al., 2006a; De Lucia et al., 2006; Kormendy et al., 2009). Figure 4.5 show us that the u-r colours of the SPMs are bluer than the ETG population, so we assume that recent star-formation in a system will have a significant impact on the visible colours of our objects.

To investigate the star formation histories of the SPMs further, we study simple models in which a young population, formed in an instantaneous starburst, is superimposed on an old population that is also formed in an instantaneous event. Stellar populations are modelled using the latest version of the population synthesis code of Bruzual & Charlot (2003). This is illustrated in Figure 4.7, where the idealised early type galaxy model is parametrised by two instantaneous starbursts; the first one was fixed to 10 Gyr in the past (since the bulk of the stars in early-type galaxies form at high redshift). The instant of the second burst is allowed to vary and we selected values between 0.2 Gyr and 0.6 Gyr ago. The horizontal and vertical lines indicate the mass fraction of the young stellar population contributed by the second burst. We assume that the old population is formed at $z = 3$ and has solar metallicity, since this is typical of the old, metal-rich stellar populations that dominate nearby early-type galaxies (e.g. Trager et al., 2000). Our models assume a monolithic collapse and no star formation for early-type galaxies in the last 10 billions years. While this is useful to compare ETG-like object, it should not be interpreted as a rigorous way to model ETGs. The free parameters in the code are the age, mass fraction and metallicity of the recent (young) starburst and the average dust content ($E_{(B-V)}$) of the system. Metallicity is an important parameter when it comes to colour analysis, due to its strong correlation with colour changes. More metals result in a redder stellar population. This is due to the two phenomena of *line blanketing*, since metals in the atmosphere of stars absorb preferentially blue

light, and *opacity*, due to the the energy absorption of the metals from the interior of the stars inducing red giants to swell up more.

We explore ages for the recent starburst between 0.2 and 0.6 Gyrs, which bracket the coalescence timescales for major mergers in the literature (Cox et al., 2006a; Lotz et al., 2008). We explore metallicities between 0.75 and 2 $Z_{\odot}$ which is the scatter in the mass-metallicity relation of galaxies in our mass range in the local Universe (Tremonti et al., 2004). We assume a median $E_{(B-V)}$ of 0.05, derived by recent UV-optical studies of nearby early-type galaxies (Kaviraj et al., 2007b; Schawinski et al., 2007b).

Early-type galaxies are largely devoid of gas. Gas fractions in early-types within the mass range considered in this study are typically (much) less than 5% (Kannappan, 2004; Young, 2002). Mergers that have two early-type progenitors are therefore very unlikely to produce more than 5% in mass fraction of young stars. By comparing the $(u-r)$ and $(g-r)$ colours of the simple models with the observed colours of the SPMs, we estimate how many of our postmergers may be the product of mergers between two early-types and therefore how many are likely to require at least one late-type progenitor.

This analysis is limited by the lack of a complete knowledge of our objects' star-formation history. A way around is possible by making their emission line signatures a significant discriminant. The merger event cannot be dated but we can safely assert that star-forming SPM should be modelled with a younger star-burst than AGN showing ones. The same applies when comparing the AGN dominated objects with Quiescent or LINER SPMs. Basing our approach on these assumptions we compare the object with different models. Our analysis is shown in Figure 4.7. For star-forming and mixed star-forming/AGN emission lines spheroidal post-mergers we model the youngest star-burst in our range at 0.2 Gyr. We find that all of these objects have only a tiny fraction of their stars in the most recent star-burst. The situation is significantly different for the other objects in our sample. 7 out of 10 (with $g-r<0.63$) AGN hosting SPMs need more than 5% of their stars to have formed recently. As mentioned before, this scenario is unlikely to happen during a merger of ETGs. The same applies for LINER and quiescent galaxies: they need a substantial star-formation episode to explain their colours. In particular 1/3 of the LINER and quiescent objects have colours consistent with a spiral-spiral mergers. Changing the metallicity in the models does not alter our results; in the most extreme cases of high-metallicity starburst even more galaxies get beyond the 5% limit.

Although we previously employed a control sample to compare the colours, the masses and the emission-line activity of our objects, we did not used it in this

section; the model here described represents an ideal elliptical galaxy going through two instantaneous bursts of star formation, which is an incredible simplification of how early-type galaxies form. Comparing the model to the control might give us some insights on the life of real ellipticals, but it will not be contributing in improving our understanding of the SPM.

The colours do not include the AGN contribution. The percentage is definitely sensitive to the assumptions, and we go from a minimum of 33% of our galaxies being spiral spirals mergers to a maximum of about 80%. We average the different models giving higher weights to more likely models and we are confident that $\sim$55% are likely to have formed in a merger involving at least one gas-rich i.e.late-type galaxy, with only a minor fraction formed in a merger between two early-type objects. The remaining objects have colours in a locus of the colour-colour diagram too susceptible to the changes of the parameters to allow a secure prediction.

4.6 Discussion

Understanding post-merger galaxies gives more solid foundation to galaxy evolution models. Most of our results confirm previous expectations, such as a brief transition from blue to red in colour magnitude space after some cataclysmic event which deeply alters their morphology. Our colour and emission line results point directly to this scenario. The colours of our spheroidal post-mergers sit perfectly in a region between the red and blue galaxies.

The emission line activity is also paramount in understanding what part these transient objects play in the evolution of massive galaxies. We find only a minor fraction of the sample to have ongoing star-formation, and yet the colours indicate a young stellar population to be present. This result, combined with the high incidence of AGN-like activity in the core of our galaxies, is another indication of the deep connection between the quenching of star formation and the ignition of the active galactic nucleus.

The first of our findings is very simple. The total mass of the SPM compared to the mass of galaxy pairs in the original Galaxy Zoo merger catalogue implies these objects are remnants of major merger events. This result holds against a diametrically different check: there is evidence that bulgeless galaxies can maintain their nuclear region status quo even during merger if the mass ratio between the two objects is less than $1:4$ (Brook et al., 2012; Simmons et al., 2013).

The other result in our progenitors discussion is the statistical prediction, based on a colour-colour analysis, of the morphology of the parent population of our

spheroidal post-mergers. While having an ulterior confirmation that the end product of a spiral-spiral merger can be a spheroidal galaxy (Toomre, 1976, 1977) is a good result per se, although the more considerable finding is that a good fraction (15%) of SPMs are more likely the product of a elliptical-elliptical collision. These galaxies are clear evidence of dissipationless dry mergers, which are the mechanism which has been advocated to explain the mass build up of ETGs at $0 < z < 1$ (Bell et al., 2005; van Dokkum, 2005). It is also interesting to point out that mergers between ETGs have been put forward to explain massive ETGs of unusual shape, e.g. Graham et al. (2012).

If resources were no problem it would have been interesting to obtain independent metallicity analysis for the sample. Using that data, we could constrain the star-formation history in such a way that both the progenitor analysis and the feedback timescale would be tailored more precisely to each individual galaxy. Another worthwhile approach in the construction of a detailed galaxy evolution model would need well matched and homogeneously analysed sample of galaxies in the pre-merger phase.

Chapter 5

Star-forming Early-type galaxies

5.1 Introduction

Studies on the infrared properties of early-type galaxies (ETGs) are limited. It was long assumed that all ETGs shared a common destiny of passive ageing. It is generally believed that the far-infrared emission from these objects depends upon the dust heating from the old stellar radiation field (Lonsdale Persson & Helou, 1987; Buat & Deharveng, 1988; Rowan-Robinson & Crawford, 1989; Sauvage & Thuan, 1992, 1994; Walterbos & Greenawalt, 1996). This interpretation is correct for a large proportion of early-types, and evidence for their passiveness and age derives from relatively low Hα and UV emission .

However, evidence in the last two decades demonstrates that there is a more active sub-population of ETGs that require in-depth examination. As mentioned in Chapter 3, estimating the star-formation rate from the far-infrared is dependent on the quantity of dust and the presence of a young stellar population. The general ETG properties make the FIR seem unsuitable to extract a SFR value for these objects. However, it has been argued that even for early-types, the 40 to 120 μm emission is still dominated by young stars (Devereux & Young, 1990; Devereux & Hameed, 1997). Past studies of star formation in ETGs have employed UV as the principal marker of Star-formation. Unfortunately the UV has limitations in terms of the UV upturn and dust obscuration so we need complimentary information in the longer wavelengths to get a more complete picture. The advantage of using UV data is shown in Figure 5.1. A small mass fraction (<3%) of young (<1 Gyr old) stars strongly affects the rest-frame UV at wavelengths smaller than 3000Å, while its influence on the optical part of the spectrum is relatively weak and could be confused for other phenomena (Kaviraj et al., 2008). Optical colours can be used as estimator but they are not at all precise. Our models in chapters 4 worked because we were

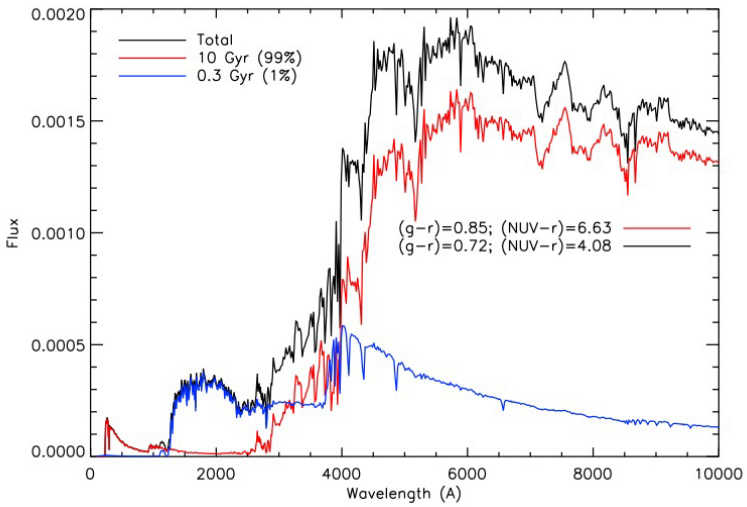


Figure 5.1: This plot shows the sensitivity of UV to small mass fractions of a young stellar population. The model was constructed by us with a 99% old stellar component (10 Gyrs) and 1% young stars (0.3 Gyrs), respectively in red and blue in the plot. The combined SED is shown in black, and its UV output comes exclusively from the young stellar component. The stellar populations were computed using the synthesis code of Bruzual & Charlot (2003), using a Chabrier initial mass function (Chabrier, 2003).

comparing ETG-like objects to an ideal (and somewhat) unreal ETG. Comparing real early-types with that model will probably suggest unphysical star-formation in our objects. In most cases if we use just the visible filters, we would not notice the presence of recent star formation. However if we use a UV sensitive telescope, the difference between an old stars dominated and a young stars dominated spectrum is so large that we can confidently determine recent star formation. Under these conditions, using UV is an obvious choice to better understand the evolution of galaxies and their recent star formation history.

Nevertheless, UV photometry has its limitations. The analysis of the rest-frame UV properties of galaxies at lower redshifts (z <0.2) is complicated by the fact that their UV spectra may contain contributions from both young and old (> 9 Gyrs old) stellar populations. This phenomenon, known as the *UV upturn*, is produced by core helium-burning stars on the evolved horizontal branch (HB) (Lee & Yi, 1999). Another problem is dust obscuration. Silicate dust grains absorb shorter wavelengths, causing a flux loss. To solve this issue, several spectroscopic indicators can be employed, such as the $H\beta$ index or higher order Balmer lines such as $H\gamma$ and $H\delta$ and the D4000 break.

For a more complete understanding we need to look at longer wavelengths, as a significant amount of UV photons produced by young stars are absorbed and

subsequently re-emitted in the Far-Infrared/Submillimetre. Although powerful, the dust-star-formation connection (Kennicutt, 1998) is not perfect (dust can be heated up by an old stellar field). But, when applied with the right methodology, this connection can give us information about the general properties of galaxies. It has been difficult to investigate this connection for ETGs: being mostly gas and dust-poor, it was determined that only 12% of ETGs have a significant amount of warm dust (Bregman et al., 1998). For a long time, we did not have instruments sensitive enough to probe the colder dust seen dominating other galaxies in the local universe (Dunne & Eales, 2001; Vlahakis, Dunne & Eales, 2005). In recent years, ETGs have been probed with more accuracy and an increasing number of objects with cold dust have been detected.

Several studies have examined the active side of early-type galaxies via their UV emission, dust or gas content (Zabludoff et al., 1996; Goto et al., 2003; Quintero et al., 2004; Fukugita et al., 2004; Temi et al., 2004; Leeuw et al., 2004; Yi et al., 2005; Martin et al., 2005; Vlahakis, Dunne & Eales, 2005; Temi, Brighenti & Mathews, 2007; Kaviraj et al., 2007a; Stickel, Klaas & Lemke, 2007; Kaviraj et al., 2008; Leeuw et al., 2008; Savoy, Welch & Fich, 2009; Schawinski et al., 2009; Skibba et al., 2011; Rowlands et al., 2012). These studies play a fundamental role in expanding our knowledge of the general ETG population. They demonstrate that early-type galaxies are not old and passively evolving. Given that fact that they dominate the stellar mass density in the local Universe (Bernardi et al., 2003; Kaviraj et al., 2013a), it is clearly desirable to understand the processes that drive the continuing star formation in these systems. For this reason, we focus on the most active class of early-types; we set out to compose a catalogue of local star-forming early-type galaxies (SF-ETGs).

This chapter focuses on the composition and analysis of the largest catalogue of star-forming early-type galaxies in the local Universe. In section 5.2 we discuss the general properties of our FIR-selected ETG sample. In section 5.3 we study their local environments, while in section 5.4 we discuss their UV-optical colours, star-formation properties, and the IRAS-derived dust content of our ETGs. In section 5.5 we discuss their emission-line properties. We present a discussion of our findings in section 5.6.

5.2 A sample of FIR-detected early-type galaxies

To construct our sample we start with the Imperial IRAS-FSC Redshift Catalogue (IIFSCz; Wang & Rowan-Robinson, 2009), which has 60303 galaxies selected at

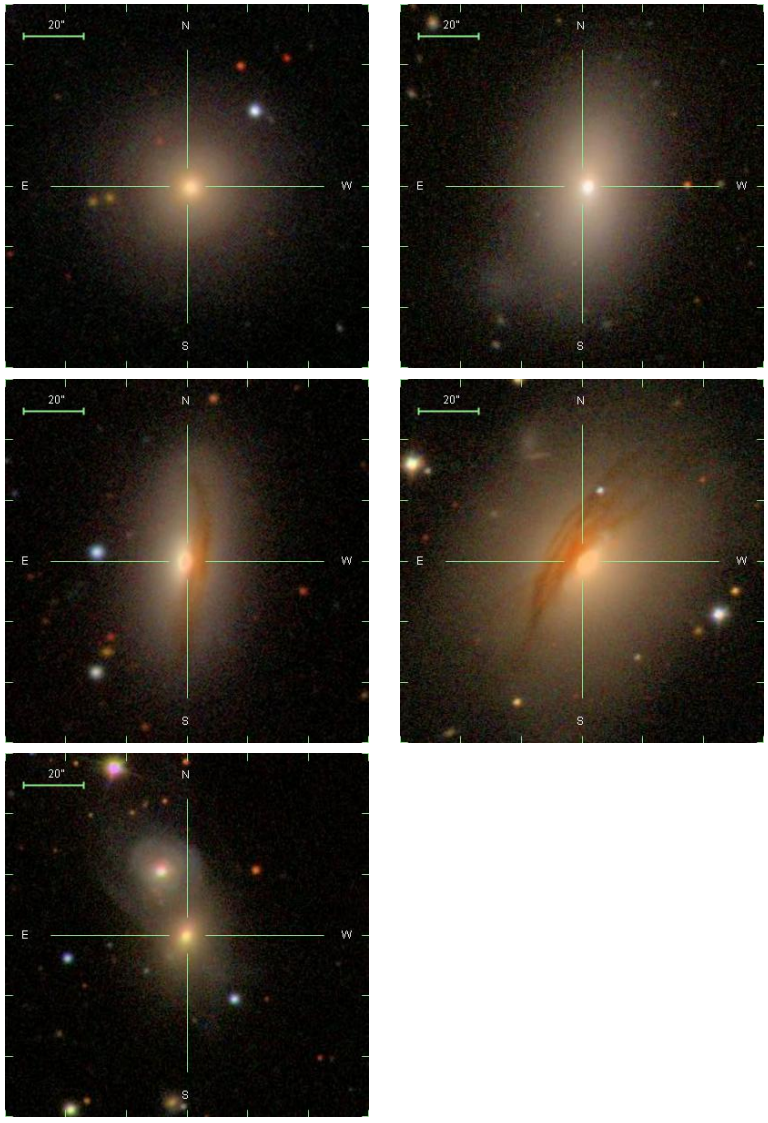


Figure 5.2: Examples of the 5 morphological star-forming ETG sub-classes. In order we have, relaxed, disturbed, dusty, dusty and disturbed and merging.

60 μm from the IRAS Faint Source Catalogue (FSC;Moshir, Kopman & Conrow (1992)), cross-matched to the SDSS DR6 (Adelman-McCarthy et al., 2006). The IIFSCz catalogue includes accurate positions, identifications (optical, NIR and/or radio), and spectroscopic redshifts (55% of the sample, e.g. from the Sloan Digital Sky Survey York et al., 2000). For our study we focus exclusively on the subset of the IIFSCz that has SDSS spectra and in which galaxies have $M(r) < -19.03$ and redshifts $z < 0.05$. The magnitude and redshift cuts make our sample volume-limited, because the SDSS has a spectroscopic limit of $r \sim$17.77. We visually inspect all of the galaxies in the IIFSCz (after our magnitude and redshift cuts are applied) to select 382 objects that have early-type morphology. The ETGs are further divided into the following morphological classes:

- Relaxed ETGs (159 galaxies), which do not show any morphological disturbances at the depth of the standard SDSS images
- Disturbed ETGs (89 galaxies), which show morphological disturbances
- Dusty ETGs (44 galaxies), which exhibit dust features but no morphological peculiarities
- Disturbed and dusty ETGs (71 galaxies), which show both dust features and morphological disturbances
- Merging ETGs (19 galaxies), which are involved in ongoing mergers with other galaxies

In Figure 5.2 we show examples of the different morphological sub-classes.

Finally, we cross-match the resulting sample of 382 galaxies with the GALEX Data Release 6 (Martin et al., 2005) to add GALEX far-UV and near-UV photometry to our catalogue.

5.2.1 Control samples

To enable us to compare our FIR-detected ETGs to the general galaxy population we construct two control samples. The first consists of a random sample of 806 late-type galaxies from the IIFSCz. The second is a sample of 800 ETGs from the catalogue of (Kaviraj et al., 2007b), which were also selected by eye in the same way as our FIR-detected ETGs. Both control samples have the same redshift and magnitude distribution as our sample of FIR-detected ETGs.

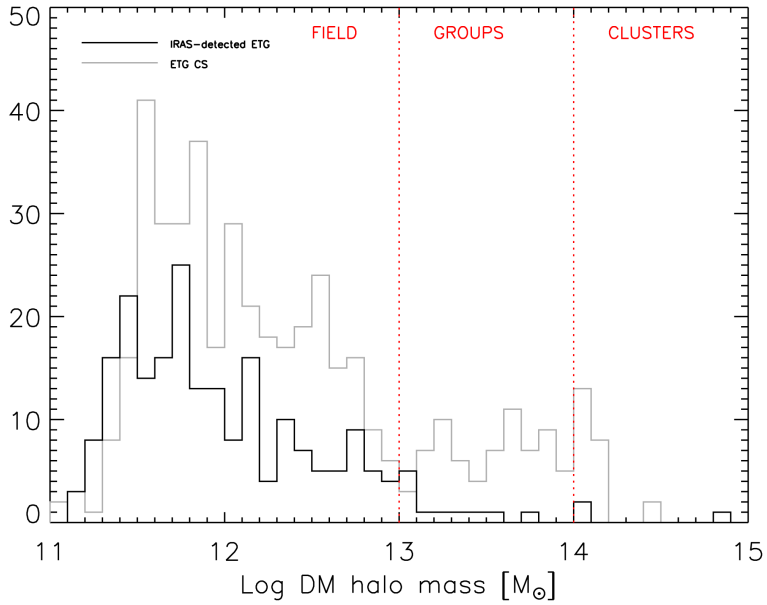


Figure 5.3: We compared the environments of our SF ETGs with an elliptical control sample. The environment parameter is the group mass from the Yang catalogue (Yang et al., 2007). We run a KS test and we find that the probability that the two samples are the same is $< 10^{-5}$.

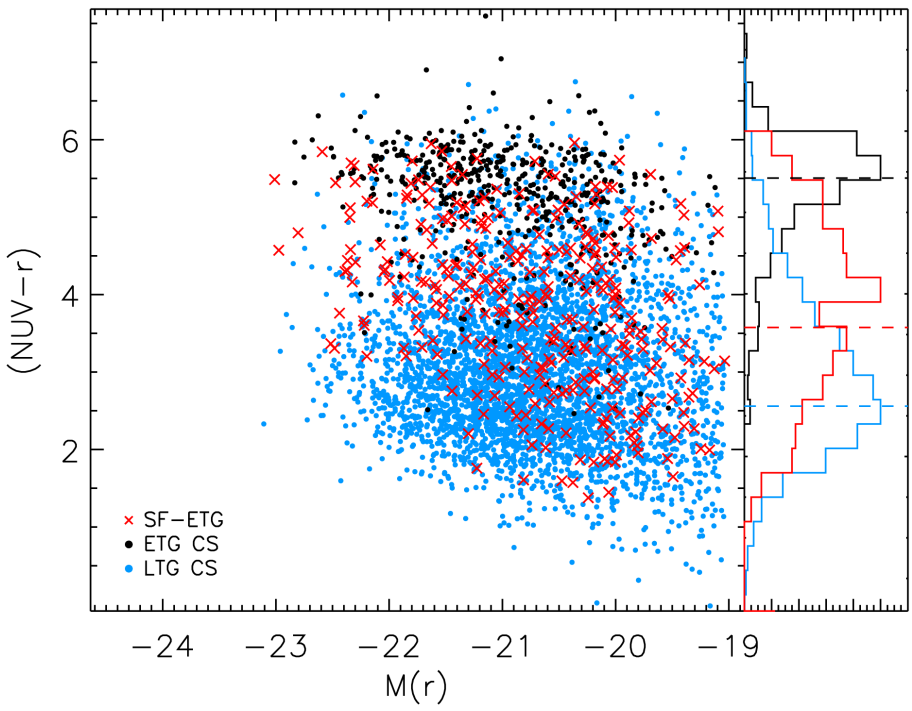


Figure 5.4: UV-optical colours of the FIR-detected ETGs (red), the early-type control sample (black) and the late-type control sample (blue).

5.3 Environment

We begin by comparing the local environments of our FIR-detected ETGs with the ETG control sample (Fig 5.3). The environment parameter employed here is the (dark matter) halo mass from the catalogue of Yang et al. (2007), M_h. We introduced this parameter in Chapter 3, when we calculated the velocity group dispersion of our infrared-selected mergers. M_h is a good estimator of the environment as isolated galaxies will have a smaller halo, while galaxies in denser environments will inhabit larger halos. Unlike the general ETG population, the FIR-detected ETGs reside almost exclusively in halos with masses less than 10^{13} $M_\odot$ (which correspond to groups and the field). A KS test indicates that the probability that the two samples are drawn from the same parent environment distribution is $< 10^{-5}$. The preponderance of low-density environments for the FIR-detected ETGs appears consistent with previous work that suggests that the star formation in the ETG population is driven by interactions (which are known to be more frequent in lower density environments, see e.g. Darg et al., 2010a) and not via internal processes such as stellar mass loss (Kaviraj et al., 2012; Carpineti et al., 2012). It is also interesting to note that the relaxed SF-ETGs show no preference for higher density regions, which also implies that the star formation in these objects is also likely to be driven by interactions. It is worth noting here that the shallow depth of the standard SDSS images (54 s exposures) means that tidal features from mergers (especially those from minor interactions) are not visible. Thus the relaxed ETGs quite possibly do carry tidal features, which only become visible in deeper imaging (see e.g. Kaviraj et al. (2011); Lee & Yi (2013))

5.4 Colours, star formation and properties of the inter-stellar medium

Before we can discuss star-formation properties, we need to find evidence of a young stellar component. To do so, we need UV emission, or alternatively, optical colours consistent with star-forming galaxies. We use near-UV colour from GALEX and optical colours from the SDSS to achieve this. Figure 5.4 presents the UV-optical colours of the FIR-detected ETGs, compared to the LTG and ETG control samples. The FIR-detected ETGs primarily lie in the green valley and blue cloud with very few occupying the broad UV red sequence on which most of the control ETGs lie. Indeed, the colours of the FIR-detected ETGs are more consistent with those of the control LTGs (a KS test indicates a probability of 23% that they are drawn from

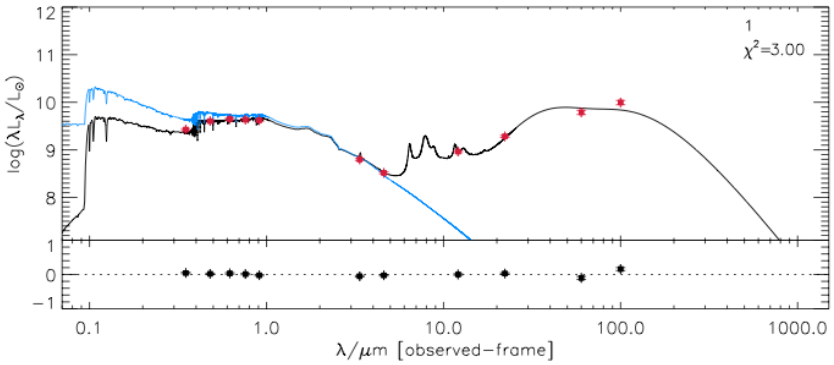


Figure 5.5: An example of the output SED produced by `MAGPHYS`. Our data is in red, the purely-star-forming model is blue and the composite is in black.

the same parent $(NUV - r)$ distribution) than the control ETG sample.

To analyse the star-formation properties of the sample we use the `MAGPHYS` code (da Cunha, Charlot & Elbaz, 2008), which assumes that UV-optical flux emitted by stars is absorbed by dust, and re-radiated in the far-infrared. Maximum-likelihood estimates for parameters (e.g. stellar mass, star formation rate, dust mass, etc.) are calculated by comparing galaxy photometry to a library of `MAGPHYS` model spectra (covering the submillimetre to the ultraviolet), which include a wide variety of stochastic star-formation histories, metallicities and dust attenuations, that are matched to dust-emission models using the aforementioned energy-balance method. Stellar populations are modelled using the latest version of the population synthesis code of Bruzual & Charlot (2003), using a Chabrier initial mass function (Chabrier, 2003). This is defined as:

$$\xi(m) = \begin{cases} km^{-\alpha} & \text{for } m > 1M_{\odot}. \\ 0.086\frac{1}{m}\exp\frac{(-log(m)-log(0.22))^2}{2\times 0.57^2} & \text{for } m < 1M_{\odot}. \end{cases} \tag{5.1}$$

where m is in solar masses, k is a normalisation coefficient (with a value of 0.135) and $\alpha = 2.3 \pm 0.3$.

The infrared models contain SEDs with different temperature dust components:

- Polycyclic aromatic hydrocarbons (PAHs) (T $<$ 2000K)
- Hot dust (130-250 K)
- Warm dust in birth clouds (30-60 K)
- Cold dust grains in the ISM (15-25 K)

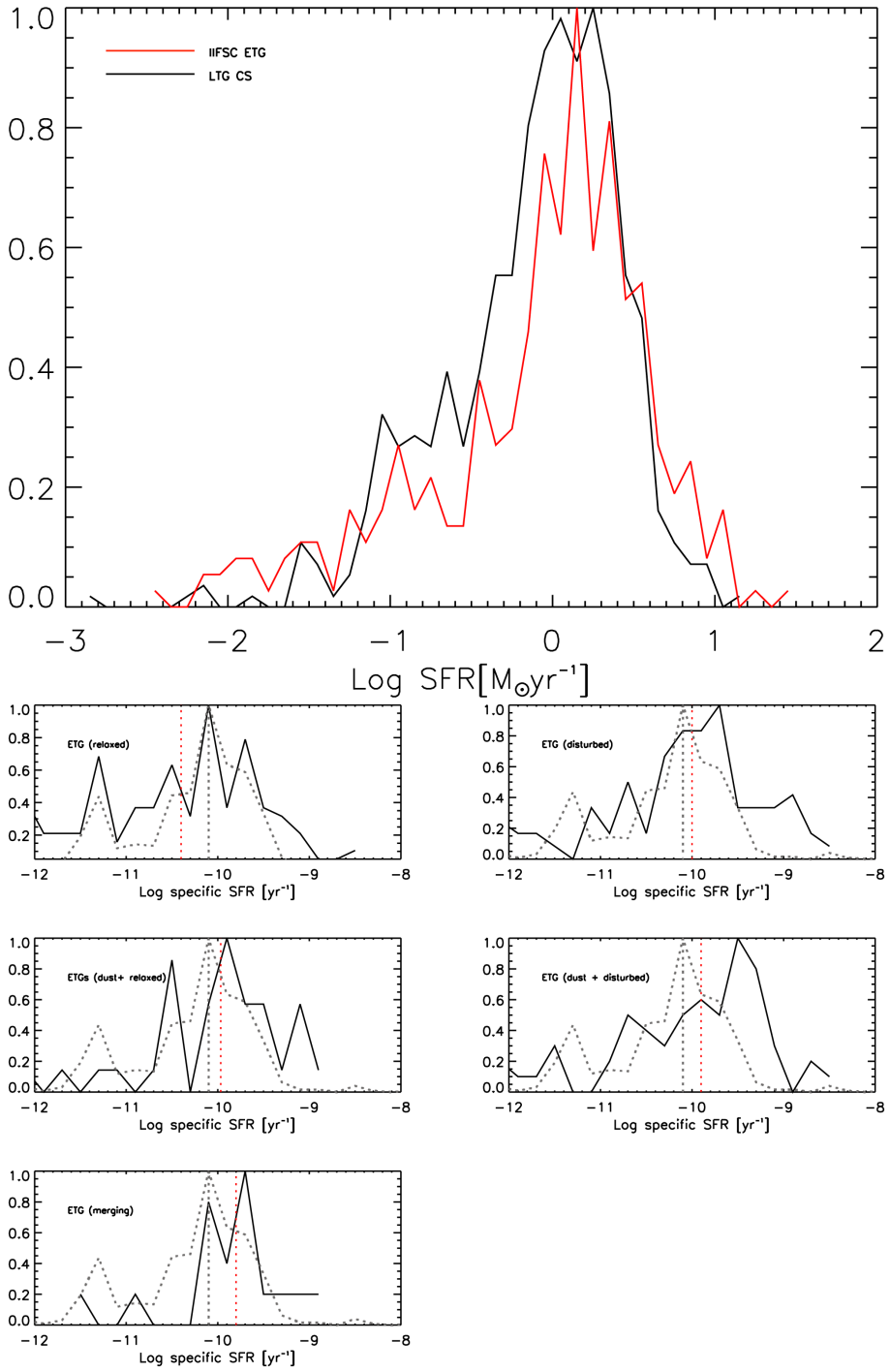


Figure 5.6: TOP: MAGPHYS-derived star formation rates (SFRs) of the FIR-detected ETGs and LTG control sample. The median SFR is $1.1 M_{\odot} yr^{-1}$. BOTTOM: Specific SFRs of FIR-detected ETG split by morphological sub-categories. The grey dots in every panel are the LTG control sample. The dotted red vertical lines are the median SSFR of the different subcategories of FIR-detected ETGs

We want to maximise the quality of the different parameters we can extract with Magphys, so we try to use additional flux measurements. Ideally the larger the variety of flux inputs, the better the constraints on the parameters. We tried different combinations of filters with the aim of finding the narrowest marginalised likelihood distribution of each physical parameter of the observed galaxy. The best results for this sample are produced when we employ the SDSS data, the 60μm and the 100μm data and data from the WISE All-Sky survey (Wright et al., 2010). We also explored using 2MASS data (Skrutskie et al., 2006). When we included the 2MASS data, the χ^2 and the spread of some likelihood distributions increased significantly for all the objects, due to the difference in sensitivities and aperture of the 2MASS sample. In Figure 5.5 we see an example of the synthetic spectral energy distribution output that `MAGPHYS` produces. From that SED, the program calculates probability distributions for stellar mass, star-formation rate, dust mass and dust luminosity, inter-stellar medium and birth cloud temperature, and the optical depth. We improve the analysis by employing the χ^2 measurement and select only objects where the fluxes are in agreement with the models. Out of the 382 SF-ETGs only 337 have a reduced χ^2 which is deemed good (< 2). The object shown in Figure 5.5 has $\chi^2 = 3$ and a reduced $\chi^2 = 0.28$. Using the same criteria, the LTG control sample is downsized from 806 to 602 objects.

The top plot of Figure 5.6 shows the histogram of star formation rates (SFRs) for FIR-detected ETGs and the control sample. The median SFR is $1.1 M_{\odot} yr^{-1}$. It is worth noting that this is in agreement with the corresponding value for the LTGs ($0.9 M_{\odot} yr^{-1}$). This value is also in agreement with the study by Schawinski et al. (2009) of optically blue ellipticals ($0.5 M_{\odot} yr^{-1} < SFR < 50 M_{\odot} yr^{-1}$) and it is slightly larger than what has been found by Rowlands et al. (2012) in their study of submillimetre selected ETGs (median of $0.7 M_{\odot} yr^{-1}$).

In the bottom plot of Figure 5.6 we show the specific SFR (SSFR) of the FIR-detected ETGs, in different panels according to their morphological sub-categories. The LTG-CS is plotted in grey in every panel. We find that the SF-ETGs generally show similar SSFRs to the LTG control sample. Merging ETGs have the highest median SSFR. Unsurprisingly, the relaxed ETGs have lower SSFRs than both the control sample and the other categories.

Looking at Fig 5.6, its not clear that there is a sequence in SSFR across the morphological classes. The relaxed ETGs have slightly lower SSFRs but its not statistically significant. This is consistent with the fact that the relaxed ETGs are probably not actually relaxed but are just the remnants of more minor mergers which produce weaker tidal features that are less likely to be visible in the SDSS

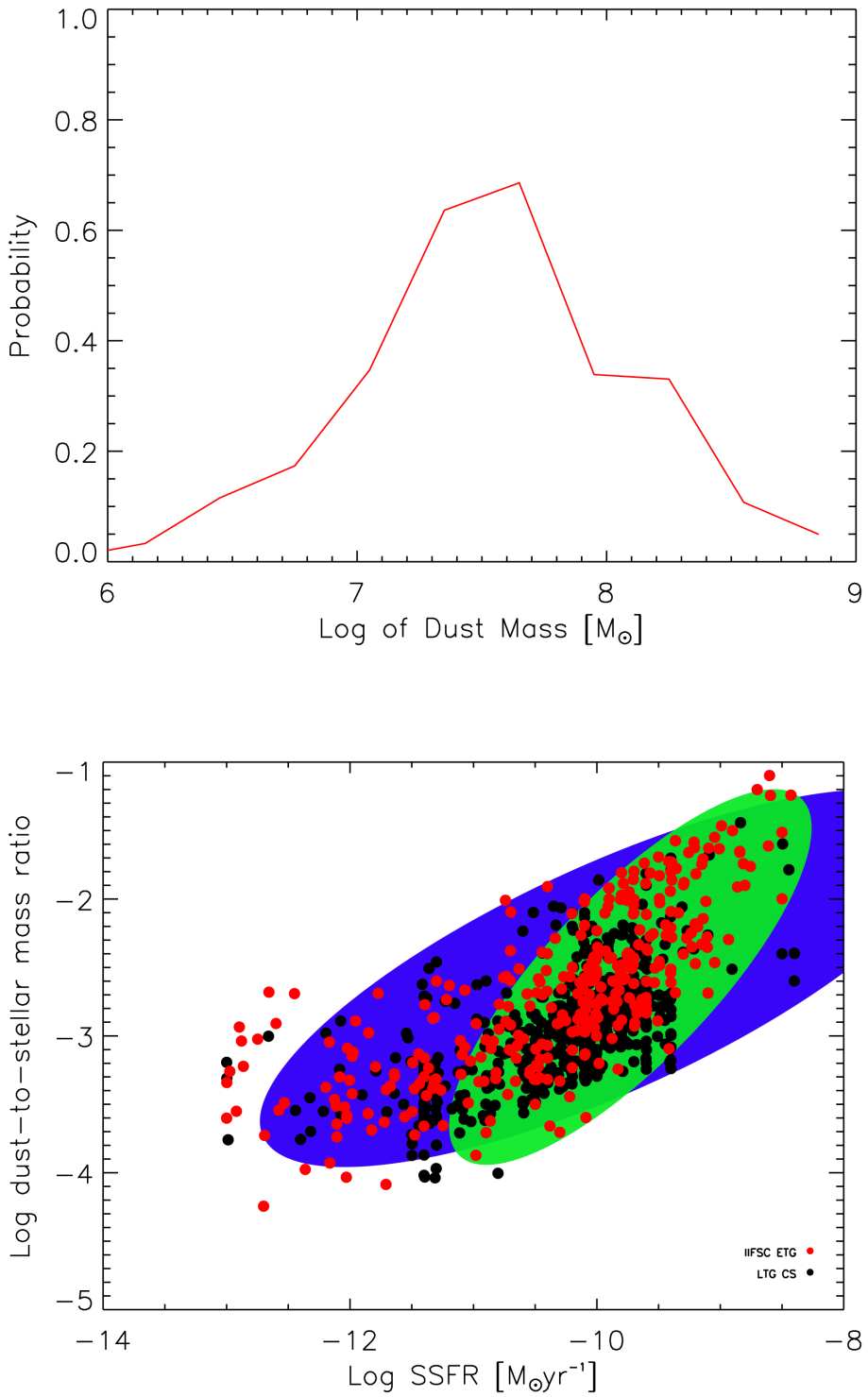


Figure 5.7: TOP: Stacked probability distributions of the dust mass from MAGPHYS for all FIR-detected ETGs. The median dust mass is $10^{7.5} M_{\odot}$. BOTTOM: Dust-to-stellar mass ratio vs SSFR of the FIR-detected ETGs (in red) and the late-types control sample (in black). For comparison, the green ellipse is the locus of the da Cunha et al. (2010) galaxy sample and the blue ellipse is the locus of the Rowlands et al. (2012) ETG sample.

.

images.

The different morphological types are probably the result of different types of mergers rather than being on some sort of evolutionary sequence. The relaxed ETGs are probably the result of fairly small minor mergers with satellites that are not particularly dusty. The dusty ETGs are probably the result of mergers with small dusty satellites that are not particularly big. The disturbed dusty ETGs are probably the result of mergers with relatively large, dustier satellites that produce more noticeable tidal features etc.

In the top panel of Figure 5.7 we show the dust mass distribution of the FIR-detected ETGs. The median dust mass is $10^{7.75} M_{\odot}$, comparable to the Rowlands et al. (2012) study of 44 far-infrared-selected ETGs ($M_{dust} \sim 10^{7.5} M_{\odot}$) and to Vlahakis, Dunne & Eales (2005), an optically selected sample of 6 ellipticals observed with SCUBA ($M_{dust} > 10^{7} M_{\odot}$). In the bottom panel of this figure, we plot the dust to stellar mass ratio against the SSFR. In agreement with previous studies (e.g. da Cunha et al., 2010; Rowlands et al., 2012), a good correlation exists between these parameters for FIR-detected galaxies, with the FIR-detected ETGs occupying a similar part of this plot as the LTG control sample. Some of our objects have a significant amount of dust (up to 10% of their stellar mass). Those same object are the most star forming ETGs in our catalogue. It has been noted already in another paper (Santini et al., 2014) that there is a good correlation between SFR and dust mass, which is probably a consequence of the Schmidt-Kennicutt relation. Strong episodes of star-formation can significantly increase the dust content in a galaxy.

In Figure 5.8 we show an estimated molecular gas mass of our sample of SF-ETGs. We estimate the gas masses using the Milky Way gas-to-dust ratio of 0.007 from Draine et al. (2007); obviously this might not be entirely correct as we have not observed them directly, but we believe that an approximated value can be very illustrative regarding the nature of the SF-ETGs. We find that FIR-detected ETGs are gas-rich galaxies; the median molecular gas fraction is around 35% of the total baryonic mass.

Our analysis indicates that SF-ETGs are strongly star-forming, but their specific star-formation rate is consistent with the general spiral galaxy population. SF-ETGs have a dust and gas mass comparable to late-type galaxies; this implies that they could sustain a prolonged star-formation spell without turning into the red passive object that one could expect.

5.5 Emission line analysis

We conclude by studying the optical emission-line properties of the FIR-detected ETGs in our study, using a standard 'BPT' analysis (see Baldwin, Phillips & Terlevich (1981); Veilleux & Osterbrock (1987); Kauffmann et al. (2003); Kewley et al. (2006)) to study the ionisation mechanisms in the IRAS-detected ETGs. The emission lines are computed using the public GANDALF code (Sarzi et al., 2006). Following Kewley et al. (2006), we use two optical emission line ratios – [OIII]/Hβ, [NII]/Hα to separate galaxies into quiescent, star-forming, seyferts and LINERs. We require line detections with $S/N > 3$. Note, once again, that galaxies classified as quiescent are those that do not have detections in all four lines.

In Figure 5.9 we present our BPT analysis. Regardless of the morphological sub-category, the FIR-detected ETGs are more active than their control counterparts. While $\sim$75% of the ETG control population are quiescent, on average only around a third of the FIR-detected ETGs are classified as quiescent, with the rest classified either as star-forming or mixed systems with both star formation and AGN (see also e.g. Carpineti et al. (2012)). We find that the SF-ETGs (except for the mergers) have a distinct increase in AGN activity compared to the LTG control sample. If we continue to assume that SF-ETGs are in the latest stages of an evolutionary route, this result is not at all striking: we expect AGN activity to help deplete the gas and dampen the intense star-formation in these objects. If we study the different morphological sub-categories in detail, we find minor differences in the dominant ionisation mechanisms. In the previous section we found evidence suggesting that the different morphological classes are not on an evolutionary sequence; this implies that the ionisation properties would be very similar across the whole range of sub-classes, which is exactly what we find here.

5.6 Discussion

Recent evidence has demonstrated that putting elliptical galaxies in a box labelled red and dead was a short-sighted and somewhat incorrect view. A new, more detailed look is necessary. The main goal we set when starting this project was to create a solid catalogue of visually classified star-forming early-type galaxies. This objective was obtainable by the use of the IIFSCz and visual inspection of the spectroscopic sample at very low redshift. If we want to understand differing attributes of passively evolving ETGs, we need to understand the exact nature of their recent evolution.

This analysis is independent of dynamical models of galaxy evolution; while

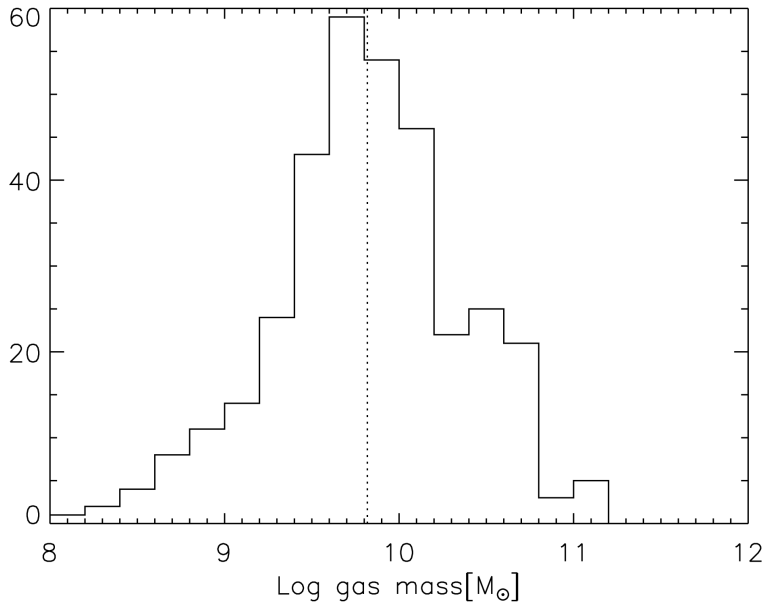


Figure 5.8: Estimated molecular gas mass of the FIR-detected ETGs. The gas mass is calculated from the dust fraction using the Milky Way gas-to-dust ratio.

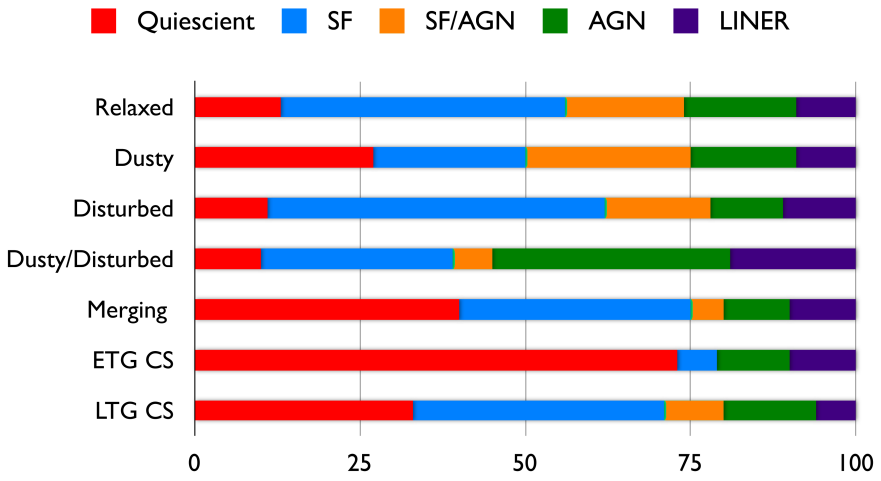


Figure 5.9: Summary of ionisation mechanisms in our FIR-detected ETGs from our BPT analysis (see text for more details). The colour-coding indicates the BPT classifications.

we obviously study the SF-ETGs in that framework, we do not need to invoke the hierarchical galaxy formation paradigm. The most interesting feature of these objects is the strong similarity with spiral galaxies across a wide range of properties. Colours, specific star-formation rate, dust and gas mass are all akin to the values we find for the late-type galaxy control sample. So, what is responsible for making our objects passive? The answer lies in the internal dynamics of our objects. AGN activity is more prevalent in SF-ETG than in the LTG control sample (apart from the mergers, but as we discussed earlier in this chapter, they might be on a different evolutionary path). Feedback mechanism could have two effects: disperse or heat up the gas and quench star-formation. Stellar feedback and stellar dynamics may also play a role in making these objects less spiral-like and more elliptical.

To answer the question we asked in this discussion, we need finer observations of ETGs with all-inclusive descriptions of the internal dynamics; these could be obtained by dedicated analysis of tracer gas movements. We also need more meticulous and precise simulations that elaborate on the exact mechanisms in a smaller scale. Some simulations (i.e. Hopkins et al. (2013)) now reach $\sim 1pc$ scale, which is enough to test feedback on giant molecular clouds. While most tests are on disk/bulge formation and feedback in active mergers, we hope that, in the near future, they will move into understanding the curious star-forming early-type galaxies.

Simulations of the star-formation histories can also help in constraining the role of minor mergers in the activation of AGNs. If we could precisely estimate how long ago that the peak of the star-burst happened then we would be able to see how delayed the beginning of the nuclear activity was.

Chapter 6

The contribution of galaxy mergers to the star-formation rate in the local Universe

6.1 Introduction

Infrared astronomy is the ideal tool to select the most star-forming galaxies in the Universe. In the previous Chapter we saw that infrared galaxies can assume a variety of morphologies. The aim of this is to explore the contribution of different morphological types of galaxies to the star-formation budget of the local Universe.

Our starting point is again the Imperial Infrared Faint source redshift catalogue (Wang & Rowan-Robinson, 2009) but this time we analyse the full spectroscopic sample of 11965 objects. This is the first large scale morphological catalogue of far infrared selected galaxies produced to date. We hope it will become the low-redshift infrared baseline for telescopes such as HERSCHEL and future IR surveys. It is important to note that this chapter is tracing only the properties IR-detected galaxies. While our results are derived using the IR-bright fraction of the galaxy population (4% of galaxies in the SDSS are detected by IIFSCz), we show towards the end of this chapter that our qualitative conclusions are also valid for the galaxy population as a whole (because the IR-bright overwhelmingly dominates the far-infrared luminosity budget of the local Universe).

The structure of this chapter is as follows: in section 6.2 we present the morphological classifications. Section 6.3 is dedicated to the study of the optical colours and the emission line activities of our sample, while section 6.4 is concerned with the galaxy main sequence and the environments of our objects. In section 6.5 we

discuss the contribution of the different morphologies to the star-formation budget of the local Universe. A discussion of our findings can be found in section 6.8.

6.2 The morphological classification

The sample we are probing is limited in both magnitude (Petrosian $r < 17.77$) and redshift ($z < 0.2$). We divided the galaxies into 3 morphological categories with the morphological classification done by eye:

- Spheroidal
- Late-type galaxy
- Merger

Every galaxy showing a dominating bulge and ellipsoidal shape is classified as spheroidal. To be classified as spiral the objects have to show a regular spiral structure with no distortion or tidal feature. The galaxies with a merger flag include interacting galaxies and objects with tidal features. Examples of these categories are shown in Figure 6.1. About 60% of the sample is composed of galaxies that either have signs of interactions, are full-on mergers or have a completely irregular shape following a merger. When it comes to infrared galaxies in the local universe, their evolution is driven by how, when and where they have interacted.

6.3 The colour magnitude distribution and nuclear emission line activity of IIFSCz galaxies

We begin by exploring the colour-magnitude distribution (CMD) of the IIFSCz. While the CMD is bimodal in the general galaxy population (Strateva et al., 2001; Blanton et al., 2003; Baldry et al., 2006), it is interesting to explore whether this is also the case for IR-bright galaxies in the local Universe. We were curious to see how the colour-magnitude relation would hold in our sample since it became clear, during the visual classification, that there was a complex assortment of objects from normal galaxies to unusual objects (like red spirals and blue ellipticals). To do so we used the *ugriz* colours from SDSS and the spectroscopic redshifts calculated by Wang & Rowan-Robinson (2009) to obtain the absolute magnitude. In Figure 6.2 we plot the *u-r* colour versus absolute magnitude in the r band. The colours were de-reddened and K-corrected according to the technique devised by Blanton

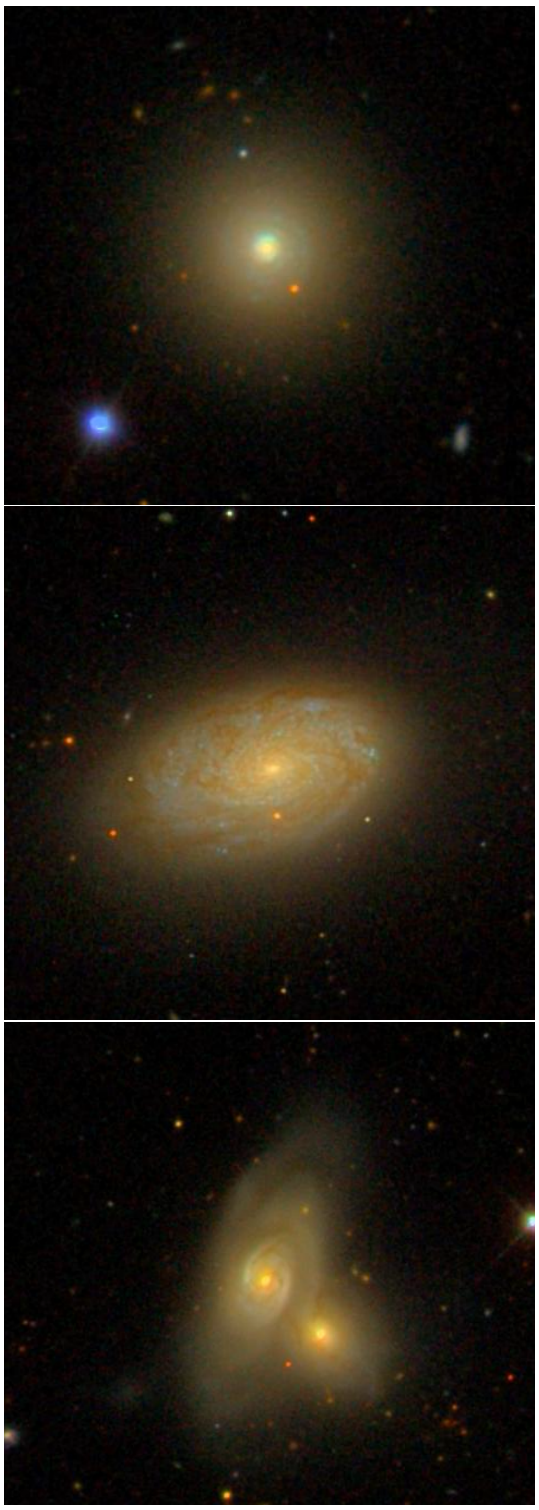


Figure 6.1: SDSS images of the 3 morphological classes. In order we have a spheroidal, a late-type galaxy and a merger.

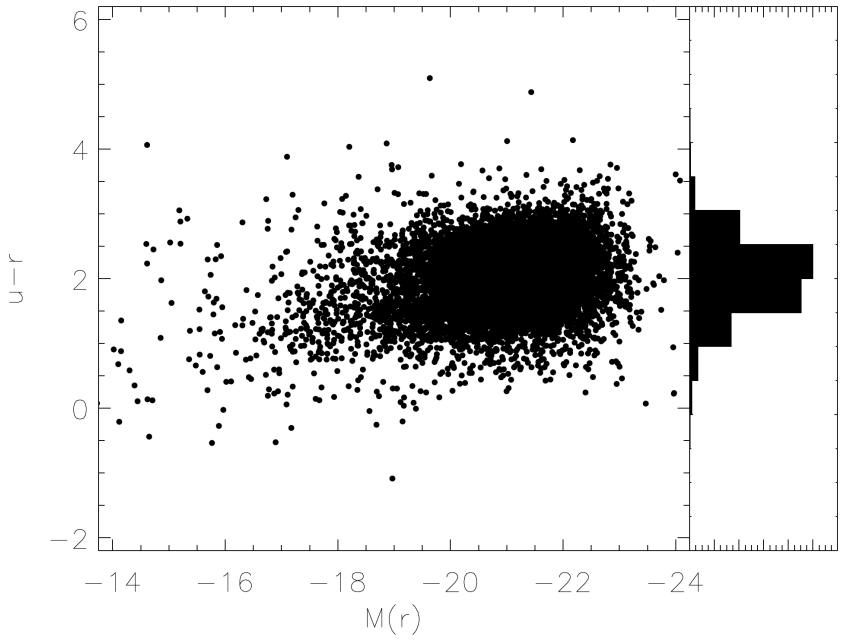


Figure 6.2: We plot *u-r* versus the absolute magnitude in the *r* band. We find no sign of bimodality in this colour-magnitude diagram: all galaxies from our sample are in an undivided distribution. This is also shown in the u-r histogram on the side.

& Roweis (2007). The most striking result is that there is no trace of a bimodality. The sample occupies a continuous distribution in the full colour space.

We were intrigued to know the reason for this departure from the galactic distribution typically presented in literature (Strateva et al., 2001; Blanton et al., 2003; Baldry et al., 2006). Our first idea was to see how the plot changed if we highlighted the different morphologies. In the top panel of Figure 6.3 we plot the Colour-Magnitude distribution for LTGs and spheroidals in our sample. It is evident that there is an almost complete overlap of the two subsets, making it clear that the well established bimodal distribution observed for normal galaxies does not hold for infrared selected galaxies. The mechanism that regulates the colours has to be independent of morphology and dependent only on the star-formation history of galaxies.

One way to give some indication about this is to study the optical emission-line properties of galaxies. We perform the BPT analysis in the same way we did before using the standard analysis (see Baldwin, Phillips & Terlevich (1981); Veilleux & Osterbrock (1987); Kauffmann et al. (2003); Kewley et al. (2006)) to study the ionisation mechanisms in the nuclear regions of these objects. Checking their emission lines is a good way to track their evolutionary paths, as we expect AGN to peak after star-formation has subsided. In the bottom panel of Figure 6.3,

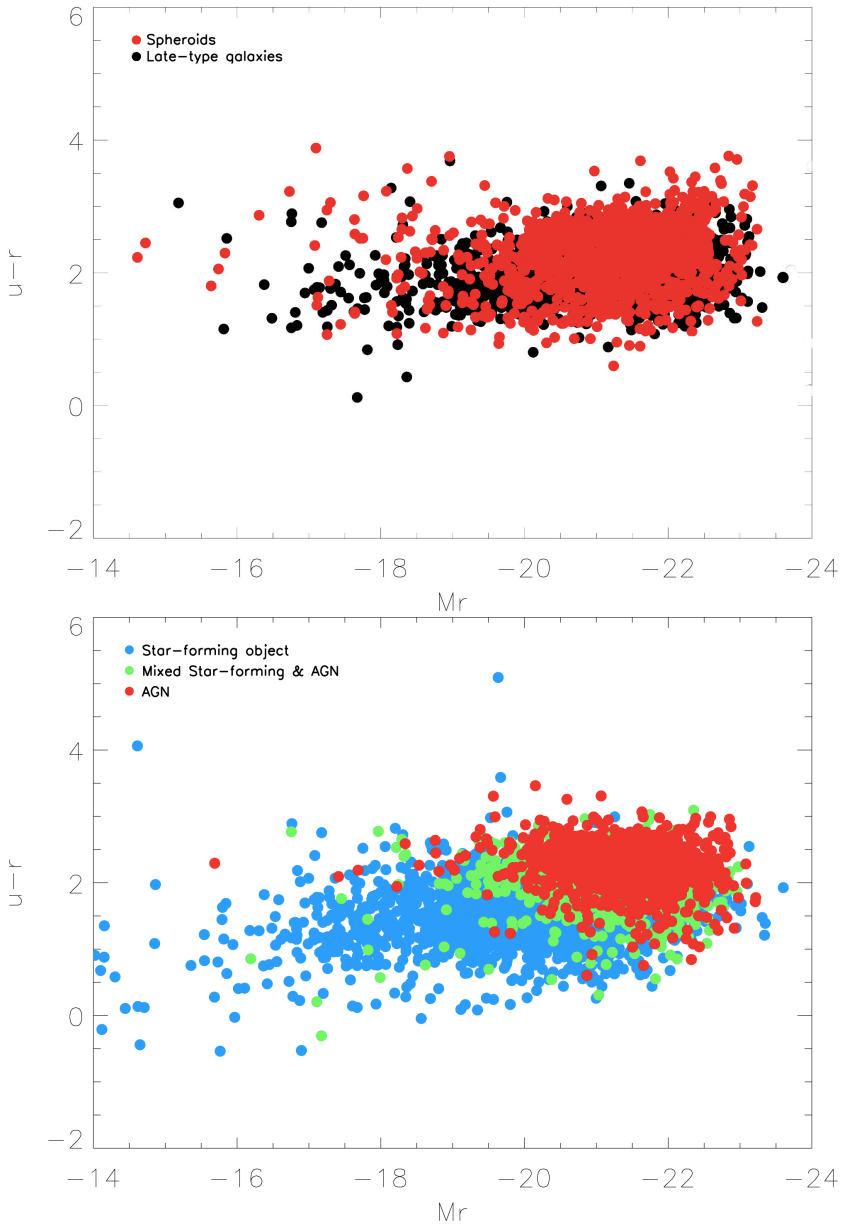


Figure 6.3: TOP: We plot the CMD for the spheroidals and LTGs in the catalogue. We find that there is no difference between the two categories in their location on the diagram. BOTTOM: We plot the CMD for different emission line classes.

we plot the CMD for different emission line signatures. We see how having an active AGN makes a galaxy redder even when there is a mix of star-formation and AGN. We see that the presence of an AGN (both dominating or in conjunction with star-formation) excludes a galaxy from being blue. This result confirms the idea that AGN activity becomes dominant after the SFR peak. Simple star-forming galaxies dominate the bluer colours of this plot. It is interesting to note some peculiarly red star-forming galaxies. It is quite likely that their sudden star formation is due to a minor merger or some secular accretion since a small starburst would leave the optical colours unchanged while having a significant impact on the UV and IR colours. This result is in agreement with what has been found in the literature (Schawinski et al., 2009; Wild, Heckman & Charlot, 2010; Schawinski et al., 2010). Emission line activity has very little to do with morphology. It is clear that this sample is largely dominated by actively star forming galaxies; as we would expect from an infrared selected group of objects.

6.4 The star-formation main sequence for different morphologies

At high redshift galaxies have a tight correlation between SFR and stellar mass (Daddi et al., 2007; Reddy et al., 2012). This correlation is called the star-formation main sequence. It has been shown that at redshift of $z \simeq 2$ mergers and normal galaxies have the same SFR in the same mass range (Santini et al., 2009; Rodighiero et al., 2011; Kaviraj et al., 2013b; Hung et al., 2013; Lamastra et al., 2013). In the previous chapters, we have shown this correlation for both mergers and Star-forming ETGs. Having a catalogue composed of various morphological types allow us not only to show the star-formation main sequence but also to verify if high-redshift assumptions hold at low redshift. This is shown in Figure 6.4.

At high redshift mergers and relaxed galaxies are not well separated on the SF main sequence. In the early universe "normal" galaxies are vigorously star-forming regardless of interactions: an extra merger is not enough to create a significant enhancement in the SFR. As we can see from the plot, the situation is different at low redshift. Mergers are significantly more star-forming than relaxed galaxies at a given mass.

Does the star formation main sequence change as a function of environment? Firstly let us look at how the different morphologies relate to environment. In the previous chapters, we discussed how a relationship with the environment might influ-

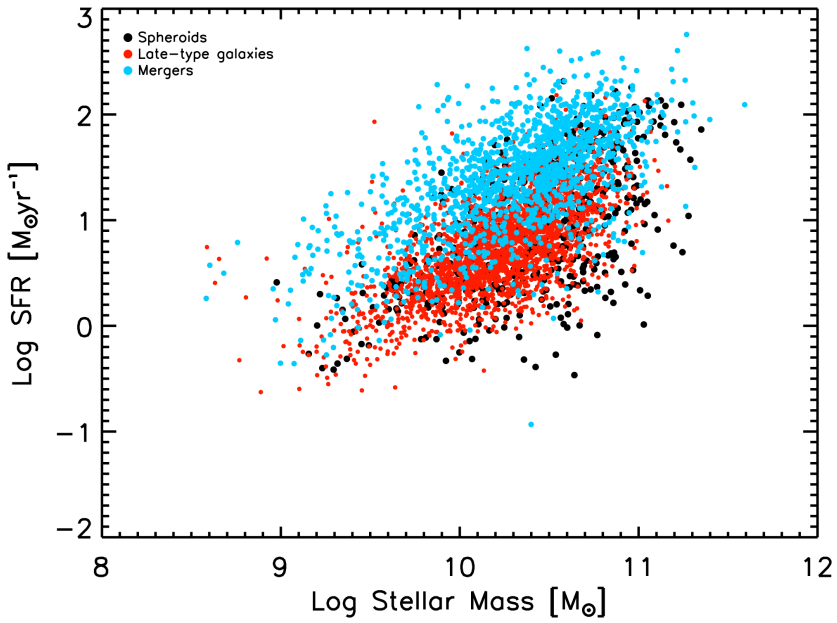


Figure 6.4: SFR as a function of galactic stellar mass for our galaxy sample. The masses are calculated using equation 4.1. Spheroidal galaxies are in black, spirals in red and mergers in blue. We see that the each morphological class follow the SF main sequence, but at low-redshift mergers have a significantly higher SFR per given mass.

ence the star-formation rate, due to infall material and cold flows. Our environment parameter is the group mass from Yang et al. (2007), and its estimation has been discussed in previous chapters. As we can see in the histogram in Figure 6.5 all morphological types in this study favour low density environments. We divide the sample into two environment bins, one representing $M_{group} < 10^{12.4} M_{\odot}$ and the other one representing $M_{group} > 10^{12.4} M_{\odot}$. The value of $10^{12.4} M_{\odot}$ is arbitrary, and was picked to have a consistent amount of objects across the bins and the morphologies. In Figure 6.6 we show the fits of the SF main sequence (divided by morphologies) to show how the SF main sequence relates to environments. The fit was calculated for each morphology in each environment bin (solid lines for low density and dashed lines for high density). We also plot the standard deviation of the linear regression for the low density objects. We see that the the fits are statistically consistent between the two environments. The influences of the environment on these distributions are only related to the stellar mass and its primordial assembly. Thus, we can consider the SF main sequence to be largely independent of environment.

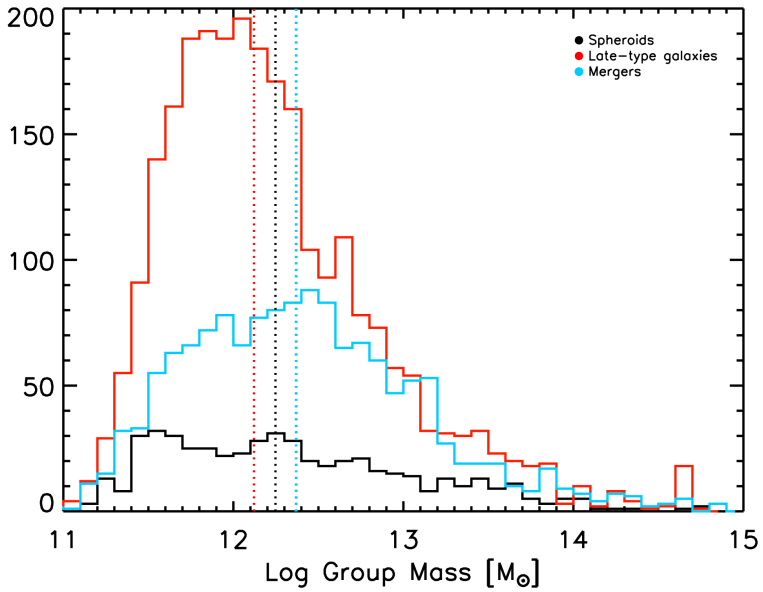


Figure 6.5: We plot the group mass as an environment density indicator for the different morphologies in the IIFSCz. The distribution for each class follows the same trend, favouring lower density environments but extending all the way to clusters ($GM > 10^{14}$). The dashed lines are the median values for the different morphologies.

6.5 The morphological contribution to the total star-formation budget of the Universe

The high-redshift SF main sequence results indicate that mergers are not the main drivers of star-formation. Moreover it has been shown that their role at high redshift ($z > 2$) is limited (Daddi et al., 2010; Rodighiero et al., 2011; Kaviraj et al., 2013b; Lamastra et al., 2013), being responsible for only 27% of the star-formation activity that goes (Kaviraj et al., 2013b). However at low redshift, Figure 6.4 shows that mergers dominate the top end of the SF main sequence. If we sum the derived SFRs in term of galaxy morphologies, we can show how the star-formation contribution is shared between morphological types. We find that mergers host 65% of the star-formation that goes on at low-redshift. LTGs host a quarter of the total SF in the local Universe, and the remaining 10% happens in spheroidal galaxies (see Figure 6.7). This result is not unexpected but it is significantly different from the high-redshift scenario. At high redshift, where the Universe's star-formation peaked, LTGs drive the SF budget. This implies that the processes that form stars in the high-redshift Universe are not related to merging processes. In the local universe quite the opposite happens: the quiescent star-formation in relaxed (i.e. non-merging) galaxies is significantly weaker than that in their merging counter-

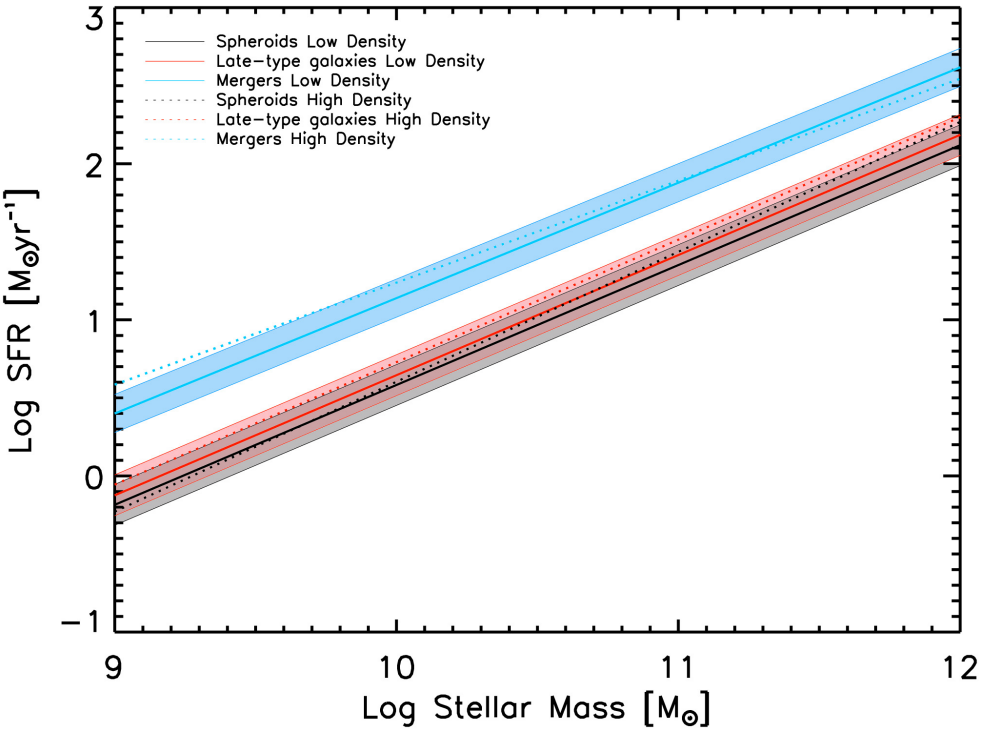


Figure 6.6: The linear fits for SF main sequence are plotted in this figure. Mergers are in blue, Spirals in red and Spheroidals in black. Solid lines represent the fits for low density environments ($M_{group} < 10^{12.4} M_{\odot}$) while dashed lines represent the fits for high density environments ($M_{group} > 10^{12.4} M_{\odot}$). The shaded areas correspond to the standard deviation about the linear fits of the low density objects. We see no significant differences between the two environments.

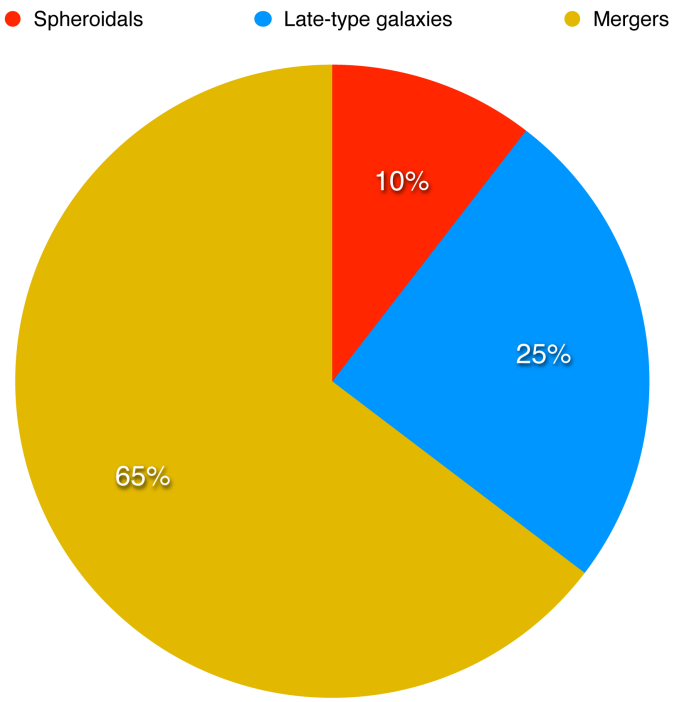


Figure 6.7: This pie chart shows the percentage of the star formation budget apportioned in terms of morphological class (Merger, Late-type or spheroidal). Mergers are clearly the main contributors of new stars in the IIFSCz.

parts, at least in the IIFSCz.

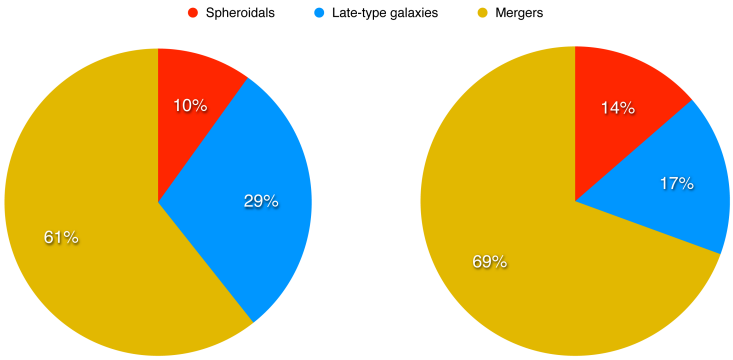


Figure 6.8: These pie charts show the percentage of the star formation budget apportioned in terms of morphological class on the LEFT for low density environments ($M_{group} < 10^{13} M_{\odot}$) and on the RIGHT for high density environments ($M_{group} > 10^{13} M_{\odot}$).

The overwhelming role played by mergers in the SF budget of the Universe does not depend on the environment of our objects. In Figure 6.8 we see two pie charts showing the SF budget for low (LEFT - $M_{group} < 10^{13} M_{\odot}$) and for high (RIGHT - $M_{group} > 10^{13} M_{\odot}$) density environments. These charts are not significantly different from Figure 6.7 and the dissimilarities are due to tendency of late-type galaxies to favour slightly lower densities (see Figure 6.6). The way the SF budget is divided is

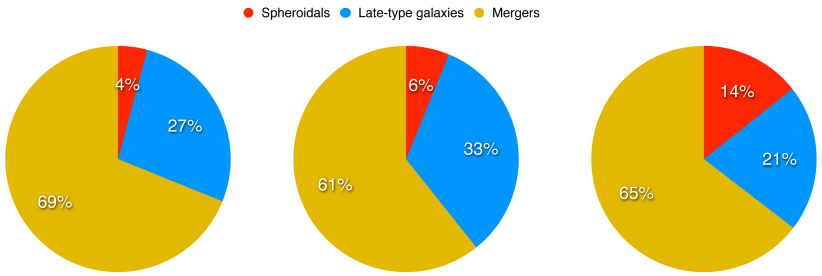


Figure 6.9: These pie charts show the percentage of the star formation budget apportioned in terms of morphological class (Merger, Late-type or spheroidal) and total stellar mass (from left to right: low mass ($M_{star} < 10^{9.5} M_{\odot}$), normal mass ($10^{9.5} M_{\odot} < M_{star} < 10^{10.5} M_{\odot}$) and high mass ($M_{star} > 10^{10.5} M_{\odot}$) galaxies). While relaxed configurations are biased towards extreme masses, the merger distribution is quite constant. Once again, mergers are clearly the main contributors of new stars in the infrared bright galaxies.

only marginally influenced by environment.

Do the morphological contributions to the star formation budget change as a function of stellar mass? In Figure 6.9 we see the three pie charts representing

the SF budget for low mass ($M_{star} < 10^{9.5} M_{\odot}$), intermediate mass ($10^{9.5} M_{\odot} < M_{star} < 10^{10.5} M_{\odot}$) and high mass ($M_{star} > 10^{10.5} M_{\odot}$) galaxies. We find that the fractional morphological contributions are relatively insensitive to stellar mass. The contribution of mergers, in particular, remains similar regardless of the stellar mass range considered. The somewhat larger contribution of spheroidal galaxies in the highest mass bin is expected to be driven partly by the fact that these galaxies dominate the high-mass end of the luminosity function (Bernardi et al., 2003).

It is clear that mergers play a dominant role in the IIFSCz, but are our results generally representative of the local Universe? The IIFSCz galaxies represent 4% of the galaxies observed in the SDSS. Let us assume that all galaxies that are *undetected* in the IIFSCz are relaxed (i.e. not mergers), and that their star formation distribution peaks just below the IRAS detection limit (which is likely to be a gross overestimation). For simplicity let us also assume that the distribution of star formation for this undetected sample peaks just under the detection limit. We can then calculate an upper limit to the contribution of these galaxies to the total star formation budget. Since we selected the catalogues with the same limit both in volume and in magnitude, we believe that the result will be an overestimation of the true value. We find that the undetected galaxies can be responsible at most 22% of the SF budget in the local Universe (Figure 6.10). Taking this into account leaves our main results unaffected. Thus, we find that *mergers must drive at least half the star formation budget in the local Universe.* The IIFSCz might be only representative of 4% of galaxies in the local Universe but they are the top 4% for star-formation. Consequently our result can be extended; galaxy mergers are the driver of star formation in the local Universe.

6.6 Discussion

The main goal of this thesis is to study the peculiar steps in the galactic evolutionary ladder from mergers to early-types, showing the importance of mergers in the local Universe. Having a more in-depth study of the full spectroscopic Imperial Infrared faint source catalogue was started for that reason. Infrared galaxies have been discussed in great detail over the past 30 years, and yet most morphological studies are very limited in either the quantity of objects or the depth of the analysis.

Our aim is to scrutinise the properties of these galaxies according to morphologies, colours, emission lines, environment and stellar masses. Classifying the entire catalogue was the hardest task. We took a lot of care in having a proper and solid classification. We find that morphology has no impact on the emission line activity

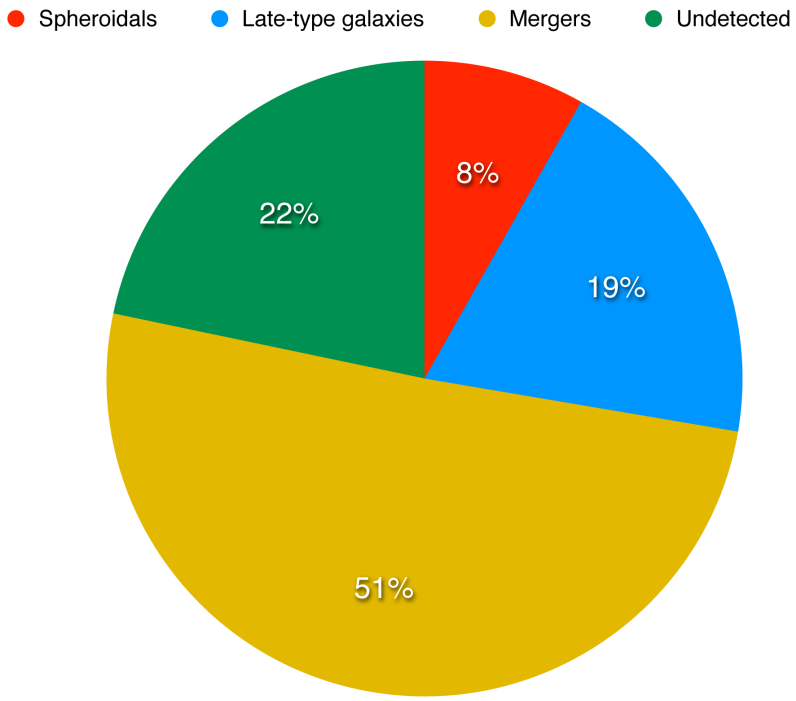


Figure 6.10: This pie chart shows the percentage of the star formation budget apportioned in terms of morphological class (Merger, Late-type or spheroidal) plus an estimation of the contribution to the SF budget by the undetected galaxies. Mergers are clearly the main contributors of new stars in the local Universe.

and that it is independent of environment.

Very interesting results come from the colour magnitude diagrams (Figures 6.2 and 6.3). From the general plot we find that there is no bimodality in the sample, showing an uninterrupted presence of galaxies from the bluest to the reddest colours. Adding morphologies to the analysis, we find an even more interesting result: the continuous distribution of galaxies across the colour-magnitude space is independent of galaxy class. These galaxies are truly special, not only because of their infrared bright status. Their general characteristics (which may or may not match with the a priori expectation) depend exclusively on their formation and interaction histories. We find that galaxies that are Seyfert or LINER sit in the red part of the CMD and might be responsible, through a feedback mechanism, for the reddening of galaxies. This confirms the absence of blue AGN-hosts in the local universe.

We looked at the star-formation rate. Our analysis confirmed that the SFR has a good correlation with the total stellar mass of the object; this correlation is known as the SF main sequence. In this chapter we look at the nature of the SF main sequence at low redshift and for different morphologies. The correlation is very different in the local Universe. Here mergers have higher star-forming rates than other galaxies, unlike in the high-redshift Universe.

This result sparked our curiosity and we looked at the star-formation budget of galaxies in the IIFSCz. Mergers clearly dominate the SF budget and this result is both mass and environment independent. We thought of ways to generalise this finding. Obviously, the sample is not a good representation of the average galaxy population, but we believe it represents the most star-forming galaxies in the universe. The assumption in the final section is that if a local galaxy is highly star-forming it will be bright in IR. So having an all sky survey, we are claiming to have access to the most star-forming objects in the local universe. As we have seen in section 2 using either $H\alpha$ or monochromatic UV underestimates the SFR so while it might not be a fool proof assumption, we are quite confident in it (and we are trying to be consistent with our choice of estimator). Our working assumption aims to create an overestimation of the SFR for undetected objects; we assume that each undetected galaxy has a SFR just below the detection limit. Even under that condition, galaxy mergers are still the main contributors to the SF budget in the local Universe. This result has never been quantified before and only through the use of a morphological catalogue of infrared galaxies we have been able to achieve it.

More work is necessary on these galaxies. It would be interesting to understand better their star-formation histories to shed more light on their evolution. A high

resolution infrared study would also help in understanding the types of mergers these galaxies went through. Finally, we hope that wider and deeper Infrared surveys will start using morphological classifications as a standard tool, not as a novelty item.

Chapter 7

Conclusions

7.1 Introduction

In this Thesis, a study of the nature and evolution of interacting galaxies has been presented using morphological classification as the primary investigative tool. By complementing the optical observations with ultraviolet and infrared data, we have studied the properties of the transitional classes of the galaxy evolution paradigm.

The main focus of this thesis is the analysis of the different stages galaxies go through after a merger. Chapter 1 and Chapter 2 are introductory chapters describing the current view of galaxy evolution, the state of simulations and a detailed summary of the tools, techniques and surveys used in this work. The properties of galaxy mergers from an infrared perspective are discussed in Chapter 3. Chapter 4 deals with the extensive descriptions of spheroidal post-mergers, while Chapter 5 focuses on the attributes of local star-forming early-types. Chapter 6 describe the construction of the IIFSCz morphological catalogue as well as discussing its general star-formation properties.

Some original aspects of this thesis include: 1.) the first detailed analysis of spheroidal post-mergers; 2.) the first infrared-blind study of the properties of merging galaxies; 3.) a multi-wavelength catalogue of local star-forming early-type galaxies; 4.) the largest morphological survey of far-infrared selected objects, 5) the first estimate of how different morphologies contribute to the SF budget of the local Universe. A full summary of the work presented in this thesis is provided in the current chapter.

7.2 Merging galaxies as seen in the infrared

We have cross-matched the IIFSCz and the GZ mergers catalogue to study the infrared properties of local galaxy mergers. We find that only 18% of the mergers are IRAS detected and they correspond to the high-flux end of the infrared flux distribution.

The IR detected mergers are mostly late-type galaxies (98%) with the exception of a few gas rich and/or multiple mergers involving early-types. The sample has a median IR luminosity of $10^{11} L_{\odot}$ and a median star-formation rate of around $15 M_{\odot}\ yr^{-1}$. They reside in low density environments but we do not find any apparent dependence between group richness and L_{IR}.

Their SFR seems to depend on the total mass of the system but has no dependence on the mass ratio of the progenitors. Studying the emission line ratios, we find that the AGN fraction increases dramatically for ULIRGs, where we have a clear AGN signature from the BPT diagram, despite being strongly star-forming systems. This might be an indication of very powerful AGN in ULIRGs.

Another interesting characteristic of ULIRGs is that they are all in a late merger stage (nearly or already coalesced), which allows us to calculate a timescale for their formation based on dynamical considerations. If the non-coalesced purely star-forming LIRGs in our sample are a reasonable parent population for ULIRGs, we can measure their separation and then, under this assumption, a value for the temporal separation between the two stages. Galaxies take 145±120 Myr to evolve from LIRGs to ULIRGs.

There is sufficient evidence to suggest that the average merger detected in the infrared is a spiral-spiral LIRG, which lives in a low density environment, has a moderate SFR and possibly some form of AGN activity.

7.3 Post-merger galaxies with spheroidal morphologies

We have studied a sample of 30 bulge-dominated or spheroidal post-mergers (SPMs) in the local Universe. These are, by virtue of their morphology, plausible progenitors of early-type galaxies. They are a subset of (Darg et al., 2010a) sample, who have produced a large, homogeneous catalogue of mergers, through direct visual inspection of the entire SDSS spectroscopic sample using the Galaxy Zoo project.

The vast majority of the SPMs inhabit low-density environments (groups and the field), consistent with the expectation that the high peculiar velocities in high-

density environments make conditions difficult for galaxy merging. Our SPM sample is generally bluer than a control sample of early-type galaxies but redder, on average, than the merging population. This indicates that the peak of star formation activity takes place during the merger phase. 84% of SPMs exhibit emission-line activity. 42% show Seyfert-like emission, 26% are LINERs and 16% are classified as star-forming. In contrast, the control sample of early-type galaxies is dominated by quiescent objects, while the mergers are dominated by star-forming galaxies. The rise in the AGN fraction in the post-merger phase (compared to mergers) suggests that the AGN phase probably becomes dominant only in the very final stages of the merging process. Comparison of the SPMs to the ongoing mergers in the Darg et al. sample indicates that they are likely to be the remnants of major mergers.

Since major mergers are expected to coalesce on timescales of less than 1 Gyr, we have compared the colours of SPMs to models in which a young stellar population (with an age between 0.2 Gyr and 0.6Gyr) and variable stellar metallicity (between $0.75Z_{\odot}$ and $2Z_{\odot}$) is superimposed on an old population that forms at $z = 3$ (since the bulk of the stars in early-type galaxies are known to be old). We have found that, under these assumptions, the vast majority of the SPMs are likely to have formed more than 5% of their stellar mass in the recent merger driven burst. Since early-type galaxies themselves are rather gas-poor objects, our results indicate that $\sim$55% of SPMs are products of major mergers in which at least one of the progenitors is a late-type galaxy.

7.4 Star-forming early-type galaxies

We have presented a catalogue of local star-forming early-type galaxies. It contains 382 SF-ETGs with $M(r) < -19.03$ and $z < 0.05$. The sample is divided according to morphological peculiarities. We have 159 relaxed ETGs, 44 ETGs that show dust features, 89 ETGs with clear asymmetries in their shape, 71 dusty and disturbed ETGs and 19 ETGs which are merging. We use two control samples to highlight the properties of the SF-ETGs. As a background for the infrared properties we use a sample of 800 late type galaxies (LTG-CS) randomly selected from the 4927 IRAS-SDSS LTGs that have the same magnitude and redshift cut as our sample. We also use a randomly selected sample of early type galaxies from SDSS. The same cuts were applied by us before using it, leaving us with 492 objects (ETG-CS). Looking at the environment our galaxies live in, we find that the SF-ETGs are mostly in the field. They tend to prefer a lower density environment compared to the ETG-CS.

We analyse the FIR (8-1000μm) luminosity of the SF-ETGs and then we use the

routine MAGPHYS to extract the SFR. The median value for the SFR is $1.1 M_{\odot} yr^{-1}$. This is comparable to the SFR in LTGs ($0.9 M_{\odot} yr^{-1}$). When we study the specific SFR we find that SF-ETGs tend to have a higher star-formation rates than LTGs of equal mass.

The colours are another interesting aspect of our sample. Based on optical *NUV-r* colours alone the KS-test suggests that there is only 23% probability that the SF-ETGs and LTG-CS are extracted from the same population. This probability becomes negligible when we use the near ultraviolet.

We also use MAGPHYS to extract a reasonable dust mass estimate combining the data from IRAS and simulated light curves. We find that the median dust mass is $10^{7.5} M_{\odot}$, which is comparable to other studies in the literature.

We find a trend in the dust mass versus SFR, which is expected, as both parameters depend on the stellar mass of the galaxy. Once that is taken into account, by simply dividing the dust mass and the SFR by the stellar mass, we still find a strong correlation. This has been interpreted in the literature as evidence for recent starbursts and evolutionary changes.

Finally we use the BPT technique to study the emission line activity of the sample. Mergers have the highest fraction of quiescent galaxies and the lowest fraction of AGN out of the SF-ETGs, while dusty disturbed galaxies have a high fraction of both AGN, SF and LINER galaxies. The disturbed galaxies have the highest fraction of SF, which is probably induced by the tidal-stress, but can not explain the high fraction of SF in the morphologically relaxed SF-ETGs . Dusty galaxies exhibit all activities without favouring a particular one. We also looked at the ETG-CS, and found that they are dominated by quiescent galaxies.

In general, the average star-forming early-type galaxy is a galaxy with a sub-LIRG luminosity and a significant star-formation rate($> 1 M_{\odot} yr^{-1}$). It dwells in a low density environment, has optical colours comparable to a late type galaxy, has some morphological substructure and possibly some form of AGN.

7.5 The morphological classification of the IIFSCz

We completed the morphological classification of the Imperial Infrared Faint-Source Redshift Catalogue, dividing the 11965 objects in three main classes: spheroidals, late-type galaxies and mergers based on their SDSS composite image.

The colour distribution of the IIFSCz objects is very interesting. The color-

magnitude diagram for the entire sample shows that there is no bimodality trend (blue cloud/red sequence) between our galaxies, as we can see a continuous presence of galaxies from the bluest to the reddest colours. The high number of peculiar objects (40% of the sample) might make us biased toward green valley objects, but even when the morphologies are considered we see that the distribution of galaxies in the CMD is unchanged. What seems to matter for the type of emissions we can extract from BPT diagrams is that galaxies which host an AGN (Seyfert or LINER) sit in the red part of the CMD and might be responsible through feedback mechanism for the reddening of the galaxies. This result goes to confirm, once again, the absence of blue AGN-hosts in the local universe (Schawinski et al., 2009).

Focusing on the SFR, we find a good correlation between the SFR and the total stellar mass of the objects; this relationship is known as the SF main sequence. At high redshift the SF main sequence is independent of morphology but in the local Universe we find that, at any given mass, merger galaxies are more star-forming than relaxed types (spheroidal and LTG). We study the type of environments our objects reside in and find that the vast majority of the IIFSCz galaxies dwell in lower density environments (groups and fields). We look at possible variation of the SF main sequence at low and high density environments. We find the distributions consistent with each other. This indicates that the SF main sequence for IR-bright galaxies is independent of environment.

Our analysis of the sample properties focused on the advantage of having such a large sample of FIR selected galaxies to explore how different galaxies contribute to the total star-formation in the local Universe. At high redshift LTGs are the main contributor to the Universe SF budget, due to higher SFR of non-interactive galaxies. This does not hold for the galaxies in the IIFSCz. Mergers dominate the star-formation budget of local IR-bright galaxies. This result is independent of environment and mass. We also estimate the upper limit for the contribution of IR-undetected galaxies to the SF budget. We find that non-bright IR galaxies contribute at the most to 22% of the SF budget of the Universe. This result tells us that galaxy mergers are the principal driving force behind star-formation in the local Universe.

7.6 Overall conclusions

One of the main characteristics that is common to all our different samples is that the galaxies we studied are all in low density environments. The conclusions that are drawn are specific for red and passive early-type galaxies that reside in the field

or in the low density outskirts of groups and clusters.

The lack of gas in ETGs can be explained by two mechanisms: either by a recent and significant star-formation event or by AGN feedback. These mechanisms can happen together, with the star-formation quenched by the winds driving out the gas from the core. Remarkable starbursts do not need a major merger event to be generated, a minor merger could be sufficient under the right conditions to produce a sufficient star-formation rate. Small minor mergers are also less visually noticeable, which can help explain the prolonged activity in star-forming ETGs.

Minor mergers obviously cannot be held responsible for the radical morphological change we expect from a late-type galaxy evolving into an early-type galaxy. Only the tidal stresses of a major merger can change the orbital pattern on such a wide scale. Studying the optical colours of spheroidal post-mergers, we found that a gas rich merger is not always the most likely candidate.

So how does a low-redshift, low-density, gas-poor and ageing early-type galaxy come to form? It forms through a series of merger events: an original major spiral-spiral collision alters the general structure of the galaxy. More merger events are necessary to increase mass, fuel star-forming events and to turn on the AGN so that the galaxy can free itself of the gas and be on its way to be red and passive. The traditional picture of an early-type being the quick end result of a LTG-LTG merger is too simplistic to explain the variety and complexity that we observed in active ETGs and a reasonable evolutionary picture needs to take into account the numerous interactions a galaxy might encounter in its life. A minor merger might have a limited impact in changing morphologies, but can produce Infrared bright star-bursts.

What we have tried to highlight throughout this work is that galaxy evolution is an incredibly complex process. This is the reason why simulations cannot reproduce real objects: when scaled down to basic parameters we lose the subtlety of the mechanism and the predictions end up being highly limited. Multi-wavelength observations and classifications become paramount to indicate what is allowed and what is forbidden in our Universe. Computer models can be expanded which in turn will lead to more detailed explanations and new predictions. Observing galaxy evolution is like trying to create a single coherent movie from different snapshots of different objects. We have a solid theoretical backbone and we have an interesting array of simulated scenarios. What we need is to expand our knowledge through observations confirming the expectations from literature or pointing out new phenomena and we hope that this thesis has produced exactly that.

References

Aarseth S. J., Fall S. M., 1980, ApJ, 236, 43

Adelman-McCarthy J. K. et al., 2008, ApJS, 175, 297

Adelman-McCarthy J. K. et al., 2006, ApJS, 162, 38

Alatalo K. et al., 2011, ApJ, 735, 88

Baker J. G., Menzel D. H., 1938, ApJ, 88, 52

Baldry I. K., Balogh M. L., Bower R. G., Glazebrook K., Nichol R. C., Bamford S. P., Budavari T., 2006, MNRAS, 373, 469

Baldwin J. A., Phillips M. M., Terlevich R., 1981, PASP, 93, 5

Bamford S. P. et al., 2009, MNRAS, 393, 1324

Barnes J., Efstathiou G., 1987, ApJ, 319, 575

Barnes J., Hut P., 1986, Nature, 324, 446

Barnes J. E., 1992, ApJ, 393, 484

Barnes J. E., Hut P., 1989, ApJS, 70, 389

Barton E. J., Geller M. J., Kenyon S. J., 2000, ApJ, 530, 660

Bell E. F., McIntosh D. H., Katz N., Weinberg M. D., 2003, ApJS, 149, 289

Bell E. F. et al., 2005, ApJ, 625, 23

Bender R., 1996, in IAU Symposium, Vol. 171, New Light on Galaxy Evolution, Bender R., Davies R. L., eds., p. 181

Bender R., 1997, in Structure formation and ages of elliptical galaxies, ASP Conference 116

Bernardi M. et al., 2003, AJ, 125, 1882

Bertone G., Hooper D., Silk J., 2005, Physics Reports, 405, 279

Bertschinger E., 1998, ARA&A, 36, 599

Blanton M. R. et al., 2003, ApJ, 594, 186

Blanton M. R., Roweis S., 2007, AJ, 133, 734

Blumenthal G. R., Faber S. M., Primack J. R., Rees M. J., 1984, Nature, 311, 517

Bouchet F. R., Kandrup H. E., 1985, ApJ, 299, 1

Bournaud F., Jog C. J., Combes F., 2007, A&A, 476, 1179

Bower R. G., Benson A. J., Malbon R., Helly J. C., Frenk C. S., Baugh C. M., Cole S., Lacey C. G., 2006, MNRAS, 370, 645

Bower R. G., Lucey J. R., Ellis R. S., 1992, MNRAS, 254, 589

Bregman J. N., Snider B. A., Grego L., Cox C. V., 1998, ApJ, 499, 670

Brook C. B., Stinson G., Gibson B. K., Roškar R., Wadsley J., Quinn T., 2012, MNRAS, 419, 771

Bruzual G., Charlot S., 2003, MNRAS, 344, 1000

Buat V., Deharveng J. M., 1988, A&A, 195, 60

Bunker A., Spinrad H., Stern D., Thompson R., Moustakas L., Davis M., Dey A., 2000, Proceedings of the "Galaxies in the Young Universe II"

Carlberg R. G., 1988, ApJ, 332, 26

Carpineti A., Kaviraj S., Darg D., Lintott C., Schawinski K., Shabala S., 2012, MNRAS, 420, 2139

Chabrier G., 2003, PASP, 115, 763

Chakrabarti S., Cox T. J., Hernquist L., Hopkins P. F., Robertson B., Di Matteo T., 2007, ApJ, 658, 840

Chary R., Elbaz D., 2001, ApJ, 556, 562

Clements D. L., Sutherland W. J., McMahon R. G., Saunders W., 1996, MNRAS, 279, 477

Cole S., Lacey C. G., Baugh C. M., Frenk C. S., 2000, MNRAS, 319, 168

Colina L. et al., 2001, ApJ, 563, 546

Conselice C. J., Blackburne J. A., Papovich C., 2005, ApJ, 620, 564

Conselice C. J., Rajgor S., Myers R., 2008, MNRAS, 386, 909

Cox T. J., Dutta S. N., Di Matteo T., Hernquist L., Hopkins P. F., Robertson B., Springel V., 2006a, ApJ, 650, 791

Cox T. J., Dutta S. N., Di Matteo T., Hernquist L., Hopkins P. F., Robertson B., Springel V., 2006b, ApJ, 650, 791

da Cunha E., Charlot S., Elbaz D., 2008, MNRAS, 388, 1595

da Cunha E., Eminian C., Charlot S., Blaizot J., 2010, MNRAS, 403, 1894

Daddi E. et al., 2007, ApJ, 670, 156

Daddi E. et al., 2010, ApJL, 714, L118

Dalcanton J. J., Spergel D. N., Summers F. J., 1997, ApJ, 482, 659

Darg D. W. et al., 2010a, MNRAS, 401, 1552

Darg D. W. et al., 2010b, MNRAS, 401, 1043

Dasyra K. M. et al., 2006, ApJ, 638, 745

De Lucia G., Springel V., White S. D. M., Croton D., Kauffmann G., 2006, MNRAS, 366, 499

de Vaucouleurs G., 1948, Annales d'Astrophysique, 11, 247

Devereux N. A., Hameed S., 1997, AJ, 113, 599

Devereux N. A., Young J. S., 1990, ApJL, 350, L25

Di Matteo T., Springel V., Hernquist L., 2005, Nature, 433, 604

Dole H. et al., 2006, A&A, 451, 417

Draine B., et al., 2007, ApJ, 663, 866

Dunkley J. et al., 2009, ApJS, 180, 306

Dunne L., Eales S. A., 2001, MNRAS, 327, 697

Efstathiou G., 1992, MNRAS, 256, 43P

Efstathiou G. et al., 2002, MNRAS, 330, L29

Eggen O. J., Lynden-Bell D., Sandage A. R., 1962, ApJ, 136, 748

Fall S. M., Efstathiou G., 1980, MNRAS, 193, 189

Ferreras I., Lisker T., Pasquali A., Kaviraj S., 2009, MNRAS, 395, 554

Ferreras I., Silk J., 2000, ApJL, 541, L37

Fixsen D. J., Dwek E., Mather J. C., Bennett C. L., Shafer R. A., 1998, ApJ, 508, 123

Foster P. N., Boss A. P., 1996, ApJ, 468, 784

Freedman W. L. et al., 2001, ApJ, 553, 47

Fukugita M., Nakamura O., Turner E. L., Helmboldt J., Nichol R. C., 2004, ApJL, 601, L127

Goodman J., Heggie D. C., Hut P., 1993, ApJ, 415, 715

Goto T. et al., 2003, PASJ, 55, 771

Graham A. W., Spitler L. R., Forbes D. A., Lisker T., Moore B., Janz J., 2012, ApJ, 750, 121

Hatton S., Devriendt J. E. G., Ninin S., Bouchet F. R., Guiderdoni B., Vibert D., 2003, MNRAS, 343, 75

Hauser M. G., Dwek E., 2001, ARA&A, 39, 249

Heavens A., Panter B., Jimenez R., Dunlop J., 2004, Nature, 428, 625

Heger A., Woosley S. E., 2002, ApJ, 567, 532

Hernquist L., 1988, Computer Physics Communications, 48, 107

Hopkins P. F., Cox T. J., Hernquist L., Narayanan D., Hayward C. C., Murray N., 2013, MNRAS

Hopkins P. F., Quataert E., Murray N., 2012, MNRAS, 421, 3522

Hopkins P. F., Somerville R. S., Hernquist L., Cox T. J., Robertson B., Li Y., 2006, ApJ, 652, 864

Hoyle F., 1949, MNRAS, 109, 365

Hubble E. P., 1926, ApJ, 64, 321

Hung C.-L. et al., 2013, ApJ, 778, 129

Hutchings J. B., Neff S. G., 1987, AJ, 93, 14

Hwang H. S., Elbaz D., Lee J. C., Jeong W.-S., Park C., Lee M. G., Lee H. M., 2010, A&A, 522, A33

Iwasawa K. et al., 2011, A&A, 529, A106

Iye M. et al., 2006, Nature, 443, 186

Jogee S. et al., 2008, in Astronomical Society of the Pacific Conference Series, Vol. 396, Formation and Evolution of Galaxy Disks, Funes J. G., Corsini E. M., eds., p. 337

Kang X., Jing Y. P., Mo H. J., Börner G., 2005, ApJ, 631, 21

Kannappan S. J., 2004, ApJL, 611, L89

Kauffmann G. et al., 2003, MNRAS, 346, 1055

Kauffmann G., White S. D. M., Guiderdoni B., 1993, MNRAS, 264, 201

Kaviraj S., 2010, MNRAS, 406, 382

Kaviraj S. et al., 2013a, MNRAS, 428, 925

Kaviraj S. et al., 2013b, MNRAS, 429, L40

Kaviraj S., Peirani S., Khochfar S., Silk J., Kay S., 2009, MNRAS, 394, 1713

Kaviraj S., Rey S.-C., Rich R. M., Yoon S.-J., Yi S. K., 2007a, MNRAS, 381, L74

Kaviraj S. et al., 2007b, ApJS, 173, 619

Kaviraj S., Tan K.-M., Ellis R. S., Silk J., 2011, MNRAS, 411, 2148

Kaviraj S. et al., 2012, MNRAS, 423, 49

Kaviraj S., Yi S. K., Gawiser E., van Dokkum P. G., Khochfar S., Schawinski K., Silk J., 2008, MNRAS, 245, 195

Kennicutt, Jr. R. C., 1998, ARA&A, 36, 189

Kereš D., Katz N., Fardal M., Davé R., Weinberg D. H., 2009, MNRAS, 395, 160

Kewley L. J., Geller M. J., Jansen R. A., Dopita M. A., 2002, AJ, 124, 3135

Kewley L. J., Groves B., Kauffmann G., Heckman T., 2006, MNRAS, 372, 961

Khochfar S., Silk J., 2006, MNRAS, 370, 902

Khochfar S., Silk J., 2009, MNRAS, 397, 506

Kleinmann S., Keel W., 1987, Star Formation in Galaxies. C.J. Lonsdale-Persson, Washington DC: US Govt. Print. Off.

Komatsu E. et al., 2009, ApJS, 180, 330

Komiya Y., Habe A., Suda T., Fujimoto M. Y., 2009, ApJL, 696, L79

Kormendy J., Fisher D. B., Cornell M. E., Bender R., 2009, ApJS, 182, 216

Kriek M., van Dokkum P. G., Franx M., Illingworth G. D., Magee D. K., 2009, ApJL, 705, L71

Lacey C., Cole S., 1994, MNRAS, 271, 676

Lamastra A., Menci N., Fiore F., Santini P., 2013, A&A, 552, A44

Lambas D. G., Tissera P. B., Alonso M. S., Coldwell G., 2003, MNRAS, 346, 1189

Larson R. B., 2003, Reports on Progress in Physics, 66, 1651

Law K.-H., Gordon K. D., Misselt K. A., 2011, ApJ, 738, 124

Lee J., Yi S. K., 2013, ApJ, 766, 38

Lee Y. W., Yi S., 1999, in Astronomical Society of the Pacific Conference Series, Vol. 164, Ultraviolet-Optical Space Astronomy Beyond HST, Morse J. A., Shull J. M., Kinney A. L., eds., p. 86

Leeuw L. L., Davidson J., Dowell C. D., Matthews H. E., 2008, ApJ, 677, 249

Leeuw L. L., Sansom A. E., Robson E. I., Haas M., Kuno N., 2004, ApJ, 612, 837

Lehnert M. D., Heckman T. M., 1996, ApJ, 472, 546

Lintott C. J. et al., 2008, MNRAS, 389, 1179

Lonsdale Persson C. J., Helou G., 1987, ApJ, 314, 513

Lotz J. M., Jonsson P., Cox T. J., Primack J. R., 2008, MNRAS, 391, 1137

Machacek M. E., Bryan G. L., Abel T., 2001, ApJ, 548, 509

Madau P., Rees M. J., 2001, ApJL, 551, L27

Martin D. C. et al., 2005, ApJL, 619, L1

Meurer G. R., Heckman T. M., Lehnert M. D., Leitherer C., Lowenthal J., 1997, AJ, 114, 54

Mihos J. C., Hernquist L., 1994a, ApJL, 425, L13

Mihos J. C., Hernquist L., 1994b, ApJL, 431, L9

Mihos J. C., Hernquist L., 1996a, ApJ, 464, 641

Mihos J. C., Hernquist L., 1996b, ApJ, 464, 641

Milosavljević M., Merritt D., 2003, AIPC, 686, 201

Mo H. J., Mao S., White S. D. M., 1998, MNRAS, 295, 319

Moshir M., Kopman G., Conrow T. A. O., 1992, IRAS Faint Source Survey, Explanatory supplement version 2. California Institute of Technology

Naab T., Johansson P. H., Ostriker J. P., 2009, ApJL, 699, L178

Nesvadba N. P. H., Lehnert M. D., Eisenhauer F., Gilbert A., Tecza M., Abuter R., 2006, ApJ, 650, 693

Neugebauer G. et al., 1984a, ApJL, 278, L1

Neugebauer G. et al., 1984b, ApJL, 278, L83

Nikolic B., Cullen H., Alexander P., 2004, MNRAS, 355, 874

Noguchi M., 1999, ApJ, 514, 77

Osterbrock D. E., Ferland G. J., 2006, Astrophysics of gaseous nebulae and active galactic nuclei. University Science Books

Padmanabhan T., 1993, Structure Formation in the Universe. Cambridge University Press

Panter B., Jimenez R., Heavens A. F., Charlot S., 2007, MNRAS, 378, 1550

Papovich C., Dickinson M., Giavalisco M., Conselice C. J., Ferguson H. C., 2005, ApJ, 631, 101

Patton D. R., Carlberg R. G., Marzke R. O., Pritchet C. J., da Costa L. N., Pellegrini P. S., 2000, ApJ, 536, 153

Peebles P. J. E., 1982, ApJL, 263, L1

Pei Y. C., Fall S. M., Hauser M. G., 1999, ApJ, 522, 604

Pilbratt G. L. et al., 2010, A&A, 518, L1

Press W. H., Schechter P., 1974, ApJ, 187, 425

Pryke C., Halverson N. W., Leitch E. M., Kovac J., Carlstrom J. E., Holzapfel W. L., Dragovan M., 2002, ApJ, 568, 46

Puget J.-L., Abergel A., Bernard J.-P., Boulanger F., Burton W. B., Desert F.-X., Hartmann D., 1996, A&A, 308, L5

Quintero A. D. et al., 2004, ApJ, 602, 190

Reddy N. et al., 2012, ApJ, 744, 154

Renzini A., 1977, in Saas-Fee Advanced Course 7: Advanced Stages in Stellar Evolution, Bouvier P., Maeder A., eds., p. 151

Riechers D. A. et al., 2013, Nature, 496, 329

Risaliti G., Gilli R., Maiolino R., Salvati M., 2000, A&A, 357, 13

Robertson B., Bullock J. S., Cox T. J., Di Matteo T., Hernquist L., Springel V., Yoshida N., 2006, ApJ, 645, 986

Rodighiero G. et al., 2011, ApJL, 739, L40

Rowan-Robinson M. et al., 2008, MNRAS, 386, 697

Rowan-Robinson M., Crawford J., 1989, MNRAS, 238, 523

Rowlands K. et al., 2012, MNRAS, 419, 2545

Ruszkowski M., Springel V., 2009, ApJ, 696, 1094

Sahni V., 2004, Lecture Notes in Physics, Vol. 653, Dark Matter and Dark Energy. Berlin Springer Verlag, p. 141

Sánchez A. G., Crocce M., Cabré A., Baugh C. M., Gaztañaga E., 2009, MNRAS, 400, 1643

Sandage A., Sandage M., Kristian J., 1975, Galaxies and the Universe. University of Chicago Press

Sanders D. B., Mirabel I. F., 1996, ARA&A, 34, 749

Sanders D. B., Scoville N. Z., Soifer B. T., Young J. S., Danielson G. E., 1987, ApJL, 312, L5

Sanders D. B., Soifer B. T., Elias J. H., Madore B. F., Matthews K., Neugebauer G., Scoville N. Z., 1988a, ApJ, 325, 74

Sanders D. B., Soifer B. T., Elias J. H., Neugebauer G., Matthews K., 1988b, ApJL, 328, L35

Santini P. et al., 2009, A&A, 504, 751

Santini P. et al., 2014, A&A, 562, A30

Sarzi M. et al., 2006, MNRAS, 366, 1151

Sarzi M. et al., 2010, MNRAS, 402, 2187

Sauvage M., Thuan T. X., 1992, ApJL, 396, L69

Sauvage M., Thuan T. X., 1994, ApJ, 429, 153

Savoy J., Welch G. A., Fich M., 2009, ApJ, 706, 21

Schaerer D., 2003, A&A, 397, 527

Schawinski K. et al., 2007a, ApJS, 173, 512

Schawinski K., Thomas D., Sarzi M., Maraston C., Kaviraj S., Joo S.-J., Yi S. K., Silk J., 2007b, MNRAS, 382, 1415

Schawinski K. et al., 2010, ApJ, 711, 284

Schawinski K., Virani S., Simmons B., Urry C. M., Treister E., Kaviraj S., Kushkuley B., 2009, ApJL, 692, L19

Schechter P., 1976, ApJ, 203, 297

Schneider R., Ferrara A., Natarajan P., Omukai K., 2002, ApJ, 571, 30

Searle L., Zinn R., 1978, ApJ, 225, 357

Shabala S. S. et al., 2012, MNRAS, 423, 59

Shapiro P. R., Giroux M. L., Babul A., 1994, ApJ, 427, 25

Shioya Y. et al., 2008, ApJS, 175, 128

Shu F. H., Adams F. C., Lizano S., 1987, ARA&A, 25, 23

Silk J., Mamon G. A., 2012, Research in Astronomy and Astrophysics, 12, 917

Simmons B., et al., 2013, MNRAS, 443, 2199

Skibba R. A. et al., 2011, ApJ, 738, 89

Skrutskie M. F. et al., 2006, AJ, 131, 1163

Somerville R. S., 2002, ApJL, 572, L23

Somerville R. S., Primack J. R., Faber S. M., 2001, MNRAS, 320, 504

Spergel D. N. et al., 2007, ApJS, 170, 377

Spitzer L., 1978, Physical processes in the interstellar medium. Wiley-VCH

Springel V., Hernquist L., 2005, ApJL, 622, L9

Springel V. et al., 2005, Nature, 435, 629

Steinmetz M., Navarro J. F., 2002, Nature, 7, 155

Stickel M., Klaas U., Lemke D., 2007, A&A, 466, 831

Strateva I. et al., 2001, AJ, 122, 1861

Sturm E. et al., 2006, ApJL, 653, L13

Temi P., Brighenti F., Mathews W. G., 2007, ApJ, 660, 1215

Temi P., Brighenti F., Mathews W. G., Bregman J. D., 2004, ApJS, 151, 237

Toomre A., 1976, in Bulletin of the American Astronomical Society, Vol. 8, Bulletin of the American Astronomical Society, p. 354

Toomre A., 1977, in Evolution of Galaxies and Stellar Populations, Tinsley B. M., Larson D. Campbell R. B. G., eds., p. 401

Torrey P., Cox T. J., Kewley L., Hernquist L., 2012a, ApJ, 746, 108

Torrey P., Vogelsberger M., Sijacki D., Springel V., Hernquist L., 2012b, MNRAS, 427, 2224

Trager S. C., Faber S. M., Worthey G., González J. J., 2000, AJ, 119, 1645

Treister E. et al., 2009, ApJ, 706, 535

Treister E., Natarajan P., Sanders D. B., Urry C. M., Schawinski K., Kartaltepe J., 2010, Science, 328, 600

Tremonti C. A. et al., 2004, ApJ, 613, 898

Tweed D., Devriendt J., Blaizot J., Colombi S., Slyz A., 2009, A&A, 506, 647

Vader J. P., Simon M., 1987, Nature, 327, 304

van Dokkum P. G., 2005, AJ, 130, 2647

Veilleux S., Osterbrock D. E., 1987, in NASA Conference Publication, Vol. 2466, NASA Conference Publication, Lonsdale Persson C. J., ed., pp. 737–740

Venkatesan A., Nath B. B., Shull J. M., 2006, ApJ, 640, 31

Verma A., Lehnert M. D., Förster Schreiber N. M., Bremer M. N., Douglas L., 2007, MNRAS, 377, 1024

Vlahakis C., Dunne L., Eales S., 2005, MNRAS, 364, 1253

von Hoerner S., 1963, Zeitschrift für Astrophysik, 57, 47

Walterbos R. A. M., Greenawalt B., 1996, ApJ, 460, 696

Wang L., Rowan-Robinson M., 2009, MNRAS, 398, 109

White S. D. M., 1978, MNRAS, 184, 185

White S. D. M., Frenk C. S., 1991, ApJ, 379, 52

White S. D. M., Rees M. J., 1978, MNRAS, 183, 341

Wild V., Heckman T., Charlot S., 2010, MNRAS, 405, 933

Wright E. L. et al., 2010, AJ, 140, 1868

Yang X., Mo H. J., van den Bosch F. C., Jing Y. P., 2005, MNRAS, 356, 1293

Yang X., Mo H. J., van den Bosch F. C., Pasquali A., Li C., Barden M., 2007, ApJ, 671, 153

Yi S. K. et al., 2005, ApJL, 619, L111

York D. G. et al., 2000, AJ, 120, 1579

Young L. M., 2002, AJ, 124, 788

Younger J. D., Hayward C. C., Narayanan D., Cox T. J., Hernquist L., Jonsson P., 2009, MNRAS, 396, L66

Zabludoff A. I., Zaritsky D., Lin H., Tucker D., Hashimoto Y., Shectman S. A., Oemler A., Kirshner R. P., 1996, ApJ, 466, 104

Zel'dovich Y. B., 1970, A&A, 5, 84